UNIVERSITY OF SOUTHAMPTON

FACULTY OF PHYSICAL SCIENCES AND ENGINEERING

Physics and Astronomy

B physics from lattice QCD: A study of $B_s \to K\ell\nu$, $B_s \to D_s\ell\nu$ and $B_s \to \phi\ell^+\ell^-$ form factors

by

Edwin Lizarazo

Thesis for the degree of Doctor of Philosophy

March 2018

UNIVERSITY OF SOUTHAMPTON

ABSTRACT

FACULTY OF PHYSICAL SCIENCES AND ENGINEERING
Physics and Astronomy

Doctor of Philosophy

B PHYSICS FROM LATTICE QCD: A STUDY OF $B_S \to K\ell\nu$, $B_S \to D_S\ell\nu$ AND $B_S \to \phi\ell^+\ell^-$ FORM FACTORS

by Edwin Lizarazo

The Standard Model of particle physics currently stands as our most complete theory of fundamental particles and interactions. It is a well tested physics theory but tensions have been found between theoretical predictions and experimental results. These discrepancies can be either a sign of New Physics or the result of insufficient control over theoretical and experimental uncertainties. In order to detect/rule-out new physics effects in the flavour sector it is important to improve our understanding of flavour changing processes which occur at tree and loop level in the Standard Model.

Semileptonic B decays provide promising channels to test the Standard Model and search for signs of New Physics. While the B-factories and LHCb carry out measurements of B-meson observables, theoretical determinations of form factors are necessary for the extraction of Cabibbo-Kobayashi-Maskawa matrix elements, the determination of differential branching fractions and angular distributions amongst other quantities.

In this work we present the calculation of $B_s \to K\ell\nu$, $B_s \to D_s\ell\nu$ and $B_s \to \phi\ell^+\ell^-$ form factors using the Columbia interpretation of the relativistic heavy quark action for the b-quark and the domain wall fermion action for light, charm and strange quarks. In conjunction with future experimental data, our form factor results for $B_s \to K\ell\nu$ and $B_s \to D_s\ell\nu$ decays will provide a new method to extract the CKM matrix elements $|V_{ub}|$ and $|V_{cb}|$, test the forward backward asymmetry and measure the ratios $R(K)$ and $R(D_s)$. Similarly, $B_s \to \phi\ell^+\ell^-$ form factors will allow for the reconstruction of many observables that offer important tests of the Standard Model and New Physics scenarios.

Contents

List of Figures

List of Tables

Declaration of Authorship

I, Edwin Lizarazo , declare that the thesis entitled *B physics from lattice QCD: A study of* $B_s \to K\ell\nu$*,* $B_s \to D_s\ell\nu$ *and* $B_s \to \phi\ell^+\ell^-$ *form factors* and the work presented in the thesis are both my own, and have been generated by me as the result of my own original research. I confirm that:

- this work was done wholly or mainly while in candidature for a research degree at this University;
- where any part of this thesis has previously been submitted for a degree or any other qualification at this University or any other institution, this has been clearly stated;
- where I have consulted the published work of others, this is always clearly attributed;
- where I have quoted from the work of others, the source is always given. With the exception of such quotations, this thesis is entirely my own work;
- I have acknowledged all main sources of help;
- where the thesis is based on work done by myself jointly with others, I have made clear exactly what was done by others and what I have contributed myself;
- parts of this work have been published as: [18], [19] and [20]

Signed:.....

Date:.....

Acknowledgements

I would like to thank my main supervisor Professor Jonathan Flynn for all his patience and dedication without which the successful completion of this work wouldn't have been possible, I would also like to thank Dr. Oliver Witzel and Dr. Andreas Jüttner for their continuous support. Finally, I would like to thank my wife Carolina and my children Logan, David and Daniel for always being there and being my greatest source of inspiration.

Chapter 1

Introduction

The Standard Model (SM) of particle physics is a relativistic quantum field theory which describes all known interactions between fundamental particles. In the development of the SM quark flavour physics has played a central role: the Glashow-Iliopoulos-Maiani (GIM) mechanism [21] predicted the charm quark, CP violation in $K^0\overline{K}^0$ predicted the third generation of quarks [22], and the Cabibbo-Kobayashi-Maskawa (CKM) matrix [22, 23] provides a single source for information on CP violation in the quark sector. Although the SM is a well tested model whose latest success was given by the discovery of the Higgs boson [24, 25] it has its shortcomings, for example:

- The observed Higgs mass can only be justified within the SM by the fine tuning cancellation between quadratic radiative corrections and the bare Higgs mass.
- The amount of CP violation in the SM is to small to produce the observed matter-antimatter asymmetry [26–29].
- It doesn't explain the origin of dark matter.

New Physics (NP) extensions of the SM have been proposed to address this issues by including heavier particles related to higher energy phenomena.

In the search for NP signals weak decays of hadrons containing a bottom quark provide an ideal testing ground. Tree-level decays such as $B_s \to K\ell\nu$ and $B_s \to D_s\ell\nu$ can be used to extract the CKM matrix elements $|V_{ub}|$ and $|V_{cb}|$, respectively, and hence to test the unitarity of the CKM matrix. Whilst processes mediated by flavour changing neutral currents, such as the decay $B_s \to \phi\ell^+\ell^-$, which are highly suppressed in the SM, provide an opportunity to discover and probe NP effects.

Any possible deviations between experimental measurements and theoretical predictions can only be confirmed as signs of NP when both theoretical and experimental uncertainties are under control. The quantity and quality of experimental measurements for

exclusive $b \to u$, $b \to c$ and $b \to s$ decays has increased greatly over the years reducing the sources of experimental uncertainty. Theoretical understanding of strong and weak interactions of quarks has also significantly increased both through the development of effective theories and by improvements on lattice simulations.

The running coupling of the strong force as a function of energy is such that the tools needed to study hadronic decays are energy regime dependent. At short distances, or equivalently high energies perturbation theory can be safely applied, whilst for large distances the phenomenon of quark confinement calls for a non-perturbative approach, namely Lattice Quantum Chromodynamics (LQCD).

In LQCD continuum space-time is replaced by a four dimensional finite Euclidean space-time grid [30] and the path integral is computed numerically. The use of a finite size lattice introduces finite-volume effects which are minimized by requiring that the mass of the lightest propagating particle in the theory, namely the pion, is such that $m_\pi L \gg 1$ where L is the side length of the lattice. Moreover, the discretization of space-time introduces discretization errors which should vanish as the lattice spacing goes to zero.

Currently available lattice QCD gauge ensembles are generated with an inverse lattice spacing around or below 3 GeV whilst the mass of the b quark is $m_b = 4.18^{+0.04}_{-0.03}$ GeV [6] meaning that $m_b a > 1$ and hence proper control of discretization errors is not possible using conventional lattice calculations. For this reason, simulations of b quarks are performed using effective theories such as heavy quark effective theory (HQET) [31–36], non-relativistic QCD (NRQCD) [37–39] or the relativistic heavy quark action (RHQ) [40–42].

In this work we present our determination of the form factors which parametrize the hadronic matrix elements for the tree-level decays $B_s \to K\ell\nu$ and $B_s \to D_s\ell\nu$, and for the rare decay $B_s \to \phi\ell^+\ell^-$. Our simulations are based on RBC-UKQCD's set of 2+1 flavour gauge field configurations [7, 10–12] generated with the Iwasaki gauge action [43] and the domain-wall fermion action [13, 14, 44]. In the valence sector we generate light, strange and charm propagators using the domain-wall fermion action and we simulate the heavy b-quarks using the RHQ action [40–42].

This dissertation is organized as follows. In Chapter 2, we give an introduction to the SM, starting from its Lagrangian formulation we then discuss the spontaneous symmetry breaking of $SU(2)_W \times U(1)_Y$ to $U(1)_{EM}$, electroweak interactions of quarks, chiral symmetry and effective Lagrangians, we then introduce the continuum phenomenology which justifies and will be benefited by the results obtained from this dissertation. We finalize this chapter by introducing the form factors which are the main quantities of interest in this work. In Chapter 3 we give an introduction to the theoretical foundations of LQCD including an overview of gauge and fermionic actions, Euclidean correlators and discrete symmetries. In Chapter 4 we discuss the process to extract form factors from lattice simulations from ratios of two-point and three-point functions. We then

discuss operator renormalization and improvement, that is, the process by which lattice results are identified with the continuum theory. We complete this chapter by our independent calculation of the $\mathcal{O}(a)$ improvement terms for tensor and pseudotensor currents. In Chapter 5 we discuss the setup of our calculations, the methods used to improve the signal obtained from our simulations and the statistical tools that we used for our data analysis. In Chapter 6 we present our results, we begin by determining effective masses and extracting the form factors at finite lattice spacing, we then renormalise and improve to $\mathcal{O}(a)$ our results and perform the chiral-continuum extrapolation so that all lattice dependence is removed from our results, and finally we perform a z-expansion to extrapolate our results to $q^2 = 0$. We present our conclusions in Chapter 7.

My personal contribution to the results presented in this dissertation is:

1. In section 4.3.2 I independently derived the $\mathcal{O}(a)$ improvement terms for tensor and pseudotensor currents Eqs (4.81) to (4.90).
2. In section 5.4.2 I determined the optimal width for the Gaussian smeared sources used for the smearing of charm-strange two point functions.
3. In section 5.4.1 I performed the tests necessary to determine the optimal source sink separation that was to be used for the extraction of form factors.
4. I performed all mass fits of sections 6.2.
5. In section 6.3.1 I determined the non-perturbative coefficient Z_V^{bb} of Table 6.4.
6. In section 6.3.1 I performed the perturbative determination of the renormalization coefficient ρ of Table 6.4 and the matching coefficients for vector currents of Table 6.5.
7. In section 6.3.2.1 I performed the charm mass extrapolation.
8. In sections 6.3.2 and 6.4.3 I analysed all the lattice data necessary to extract the form factors for all the decays studied in this dissertation.
9. In sections 6.3.3, 6.3.4 and 6.4.4 I performed the heavy meson chiral continuum extrapolation for all the decays studied in this dissertation.
10. In sections 6.3.6 and 6.4.6 I calculated all statistical and systematic errors presented in our error budget.
11. In sections 6.3.8 and 6.4.7 I performed the z-expansion to extrapolate all results from the region where the simulations were performed to $q^2 = 0$.

Chapter 2

The Standard Model

2.1 Introduction

The Standard Model (SM) of particle physics is a summary of our understanding of the interactions between fundamental particles, that is, the building blocks of the universe and three of the four fundamental forces of nature, namely the electromagnetic, weak and strong interactions. The SM has been successfully tested against experimental results and has predicted the existence of the top quark [45], the tau neutrino [46], and the Higgs boson [24, 25]. The SM however does not include the gravitational force nor does it explain the matter-antimatter asymmetry or the origin of dark matter amongst other phenomena. The shortcomings of the SM have given rise to new models such as supersymmetry [47] and string theory [48].

In this chapter we will introduce the Lagrangian formulation of the SM in section 2.2, followed by a brief description of electroweak interactions of quarks — section 2.4 —, approximate flavour symmetries — section 2.5 — and effective Hamiltonians for weak decays — section 2.6 —. Finally, in sections 2.7 and 2.8 we will discuss the continuum phenomenology and make a brief introduction to form factors.

2.2 Lagrangian Formulation

The Standard Model of particle physics is a gauge theory that describes electromagnetic, weak and strong interactions in terms of the gauge group

$$SU(3)_C \times SU(2)_W \times U(1)_Y, \tag{2.1}$$

with field content summarized in Table 2.1 and the Lagrangian

$$\mathcal{L} = \mathcal{L}_{\text{gauge}} + \mathcal{L}_{\text{fermion}} + \mathcal{L}_{\text{Yukawa}} + \mathcal{L}_{\text{Higgs}} \tag{2.2}$$

$$\mathcal{L}_{\text{gauge}} = -\frac{1}{4}\sum_{c=1}^{8} G^c_{\mu\nu}G^{c\mu\nu} - \frac{1}{4}\sum_{a=1}^{3} W^a_{\mu\nu}W^{a\mu\nu} - \frac{1}{4}B_{\mu\nu}B^{\mu\nu} \tag{2.3}$$

$$\mathcal{L}_{\text{Higgs}} = D^\mu\phi^\dagger D_\mu\phi - \frac{h}{2}(\phi^\dagger\phi)^2 + \mu^2\phi^\dagger\phi \tag{2.4}$$

$$\begin{aligned}\mathcal{L}_{\text{fermions}} = &\sum_{n,i,\alpha} i\bar{Q}_{ni\alpha}\not{D}Q^{i\alpha}_n + \sum_{n,i} i\bar{U}^i_n\not{D}U_{ni} + \sum_{n,i} i\bar{D}^i_n\not{D}D_{ni} \\ &+ \sum_{n,\alpha} i\bar{L}_{n\alpha}\not{D}L^\alpha_n + \sum_n i\bar{E}_n\not{D}E_n\end{aligned} \tag{2.5}$$

$$\begin{aligned}\mathcal{L}_{\text{Yukawa}} = &-\sum_{n,n'} Y^E_{n,n'}H^\dagger_\alpha\bar{L}^\alpha_n E_{n'} - \sum_{n,n'} Y^D_{n,n'}H^\dagger_\alpha\bar{Q}^{i\alpha}_n D_{n'i} \\ &- \sum_{n,n'} Y^U_{n,n'}H^\alpha Q^{i\alpha}_n U_{n'i} + \text{Hermitian Conjugates}\end{aligned} \tag{2.6}$$

where n, i and α are family, color and $SU(2)$ indices, respectively, and the covariant derivatives have the form

$$D_\mu\phi^\alpha = \partial_\mu\phi^\alpha + \frac{ig_w}{2}\tau^{a\alpha}_b W^a_\mu\phi^\beta + \frac{ig_1}{2}B_\mu\phi^\alpha \tag{2.7}$$

$$\begin{aligned}D_\mu Q^{i\alpha}_n(x) = &\partial_\mu Q^{i\alpha}_n(x) + \frac{ig_s}{2}\sum_{c=1}^{8} G^c_\mu\lambda^{ci}_j Q^{j\alpha}_n(x) + \frac{ig_w}{2}\sum_{a=1}^{3} W^a_\mu(x)\tau^{a\alpha}_\beta Q^{i\beta}_n(x) \\ &+ \frac{ig_1}{6}B_\mu(x)Q^{i\alpha}_n(x),\end{aligned} \tag{2.8}$$

$$D_\mu U_{ni}(x) = \partial_\mu U_{ni}(x) - \frac{ig_s}{2}\sum_{c=1}^{8} G^c_\mu\lambda^{cj}_i U_{nj}(x) - \frac{ig_1}{3}B_\mu(x)U_{ni}(x), \tag{2.9}$$

$$D_\mu D_{ni}(x) = \partial_\mu D_{ni}(x) - \frac{ig_s}{2}\sum_{c=1}^{8} G^c_\mu\lambda^{cj}_i D_{nj}(x) - \frac{ig_1}{3}B_\mu(x)D_{ni}(x), \tag{2.10}$$

$$D_\mu L^\alpha_n(x) = \partial_\mu L^\alpha_n(x) + \frac{ig_w}{2}\sum_{a=1}^{3} W^a_\mu(x)\tau^{a\alpha}_\beta L^\beta_n(x) - \frac{ig_1}{3}B_\mu(x)U^\alpha_n(x), \tag{2.11}$$

$$D_\mu E_n(x) = \partial_\mu E_n(x) + ig_1 B_\mu(x)E_n(x), \tag{2.12}$$

where g_s, g_w and g_1 denote the $SU(3)$, $SU(2)_W$ and $U(1)_Y$ couplings, respectively. In equation (2.6) we denote Yukawa couplings by $Y_{n,n'}$ and define the field strength tensors for color, weak isospin and weak hypercharge as

$$G^c_{\mu\nu} = \partial_\mu G^c_\nu - \partial_\nu G^c_\mu - g_s f^{cde}G^d_\mu G^e_\nu, \tag{2.13}$$

$$W^c_{\mu\nu} = \partial_\mu W^a_\nu - \partial_\nu W^a_\mu - g_w\epsilon^{abc}W^b_\mu W^c_\nu, \tag{2.14}$$

$$B_{\mu\nu} = \partial_\mu B_\nu - \partial_\nu B_\mu, \tag{2.15}$$

where ϵ^{abc} and f^{abc} denote the structure constants of $SU(2)_W$ and $SU(3)$, respectively. In the continuum the Standard Model Lagrangian (2.2) requires the addition of gauge fixing terms.

	SU(3)	SU(2)	U(1)
G (gluon)	8	1	0
W (W, Z and photon)	1	3	0
B (Z and photon)	1	1	0
ϕ (Higgs)	1	2	$-1/2$
Q_n (left-handed quarks)	3	2	$+1/6$
U_n (right-handed up-type quarks)	3	1	$2/3$
D_n (right handed down-type quarks)	3	1	$-1/3$
L_n (left handed leptons)	1	2	$-1/2$
E_n (right handed leptons)	1	1	-1

Table 2.1: $SU(3)_C \times SU(2)_W \times U(1)_Y$ representations for the Standard Model fields

2.3 Spontaneous symmetry breaking of $SU(2)_W \times U(1)_Y$

The potential of the Higgs Lagrangian (2.4) has an infinite set of degenerate states with minimum energy satisfying

$$|\langle 0|\phi^{(0)}|0\rangle| = \sqrt{\frac{-\mu^2}{2h}} \equiv \frac{v}{\sqrt{2}}. \tag{2.16}$$

Once a particular ground state is chosen the $SU(2)_W \times U(1)_Y$ symmetry of the Higgs Lagrangian is spontaneously broken to the electromagnetic subgroup $U(1)_{EM}$. This process rotates the original W^3 and B vector boson plane by an angle θ_W, the weak mixing angle, producing as a result the Z boson and the photon A

$$\begin{bmatrix} A \\ Z^0 \end{bmatrix} = \begin{bmatrix} \cos\theta_W & \sin\theta_W \\ -\sin\theta_W & \cos\theta_W \end{bmatrix} \begin{bmatrix} B \\ W^3 \end{bmatrix}. \tag{2.17}$$

Moreover, it follows from Goldstone's theorem [49–51] that this symmetry breaking gives rise to three massless states — Goldstone bosons —, one for each broken generator, these Goldstone bosons can nonetheless be removed from the Lagrangian using $SU(2)_W$ local gauge invariance. This can be readily seen by parametrizing the scalar doublet as

$$\phi(x) \equiv \begin{bmatrix} \phi^{(+)}(x) \\ \phi^{(0)}(x) \end{bmatrix} = \exp\left\{ i\frac{\sigma_i}{2}\theta^i(x) \right\} \frac{1}{\sqrt{2}} \begin{bmatrix} 0 \\ v + H(x) \end{bmatrix}, \tag{2.18}$$

and setting the parameter $\theta^i(x)$ which denotes the three Goldstone bosons to zero, that is, working in the unitary gauge. In equation (2.18) $H(x)$ denotes the physical Higgs and $v = (\sqrt{2}G_F)^{1/2} \approx 246$ GeV is the Higgs vacuum expectation value. We can now use equation (2.18) together with the covariant derivative (2.7) to write the kinetic piece of the Higgs Lagrangian (2.4) as

$$(D_\mu\phi)^\dagger D^\mu\phi \to \frac{1}{2}\partial_\mu H \partial^\mu H + (v+H)^2 \left\{ \frac{g_w^2}{4} W_\mu^+ W^{-\mu} + \frac{g_w^2}{8\cos^2\theta_W} Z_\mu Z^\mu \right\} \tag{2.19}$$

$$W_\mu^\pm = \frac{1}{\sqrt{2}}\left(W_\mu^1 \mp iW_\mu^2\right) \tag{2.20}$$

$$Z_\mu = \cos\theta_W W_\mu^3 - \sin\theta_W B_\mu \tag{2.21}$$

where the quadratic term for the $W^\pm$ and the Z boson indicate that the gauge bosons have acquired masses:

$$M_Z \cos\theta_W = M_W = \frac{1}{2}vg. \tag{2.22}$$

The photon on the other hand remains massless because $U(1)_{\mathrm{EM}}$ is an unbroken symmetry.

2.4 Electroweak interactions of quarks

Fermionic masses are also generated through the spontaneous symmetry breaking of $SU(2)_W \times U(1)_Y$ to $U(1)_{EM}$. In the case of quarks their masses are given by

$$\mathcal{L} = -\sum_{n,n'=d,s,b} M^D_{n,n'} \bar{Q}^{i2}_n D_{n'i} - \sum_{n,n'=u,c,t} M^U_{n,n'} \bar{Q}^{i1}_n \sigma_2 U_{n'i} + \text{hermitian conjugate}$$

where Q^{i1}_n and Q^{i2}_n are left handed quarks of electric charge $q = 2/3$ and $q = -1/3$, respectively, and

$$M^U_{n,n'} = \frac{v}{\sqrt{2}} Y^U_{n,n'} \tag{2.23}$$

$$M^D_{n,n'} = \frac{v}{\sqrt{2}} Y^D_{n,n'} \tag{2.24}$$

their corresponding mass matrices. We can now use the unitary field redefinitions

$$\begin{bmatrix} Q^1_{n,n'} \\ Q^2_{n,n'} \end{bmatrix} \to A^U \begin{bmatrix} Q^1_{n,n'} \\ Q^2_{n,n'} \end{bmatrix} \tag{2.25}$$

$$U \to B^U U \tag{2.26}$$

$$D \to B^D D \tag{2.27}$$

to write the diagonal mass matrices

$$M^U \to (A^U)^\dagger M^U B^U = \begin{bmatrix} m_u & 0 & 0 \\ 0 & m_c & 0 \\ 0 & 0 & m_t \end{bmatrix} \tag{2.28}$$

$$M^D \to (A^U V)^\dagger M^D B^D = \begin{bmatrix} m_d & 0 & 0 \\ 0 & m_s & 0 \\ 0 & 0 & m_b \end{bmatrix}, \tag{2.29}$$

where

$$V = \begin{bmatrix} V_{ud} & V_{us} & V_{ub} \\ V_{cd} & V_{cs} & V_{cb} \\ V_{td} & V_{ts} & V_{tb} \end{bmatrix} \tag{2.30}$$

is known as the Cabibbo-Kobayashi-Maskawa matrix [22, 23]. In the Standard Model the CKM matrix is a 3×3 unitary matrix, it contains 9 real parameters of which only four are independent, this can be seen by introducing the six field phases α_i, $i = \{1, 2, 3, 4, 5, 6\}$, redefining the CKM matrix as

$$\tilde{V} = \begin{bmatrix} e^{i\alpha_1} & 0 & 0 \\ 0 & e^{i\alpha_2} & 0 \\ 0 & 0 & e^{i\alpha_3} \end{bmatrix} V \begin{bmatrix} e^{-i\alpha_4} & 0 & 0 \\ 0 & e^{-i\alpha_5} & 0 \\ 0 & 0 & e^{-i\alpha_6} \end{bmatrix} \tag{2.31}$$

and noticing that an overall phase change, $\alpha_i \to \alpha_i + \omega$, leaves $\tilde{V}$ unchanged. From these we can conclude that five out of the nine real parameters that constitute the CKM matrix can be absorbed into quark field phases and the remaining four parameters are independent. These parameters can be expressed in terms of three mixing angles $\theta_1, \theta_2, \theta_3$ and the CP violating phase δ. Having introduced the CKM matrix we will now discuss charged and neutral currents. We begin by writing in terms of quark mass eigenstate fields Ψ the kinetic and mass terms of the quark Lagrangian

$$\mathcal{L}_{\text{quarks}} = \sum_{f=u,c,t,d,s,b} \sum_{l} \bar{\Psi}_{f,l}(i\not{\partial} - m_f)\Psi^l_f \tag{2.32}$$

$$= \sum_{f=u,c,t,d,s,b} \sum_{l} \bar{\Psi}_{f,l}(i\hat{\not{D}} - m_f)\Psi^l_f - \frac{g_w}{\sqrt{2}}(W^+_\mu T^{-\mu} + W^-_\mu T^{+\mu}) - \tilde{g} Z^0_\mu T^\mu_Z \tag{2.33}$$

where l indicates color indices, the currents are given by

$$T^\mu_Z = \sum_{f=u,c,t} \bar{\Psi}_{f,i}\gamma^\mu \left(\frac{1-\gamma^5}{4} - \frac{2}{3}\sin^2\theta_W\right)\Psi^i_f \sum_{f=b,s,d} \bar{\Psi}_{f,i}\gamma^\mu \left(-\frac{1-\gamma^5}{4} - +\frac{1}{3}\sin^2\theta_W\right)\Psi^i_f, \tag{2.34}$$

$$T^{+\mu} = \sum_{f=u,c,t} \sum_{f'=d,s,b} V_{f',f}\bar{\Psi}_{f',i}\gamma^\mu \frac{1-\gamma^5}{2}\Psi^i_f, \tag{2.35}$$

$$T^{-\mu} = \sum_{f=u,c,t} \sum_{f'=d,s,b} V^*_{f',f}\bar{\Psi}_{f,i}\gamma^\mu \frac{1-\gamma^5}{2}\Psi^i_{f'}, \tag{2.36}$$

and the derivatives

$$\hat{D}_\mu \Psi^i_f = \partial_\mu + i g_s \sum_{c=1}^{8} \sum_j G^c_\mu(x)(\frac{1}{2}\lambda^c)^i_j \Psi^j_f + \frac{2}{3} i e A_\mu(x)\Psi^i_f \quad \text{for f = u,c,t,} \tag{2.37}$$

$$\hat{D}_\mu \Psi_f^i = \partial_\mu + ig_s \sum_{c=1}^{8} \sum_j G_\mu^c(x)(\frac{1}{2}\lambda^c)_j^i \Psi_f^j - \frac{1}{3} ieA_\mu(x)\Psi_f^i \quad \text{for f = d,s,b.} \tag{2.38}$$

where θ_W is the weak mixing angle, G and A are the gluon and photon fields, respectively, λ^C are the Gell-Mann matrices —c.f Appendix A — and e is the electric charge of the particle in question. It can be seen from (2.34)-(2.36) that in contrast with charged currents where the CKM matrix which couples up-type and down-type quarks is present, there is no term mediating the mixing of quarks in the case of neutral currents.

2.5 Approximate flavour symmetries: chiral symmetry

The up, down and strange quark masses in the $\overline{\text{MS}}$ scheme at a renormalization scale $\mu = 2$ GeV are $m_u = 2.2^{+0.6}_{-0.4}$ MeV, $m_d = 4.7^{+0.5}_{-0.4}$ MeV and $m_s = 96^{+8}_{-4}$ MeV [6]. These masses are small compared with the scale $\Lambda_{\text{QCD}} \sim 0.3$ GeV of non perturbative strong interaction physics. It is then convenient to set $m_q = m_d = m_u = m_s = 0$ and do perturbation theory about this limit [52]. In this chiral limit the light quark Lagrangian

$$\mathcal{L}_{\text{quarks}} = \bar{\Psi}_q(i\gamma^\mu D_\mu)\Psi_q = \bar{\Psi}_q^L(i\gamma^\mu D_\mu)\Psi_q^L + \bar{\Psi}_q^R(i\gamma^\mu D_\mu)\Psi_q^R \tag{2.39}$$

has an $SU(3)_L \times SU(3)_R$ symmetry under which right and left handed quarks transform as

$$\Psi_q^L \to L\Psi_q^L \quad L \in SU(3)_L, \tag{2.40}$$

$$\Psi_q^R \to R\Psi_q^R \quad R \in SU(3)_R, \tag{2.41}$$

and a baryon number $U(1)$ symmetry under which right and left handed quarks transform by a common phase. There is also an axial U(1) transformation which leaves (2.39) invariant but which changes the measure in the path integral — c.f Eq. (3.11)— and hence it is not a symmetry of QCD [53]. The eight generators of the chiral $SU(3)_L \times SU(3)_R$ symmetry are spontaneously broken to $SU(3)_V$ by the vacuum expectation value of quark bilinears giving rise to eight Goldstone bosons, namely, $\pi^\pm$, π^0, $K^\pm$, K^0, $\bar{K}^0$ and η which can be described by the $SU(3)$ matrix

$$\Sigma = \exp\left(\frac{2i\Pi}{f}\right) \tag{2.42}$$

where f is a constant with dimensions of mass and

$$\Pi = \begin{bmatrix} \pi^0/\sqrt{2} + \eta/\sqrt{6} & \pi^+ & K^+ \\ \pi^- & \pi^0/\sqrt{2} + \eta/\sqrt{6} & K^0 \\ K^- & \bar{K}^0 & -2\eta/\sqrt{6} \end{bmatrix}. \tag{2.43}$$

Restoring the Lagrangian masses of the u, d and s quarks turns pions, kaons and the eta meson into pseudo-Goldstone bosons. It's possible to write an effective field theory for these Goldstone bosons, which respects the same chiral symmetry as QCD: this is chiral perturbation theory (ChiPT) expressed in terms of the field Σ, expressed as an exponential of the pion matrix. Σ transforms in a simple way under $SU(3)_L \times SU(3)_R$, which leads to nonlinear transformations of the Goldstone fields. The non-zero (Lagrangian) masses of the quarks can be introduced in ChiPT. This gives an effective theory which can be used to give expressions for chiral extrapolations and which suggests forms to use for chiral-continuum extrapolations, — c.f Section 6.3.3 —.

2.6 Effective Hamiltonians for Weak Decays

For energy scales that are much lower than the W boson mass, the full theory of weak decays can be replaced by an effective one in which the W and Z bosons, together with the top quark are integrated out, that is, we remove the degrees of freedom which in particular, don't appear as initial or final physical states at the scale under consideration. At lowest order the Hamiltonian that describes this effective theory can be written as

$$\mathcal{H}_{\text{eff}} = \frac{G_F}{\sqrt{2}} \sum_n V_n C_n(\mu) O_n \tag{2.44}$$

where G_F is Fermi's constant, V^n are Cabibbo-Kobayashi-Maskawa factors, O_n are local operators which govern the process in question, and $C_n(\mu)$ summarize the contributions from scales higher than μ. The Wilson coefficients $C_n(\mu)$ [54, 55] are independent of the particular decay considered and have been calculated in perturbation theory [56–58].

2.7 Continuum Phenomenology

Decays of bottom quarks into up or charm quarks are mediated by a charged W boson and occur at tree-level in the Standard Model (SM). By means of experimental measurements of the branching fraction of $B_s \to K\ell\nu$ and $B_s \to D_s\ell\nu$ decays and a theoretical calculation of the form factors f_0 and f_+ (2.68) the CKM matrix elements $|V_{ub}|$ and $|V_{cb}|$ can be extracted. The precise determination of $|V_{ub}|$ and $|V_{cb}|$ are central to testing the CKM sector of the Standard Model, test for unitarity of the CKM matrix and complement the measurements of CP asymmetries in B decays [6]. Decays of bottom quarks to down or strange quarks may occur in the SM only at loop level and the corresponding flavour changing neutral currents (FCNC) are further suppressed due to the Glashow-Iliopoulos-Maiani (GIM) mechanism [21]. As such, the decay $B_s \to \phi\ell^+\ell^-$ in which a bottom quark decays into a strange quark provides an ideal testing ground in the search for non-standard contributions to physical observables. Anomalies have been

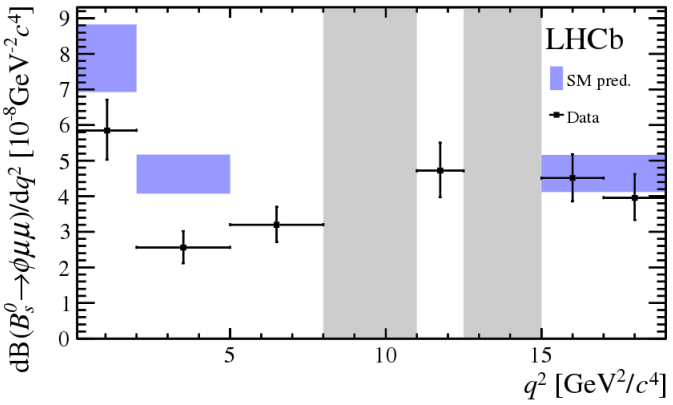

Figure 2.1: Differential branching fraction of the decay $B_s^0 \to \phi\nu^+\nu^-$, overlaid with SM predictions [1, 2] indicated by blue boxes. The vetoes excluding the charmonium resonances are indicated by grey areas. Taken from [3]

reported between SM predictions and experimental results, such as angular observables [59, 60], branching fractions [3, 61, 62], and the ratio R_K [63], but are also observed in charged tree-level $b \to c$ transitions see e.g. [64–67]. The main difficulty to conclusively establish that these anomalies are due to NP effects lies in our inability to exclude large hadronic effects as their actual cause [68–73]. In this section we will discuss some of the phenomenological applications that can be made of the form factors extracted from semileptonic B decays which can be used in the search for NP contributions and to exclude NP scenarios.

2.7.1 The $|V_{ub}|$ and $|V_{cb}|$ CKM matrix elements

These matrix elements can be obtained from the differential decay rate [8]

$$\frac{d\Gamma(B_s \to P\ell\nu)}{dq^2} = \frac{G_F^2|V_{qb}|^2}{24\pi^3 M_{B_{(s)}}^2}\left(1-\frac{m_\ell^2}{2q^2}\right)|\mathbf{k}|\left[\left(1+\frac{m_\ell^2}{2q^2}\right)M_{B_{(s)}}^2\mathbf{k}^2|f_+(q^2)|^2 + \frac{3m_\ell^2}{8q^2}(M_{B_{(s)}}^2 - M_P^2)^2|f_0(q^2)|^2\right], \tag{2.45}$$

where P is the pseudoscalar meson to which the B_s meson decays, namely, a Kaon or D_s meson, V_{qb} indicates the corresponding CKM matrix element, the emitted lepton is denoted by ℓ, $\mathbf{k}$ is the three momentum of the final state meson, $q = p - k$ where p is the momentum of the B_s meson, and f_+ and f_0 are the vector and scalar form factors —c.f. Section 2.8—.

2.7.2 Forward-backward asymmetry

If we neglect final state electromagnetic interactions the angular dependence of the differential decay rate for B_s decays to pseudoscalar final states $P = \{K, D_s\}$ is given

by [8]

$$\frac{d^2\Gamma(B_s \to P\ell\nu)}{dq^2 d\cos\theta_l} = \frac{G_F^2|V_{qb}|^2}{128\pi^3 M_{B_s}^2}\left(1-\frac{m_\ell^2}{q^2}\right)^2 |\mathbf{k}|\left[4M_{B_s}^2|\mathbf{k}|^2\left(\sin^2\theta_l + \frac{m_\ell^2}{q^2}\cos^2\theta_\ell\right) f_+^2(q^2)\right.$$
$$+\frac{m_\ell^2}{q^2}(M_{B_s}^2 - M_P^2)M_{B_s}|\mathbf{k}|\cos\theta_\ell f_0(q^2) f_+(q^2)$$
$$\left.+\frac{m_\ell}{q^2}(M_{B_s}^2 - M_P^2)^2 f_0^2(q^2)\right] \tag{2.46}$$

where m_ℓ is the lepton mass and θ_ℓ is the angle between the charged-lepton and the B_s meson momenta in the q^2 rest frame, that is, in the frame where the sum of the three momenta of the lepton and the neutrino is zero. From this angular dependency we can extract the forward-backward asymmetry

$$\mathcal{A}_{FB}^{B_s\to P\ell\nu}(q^2) \equiv \left[\int_0^1 - \int_{-1}^0\right] d\cos\theta_\ell \frac{d^2\Gamma(B_s \to P\ell\nu)}{dq^2 d\cos\theta_\ell} \tag{2.47}$$

which in the Standard Model (SM) is given by [74]

$$\mathcal{A}_{FB}^{B_s\to P\ell\nu}(q^2) = \frac{G_F^2|V_{qb}|^2}{32\pi^3 M_{B_s}}\left(1-\frac{m_\ell^2}{q^2}\right)^2 |\mathbf{k}|^2 \frac{m_\ell^2}{q^2}(M_{B_s}^2 - M_P^2) f_+(q^2) f_0(q^2)\,.$$

Deviation from SM predictions of the value of $\mathcal{A}_{FB}$ are a clear sign of NP contributions [75–77] and could be used to constrain NP models [78–81].

2.7.3 The ratios $R(K)$ and $R(D_s)$

As discussed in the introduction to this section it is necessary to rule out hadronic effects as the cause of the apparent discrepancies between theoretical predictions and experimental measurements. This makes observables which are practically free of hadronic uncertainties of particular interest. One such observable is the lepton flavour universality ratio, that is, the ratio of branching ratios involving different flavours such as [74, 82–84]

$$\mathcal{R}_P^{\tau/\mu}(q^2) \equiv \frac{d\Gamma(B_{(s)} \to P\tau\nu)/dq^2}{d\Gamma(B_{(s)} \to P\mu\nu)/dq^2} \tag{2.48}$$

$$\mathcal{R}_P^{\mu/e}(q^2) \equiv \frac{d\Gamma(B_{(s)} \to P\mu\mu)/dq^2}{d\Gamma(B_{(s)} \to Pee)/dq^2} \tag{2.49}$$

where (2.48) and (2.49) are the ratios for tree level and rare decays, respectively, and P is a Kaon or D_s meson. These ratios provide precise tests of the Standard Model predictions which are independent of the CKM matrix elements involved. Moreover, tree-level decays to τ leptons may be particularly sensitive to additional amplitudes, such as those involving an intermediate charged Higgs boson [85, 86]. The currently

experimentally measured ratios are [63, 87, 88]:

$$R_K^{[1,6]} = 0.745^{+0.090}_{-0.074} \pm 0.036 \tag{2.50}$$

$$R_K^{*[0.045,1.1]} = 0.660^{+0.110}_{-0.070} \pm 0.024 \tag{2.51}$$

$$R_K^{*[1,1.6]} = 0.685^{+0.113}_{-0.069} \pm 0.047 \tag{2.52}$$

$$R_D^{[3.5,8]} = 0.375 \pm 0.064 \pm 0.026 \tag{2.53}$$

$$R_D^{*[3.5,8]} = 0.293 \pm 0.038 \pm 0.015 \tag{2.54}$$

where the values inside the square brackets indicate the integrated q^2 region where the measurement was done, and the errors are due to statistics and systematics, respectively.

2.7.4 Differential decay rates and angular observables for $B_s \to \phi\ell^+\ell^-$

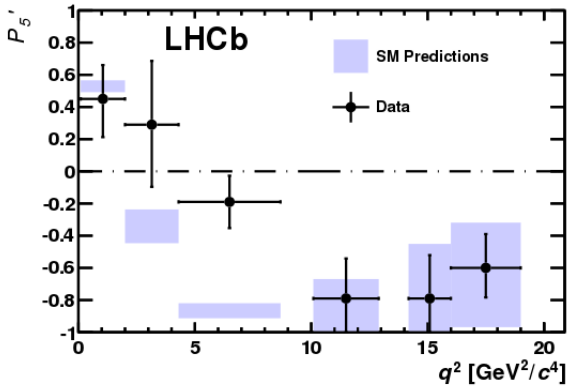

Figure 2.2: Measured values of P_5' (black points) compared with SM predictions from [4] (blue bands). Taken from [5]

The general form of the decay distribution of $B_s \to \phi\ell^+\ell^-$ is given by [58]

$$\begin{aligned}\frac{d^4\Gamma}{dq^2 d\cos\theta_\ell d\cos\theta_\phi d\phi} = \frac{9}{32\pi}\big[&I_1^s \sin^2\theta_\phi + I_1^c \cos^2\theta_\phi + (I_2^s \sin^2\theta_\phi + I_2^c \cos^2\theta_\phi)\cos(2\theta_\ell) \\ &+ I_3 \sin^2\theta_\phi \sin^2\theta_\ell \cos(2\phi) + I_4 \sin(2\theta_\phi)\sin(2\theta_\ell)\cos\phi \\ &+ I_5 \sin(2\theta_\phi)\sin\theta_\ell \cos\phi + (I_6^s \sin^2\theta_\phi + I_6^c \cos^2\theta_\phi)\cos(\theta_\ell) \\ &+ I_7 \sin(2\theta_\phi)\sin\theta_\ell \sin\phi + I_8 \sin(2\theta_\phi)\sin(2\theta_\ell)\sin\phi \\ &+ I_9 \sin^2\theta_\phi \sin^2\theta_\ell \sin(2\phi)\end{aligned} \tag{2.55}$$

where the angular coefficients I_i are functions of the seven form factors for vector final states (2.71) to (2.74) which have been analytically determined in Section 3.3 of reference [58], and the angles ϕ, θ_ϕ and θ_ℓ are defined in Appendix A of reference [58]. Integrating (2.55) over the angles we obtain the differential decay rate

$$\frac{d\Gamma}{dq^2} = \frac{3}{4}(2I_1^s + I_1^c) - \frac{1}{4}(2I_2^s + I_2^c). \tag{2.56}$$

The angular coefficients I_i are also used to obtain the twelve CP averaged angular coefficients

$$S_i^{(a)} = \left(I_i^{(a)} + \bar{I}_i^{(a)}\right) \Big/ \frac{d(\Gamma + \bar{\Gamma})}{dq^2} \tag{2.57}$$

and the twelve CP asymmetries

$$A_i^{(a)} = \left(I_i^{(a)} - \bar{I}_i^{(a)}\right) \Big/ \frac{d(\Gamma + \bar{\Gamma})}{dq^2} \tag{2.58}$$

which can be used to express previously studied observables such as the forward-backward asymmetry, $\mathcal{A}_{FB}$, with reduced experimental and theoretical uncertainties —due to the normalization factor $d(\Gamma + \bar{\Gamma})/dq^2$—. Moreover, the CP averaged angular coefficients (2.57) offer cleaner observables in which CP violating effects are washed out, whilst the CP asymmetries (2.58) offer a window into non-standard CP violation [58]. In figure 2.1 we present the LHCb result [3] for the differential branching fraction of the decay $B_s^0 \to \phi\nu^+\nu^-$ where a $\sim 2\sigma$ discrepancy can be seen between experiment and theory. Similarly in figure 2.2 we present the LHCb result [5] of the measurement of the angular observable

$$\langle P_5' \rangle = \frac{\langle S_5 \rangle}{2\sqrt{-\langle S_2^c \rangle \langle S_2^s \rangle}} \tag{2.59}$$

for the decay $B^0 \to K^{*0}\mu^+\mu^-$ where a similar discrepancy has been observed. It has been suggested [89] that these discrepancies can be explained by a negative NP contribution to the Wilson coefficient C_9 which can arise in models with flavour-changing neutral gauge bosons [89–91].

2.8 Form factors

The matrix elements for decays of B_s mesons to pseudoscalar, $P \in \{K, D_s\}$, or vector ϕ mesons are:

$$\langle P(k)|\mathcal{H}^{b\to q}|B_s(p)\rangle = \frac{G_F}{\sqrt{2}} V_{qb} \langle P(k)|\bar{q}\gamma_\mu b|B_s\rangle (\nu\gamma_\mu \ell), \tag{2.60}$$

$$\begin{aligned}\langle \phi(k,\varepsilon)|\mathcal{H}_{\text{eff}}^{b\to s}|B_s(p)\rangle = \frac{G_F}{\sqrt{2}} V_{tb}V_{ts}^* \Big\{ \Big[& C_9^{\text{eff}} \langle \phi(k,\varepsilon)|\bar{s}\gamma^\mu(1-\gamma_5)b|B_s\rangle \\ & - \frac{2m_b}{q^2} C_7^{\text{eff}} \langle \phi(k,\varepsilon)|\bar{s} i\sigma^{\mu\nu} q_\nu (1-\gamma_5) b|B_s\rangle \Big] (\bar{\ell}\gamma_\mu \ell) \\ & + C_{10}^{\text{eff}} \langle \phi|\bar{s}\gamma^\mu b|B_s\rangle (\bar{\ell}\gamma_\mu\gamma_5 \ell) \Big\}\end{aligned} \tag{2.61}$$

where $q = \{u, c\}$, ε is the polarization vector of the vector meson, the 4-momenta of the B_s and final state meson are given by p and k, respectively, and the Wilson coefficients are to next-to-next-leading logarithmic (NNLL) accuracy, which requires the calculation on the matching conditions at $\mu = m_W$ to two-loop accuracy, $C_7^{\text{eff}} = -0.304$, $C_9^{\text{eff}} = 4.211$ and $C_{10}^{\text{eff}} = -4.103$ [58]. The matrix elements in equations (2.60) and (2.61) can be

written as a linear combination of Lorentz vectors and functions of the Lorentz scalar $q^2 = (p-k)^2$ known as form factors. In the following we will show the steps followed to parametrize the matrix elements in terms of form factors. We start by noticing that the matrix elements for decays to pseudoscalar final states (2.60) contain two Lorentz vectors, namely p and k, these can be combined to obtain the basis vectors $p_+ \equiv p + k$ and $q \equiv p - k$. Matrix elements for decays to vector mesons (2.61) involve an additional basis vector —i.e. the polarization vector—. It is possible then to parametrize (2.61) using combinations of the basis vectors $p_+, q, (\epsilon^*)$, the totally antisymmetric tensor $\epsilon^{\mu\nu\rho\sigma}$ and form factors. The parametrized matrix elements have the form

$$\langle P(k)|\bar{q}\gamma^\mu \bar{b}|B_s(p)\rangle = p_+^\mu f_+(q^2) + q^\mu f_-(q^2), \tag{2.62}$$

$$\langle \phi(k,\varepsilon)|\bar{s}\gamma^\mu b|B_s(p)\rangle = ig(q^2)\epsilon^{\mu\nu\rho\sigma}\epsilon^{*\nu}p_+^\rho q^\sigma, \tag{2.63}$$

$$\langle \phi(k,\varepsilon)|\bar{s}\gamma^\mu\gamma_5 b|B_s(p)\rangle = h(q^2)\epsilon^{*\mu} + a_+(q^2)(\epsilon^*\cdot p)p_+^\mu + a_-(q^2)(\epsilon^*\cdot p)q^\mu, \tag{2.64}$$

$$\begin{aligned}\langle \phi(k,\varepsilon)|\bar{s}\sigma^{\mu\nu}\bar{b}|B_s(p)\rangle &= f_{T+}(q^2)\epsilon^{\mu\nu\rho\sigma}\varepsilon^{*\rho}p_+^\sigma + f_{T-}(q^2)\epsilon^{\mu\nu\rho\sigma}\varepsilon^{*\rho}q^\sigma \\ &\quad + g_T(q^2)(\varepsilon^*\cdot p)\epsilon^{\mu\nu\rho\sigma}q^\rho p_+^\sigma,\end{aligned} \tag{2.65}$$

$$\begin{aligned}\langle \phi(k,\varepsilon)|\bar{s}\sigma^{\mu\nu}\gamma_5\bar{b}|B_s(p)\rangle &= if_{T+}(q^2)\left[\varepsilon^{*\nu}p_+^\mu - \varepsilon_\mu^* p_+^\nu\right] - if_{T-}(q^2)\left[\varepsilon^{*\nu}q^\mu - \varepsilon^{*\nu}q^\mu\right] \\ &\quad + ig_T(q^2)(\varepsilon^*\cdot p)\left[p^\mu q^\nu - p^\nu q^\mu\right]q^\rho p_+^\sigma.\end{aligned} \tag{2.66}$$

where f_+, f_-, g, h, a_+, f_{T+}, f_{T-} and g_T are the aforementioned form factors. Having obtained the basic parametrization of the matrix elements for decays of a B_s meson to a pseudoscalar or vector mesons, we will now show how these form factors are related to the basis that is most commonly used in recent phenomenological analysis, namely, f_0, f_+, f_V, f_{A_0}, f_{A_1}, f_{A_2}, f_{T_1}, f_{T_2} and f_{T_3}. We start by introducing the form factor f_0, associated with scalar exchange and given by:

$$f_0(q^2) = f_+(q^2) + \frac{q^2}{M_{B_s}^2 - M_P^2}f_-(q^2) \tag{2.67}$$

to rewrite equation (2.62) as

$$\langle P(k)|\bar{q}\gamma^\mu\bar{b}|B_s(p)\rangle = f_+(q^2)\left(p^\mu + k^\mu - \frac{M_{B_s}^2 - M_P^2}{q^2}q^\mu\right) + f_0(q^2)\frac{M_{B_s}^2 - M_P^2}{q^2}. \tag{2.68}$$

Next we contract the matrix elements of equations (2.65) and (2.66) with the momentum transfer vector q

$$q^\mu\langle \phi(k,\varepsilon)|s\sigma^{\mu\nu}\bar{b}|B_s(p)\rangle = 2f_{T+}(q^2)\epsilon^{\mu\nu\rho\sigma}\varepsilon^{*\rho}p^\mu k^\sigma \tag{2.69}$$

$$\begin{aligned}q^\mu\langle \phi(k,\varepsilon)|s\sigma^{\mu\nu}\gamma_5\bar{b}|B_s(p)\rangle &= if_{T+}(q^2)\left[\varepsilon^{*\nu}(M_{B_s}^2 - M_\phi^2) - (\varepsilon^*\cdot q)(p+k)^\nu\right] \\ &\quad - if_{T-}(q^2)\left[\varepsilon^{*\nu}q^2 - (\varepsilon^*\cdot q)q^\nu\right] \\ &\quad + g_T(q^2)(\varepsilon^*\cdot p)\left[q^2(p+k)^\nu - (M_{B_s}^2 - M_\phi^2)q^\nu\right]\end{aligned} \tag{2.70}$$

and then we use equations (2.64), (2.69), (2.70) and follow Refs. [58, 92, 93] to obtain the final expressions for the matrix elements for $B_s \to \phi$ decays

$$\langle \phi(k,\varepsilon)|\bar{s}\gamma^i b|B_s(p)\rangle = i f_V(q^2)\frac{2m_{B_s}\epsilon^{0ijk}\epsilon_j^*(k,\varepsilon)k_k}{m_{B_s}+m_\phi}, \tag{2.71}$$

$$\begin{aligned}\langle \phi(k,\varepsilon)|\bar{s}\gamma^\mu\gamma^5 b|B_s(p)\rangle &= f_{A_0}(q^2)2m_\phi q^\mu\frac{\epsilon^*(k,\varepsilon)\cdot q}{q^2}\\ &+ f_{A_1}(q^2)(m_{B_s}+m_\phi)\left[\epsilon^{\mu *}(k,\varepsilon)-\frac{\epsilon^*(k,\varepsilon)\cdot q}{q^2}q^\mu\right]\\ &- f_{A_2}(q^2)\frac{\epsilon^*(k,\varepsilon)\cdot q}{m_{B_s}+m_\phi}\left[k^\mu+p^\mu-\frac{m_{B_s}^2-m_\phi^2}{q^2}q^\mu\right],\end{aligned} \tag{2.72}$$

$$q^\nu\langle \phi(k,\varepsilon)|\bar{s}\sigma^{\nu\mu} b|B_s(p)\rangle = 2f_{T_1}(q^2)\epsilon^{\mu\rho\tau\sigma}\epsilon_\rho^*(k,\varepsilon)k_\tau p_\sigma, \tag{2.73}$$

$$\begin{aligned}q^\nu\langle \phi(k,\varepsilon)|\bar{s}\sigma^{\nu\mu}\gamma^5 b|B_s(p)\rangle &= i f_{T_2}(q^2)\left[\epsilon^{\mu *}(k,\varepsilon)(m_{B_s}^2-m_\phi^2)\right.\\ &\left.- (\epsilon^*(k,\varepsilon)\cdot q)(p+k)^\mu\right]\\ &+ i f_{T_3}(q^2)(\epsilon^*(k,\varepsilon)\cdot q)\left[q^\mu-\frac{q^2}{m_{B_s}^2-m_\phi^2}(p+k)^\mu\right]\end{aligned} \tag{2.74}$$

where the relation between the form factors of interest f_V, f_{A_0}, f_{A_1}, f_{A_2}, f_{T_1}, f_{T_2} and f_{T_3} to the original form factors $g, h, a_+, a_-, f_{T+}, f_{T-}$ and g_T is given by

$$f_V(q^2) = (M_{B_s}+M_\phi)g(q^2), \tag{2.75}$$

$$f_{A_0}(q^2) = \frac{1}{2M_\phi}\left[h(q^2)+(M_{B_s}^2-M_\phi^2)a_+(q^2)+q^2 a_-(q^2)\right], \tag{2.76}$$

$$f_{A_1}(q^2) = \frac{h(q^2)}{M_{B_s}+M_\phi}, \tag{2.77}$$

$$f_{A_2}(q^2) = -(M_{B_s}+M_\phi)a_+(q^2), \tag{2.78}$$

$$f_{T_1}(q^2) = -\frac{1}{2}f_{T+}(q^2), \tag{2.79}$$

$$f_{T_2}(q^2) = -\frac{1}{2}\left[f_{T+}(q^2)+\frac{q^2}{M_{B_s}^2-M_\phi^2}f_{T-}(q^2)\right], \tag{2.80}$$

$$f_{T_3}(q^2) = \frac{1}{2}\left[f_{T-}(q^2)+(M_{B_s}^2-M_\phi^2)g_T(q^2)\right]. \tag{2.81}$$

2.9 Conclusion

In this chapter we have given a brief introduction to the Standard Model of particle physics, effective Hamiltonians for weak decays and form factors, these are the basic building blocks of the rest of this dissertation. We also discussed the continuum phenomenology which justifies the study of form factors for the decays $B_s \to K\ell\nu$, $B_s \to D_s\ell\nu$ and $B_s \to \phi\ell\ell$ which will be the final outcome of this dissertation.

Chapter 3

Quantum Chromodynamics

3.1 Introduction

Quantum Chromodynamics (QCD) is the theory of the strong nuclear force, it is formulated in terms of quarks and gluons which are believed to be the basic constituents of hadronic matter. The behaviour of the QCD coupling $g_s(\mu)$ which sets the strength of the interactions involving quarks and gluons is such that although at large momentum transfer perturbation theory is reliable, at hadronic scales $\mu \lesssim 1$ GeV the coupling constant is $\mathcal{O}(1)$ and perturbative methods fail. In this low energy regime lattice QCD offers the only first principles method for computing QCD observables. In this chapter we provide an overview of the formulation and basic features of lattice QCD. We begin by introducing the QCD action in the continuum in section 3.2. This is followed by an outline of the steps necessary for its discretization in sections 3.4 to 3.7. Finally in sections 3.8 to 3.12 the general methods used in lattice computations are discussed.

This chapter is based mainly on references [94–97], additional references will be given where appropriate.

3.2 The QCD action in the continuum

The continuum action of QCD in Euclidean space time can be written as[1,2]

$$S_E = \sum_{f=1}^{N_f} \int d^4x \bar{\psi}^{(f)}(x) \left(\gamma_\mu (\partial_\mu + i g_s G_\mu(x)) + M^{(f)} \right) \psi^{(f)}(x) + \frac{1}{2g_s^2} \int d^4x G_{\mu\nu}(x) G_{\mu\nu}(x) \tag{3.1}$$

[1] where I have used matrix/vector notation for the color and Dirac indices.

[2] I use M for the mass to avoid confusion once m is introduced to label lattice sites.

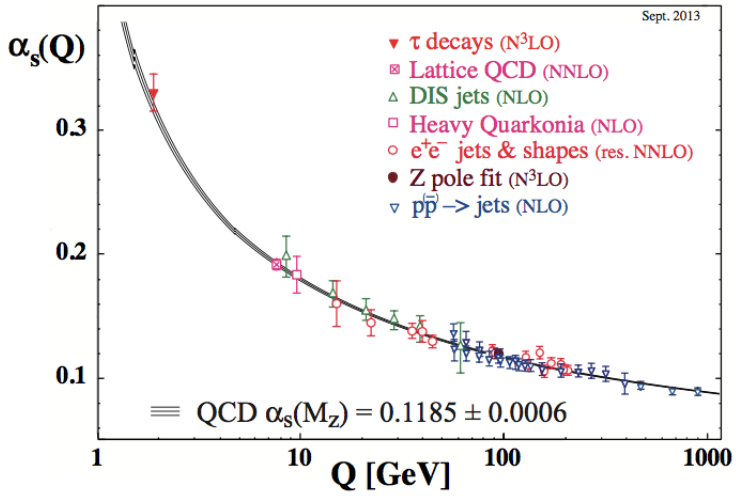

Figure 3.1: Running behaviour of the strong coupling as a function of energy scale. Taken from [6].

where the number of quark fields ψ with flavour f is denoted by N_f and the coupling strength, the gluon field and the field strength tensor are labelled by g_s, G_μ and $G_{\mu\nu}$, respectively, and we have written all indices down as we are using the Euclidean metric. The first term on the right hand side of Eq. (3.1) is known as the fermionic part of the action, denoted S_F, it deals with quark fields and quark-gluon interactions. The term that includes the field strength tensor in Eq. (3.1) is known as the gluonic part of the action, it is denoted S_G and deals exclusively with gluons, their propagation and interaction.

3.2.1 Gauge invariance

The physical content of QCD is invariant under local gauge transformations, that is, given $\Omega(x) \in SU(3)$ the quark and gluon fields must transform as

$$\psi(x) \to \psi'(x) = \Omega(x)\psi(x), \qquad \bar{\psi}(x) \to \bar{\psi}'(x) = \bar{\psi}(x)\Omega(x)^\dagger \tag{3.2}$$

$$G_\mu(x) \to G'_\mu(x) = \Omega(x)G_\mu(x)\Omega(x)^\dagger + i(\partial_\mu\Omega(x))\Omega(x)^\dagger \tag{3.3}$$

so that $S_E[\psi', \bar{\psi}', G'] = S_E[\psi, \bar{\psi}, G]$.

3.3 Asymptotic freedom and quark confinement

Nonabelian gauge theories in 4D display asymptotic freedom, where the coupling constant decreases as the energy scale at which it's measured or defined increases. In dimensional regularisation we introduce a mass scale μ, and we find that the coupling

depends on μ such that $g_s(\mu)$ decreases as μ increases — c.f Figure 3.1 —. In other regularisation schemes some other mass parameter would enter but asymptotic freedom would still be present. This means that different tools must be employed for the study of QCD at different energy scales. Asymptotic freedom [98, 99] at short distances means that because the coupling constant tends to zero perturbation theory can successfully be applied to study QCD at high energies. Conversely, at long distance the coupling constant increases, quarks become confined [100] and a non-perturbative approach such as Lattice QCD must be applied to study the interactions between quarks and gluons. In this work we are interested in the study of hadronic matrix elements and hence will use Lattice QCD as our tool of choice.

3.4 Discretization of QCD

We now introduce a 4D lattice Λ with L points in each spatial direction and N_T points in the temporal direction,

$$\Lambda = \{n = (n_1, n_2, n_3, n_4) \;\mid\; n_1, n_2, n_3 = 0, 1, \cdots, L-1; n_4 = 0, 1, \cdots, N_T - 1\}. \quad (3.4)$$

These points are separated by a lattice constant a and are populated by spinors $\psi(n)$ that carry the same color, Dirac, and flavour indices as in the continuum. With this setup the continuum action of Eq. (3.1) is discretized by replacing the path integral over fields by ordinary integrals over the field values at the points in Λ — c.f section 3.5 — and derivatives by finite differences of the form

$$\partial_\mu \psi(x) \to \frac{1}{2a}(U_\mu(n)\psi(n+\hat{\mu}) + U_{-\mu}(n)\psi(n-\hat{\mu})), \quad (3.5)$$

where μ are directional indices and the gauge field $U_\mu(n)$ —which is located on the link that connects the sites n and $n+\hat{\mu}$— has been introduced to preserve $SU(3)$ gauge invariance and $U_{-\mu}(n) = U_\mu(n-\hat{\mu})^\dagger$. It transforms under the local rotation of the color indices of the gauge fields given by an element $\Omega(n)$ of $SU(3)$ as

$$U_\mu(n) \to U_\mu^{'}(n) = \Omega(n) U_\mu(n) \Omega(n+\hat{\mu})^\dagger. \quad (3.6)$$

If we now introduce the algebra valued lattice gauge field $A_\mu(n)$ and the link variable is written as

$$U_\mu(n) = \exp\left(iaA_\mu\right) \quad (3.7)$$

then we can interpret the link variable $U_\mu(n)$ as a lattice version of the continuum gauge transporter

$$G(x,y) \propto \exp\left(i \int_{C_{xy}} A \cdot ds\right) \quad (3.8)$$

connecting the points n and $n+\mu$. Equation (3.8) is a path-ordered exponential where C_{xy} is a curve connecting the points x and y.

3.5 The Lattice path integral

Lattice QCD calculations are a non perturbative implementation of field theory using the Feynman path integral approach. By discretising and using a finite volume, the path integral is turned into an ordinary multiple integral, though with an extremely high dimension, and hence best evaluated by a stochastic Monte Carlo sampling technique.

The expectation value of an operator $\mathcal{O}$ in terms of the Lattice path integral is given by

$$\langle \mathcal{O}[\psi,\bar{\psi},U]\rangle = \frac{1}{Z}\int [d\psi][d\bar{\psi}][dU]\mathcal{O}[\psi,\bar{\psi},U]e^{-S_{\mathrm{QCD}}} \tag{3.9}$$

$$Z = \int [d\psi][d\bar{\psi}][dU]e^{-S_{\mathrm{QCD}}} \tag{3.10}$$

where

$$[d\psi][d\bar{\psi}][dU] = \prod_{n\in\Lambda}\prod_{i=1}^{N_f}\prod_{\mu=1}^{4} d\psi(n)_i d\bar{\psi}(n)_i dU(n)_\mu \tag{3.11}$$

with N_f the number of fermion fields. Given that the fermionic part of the QCD action (3.15) is quadratic in the fermionic fields these can be integrated out using the Matthews-Salam formula [101, 102] with the result

$$\langle \mathcal{O}[\psi,\bar{\psi},U]\rangle = \frac{\int [dU]\det D[U]\mathcal{O}[U]e^{-S_G[U]}}{\int [dU]\det D[U]e^{-S_G}}. \tag{3.12}$$

3.6 The Wilson gauge action S_G

The Wilson gauge action is given by

$$S_G[U] = \frac{2}{g^2}\sum_{n\in\Lambda}\sum_{\mu<\nu}\mathrm{Re}\,\mathrm{Tr}[1-U_{\mu\nu}(n)] \tag{3.13}$$

where the factor of $2/g^2$ with g the bare quark-gluon coupling has been introduced to get the correct continuum limit and

$$U_{\mu\nu}(n) = U_\mu(n)U_\nu(n+\hat{\mu})U_{-\mu}(n+\hat{\mu}+\hat{\nu})U_{-\nu}(n+\hat{\nu}) \tag{3.14}$$

is the plaquette. Other choices of gauge actions, involving more complex Wilson loops than the plaquette can be, and are, used (e.g. Iwasaki [43], DBW2 [103, 104], Luscher-Weisz [105]) they allow to improve the action by reducing discretisation effects.

3.7 Fermionic actions S_F

3.7.1 The naive fermionic action

In the absence of interactions the lattice formulation of the fermionic QCD action for a single flavour can be written as

$$S_F[\psi, \bar{\psi}, U] = a^4 \sum_{n,m\in\Lambda} \bar{\psi}(n) D(n|m) \psi(m), \tag{3.15}$$

where the Dirac operator is given by

$$D(n|m) = \sum_{\mu=1}^{4} \gamma_\mu \frac{U_\mu(n)\psi(n+\mu) - U_{-\mu}(n)\psi(n-\mu)}{2a} + M. \tag{3.16}$$

The quark propagator is given by the inverse of Eq. (3.16) and reads

$$D^{-1}(n|m) = \frac{1}{|\Lambda|} \sum_{p\in\tilde{\Lambda}} \tilde{D}(p)^{-1} \exp\left(ip(n-m)a\right), \tag{3.17}$$

where $|\Lambda| = L^3 \times N_T$ is the total number of lattice points, $\tilde{\Lambda}$ is the set of discrete lattice momenta

$$\tilde{\Lambda} = \left\{ p; ap_\mu = \frac{2\pi k}{L}; k \in \mathbb{Z}; -\frac{L}{2} \leq k < \frac{L}{2} \right\}, \tag{3.18}$$

and the momentum space propagator is given by

$$\tilde{D}^{-1}(p) = \frac{M - ia^{-1} \sum_\mu \gamma_\mu \sin(p_\mu a)}{M^2 + a^{-2} \sum_\mu \sin(p_\mu a)^2}. \tag{3.19}$$

3.7.2 The doubler problem

Equation (3.19) has one physical pole at $p = (0,0,0,0)$ and 15 unphysical ones for $p \in \mathcal{P}$ when set $M = 0$, where

$$\mathcal{P} = \{(\pi/a, 0, 0, 0), (0, \pi/a, 0, 0), \cdots, (\pi/a, \pi/a, \pi/a, \pi/a)\}. \tag{3.20}$$

These unphysical poles are called doublers and can be removed by inserting an extra term in the momentum space Dirac operator

$$\tilde{D}(p) = M + \frac{1}{a} \sum_{\mu=1}^{4} \gamma_\mu \sin(p_\mu a) + \underbrace{\frac{1}{a} \sum_{\mu=1}^{4} (1 - \cos(p_\mu a))}_{\text{Wilson term}} = \begin{cases} M, & p = 0 \\ M + 2l/a, & p \in \mathcal{P}. \end{cases} \tag{3.21}$$

where l labels the number of momentum components with $p_\mu = \pi/a$. The introduction of the Wilson term changes the dispersion relation so that there is only one lowest energy solution, all other solutions become heavy in the continuum limit and hence decouple from the theory. Unfortunately, even in the massless limit the Wilson term does not anticommute with γ_5 and hence the Wilson fermionic action [3] which in position space reads

$$\begin{aligned} S_{\text{Wilson}}[\psi,\bar{\psi},U,M] = a^4 \sum_{n,m\in\Lambda} \overline{\psi}^{(f)}(n) \Bigg[\left(M^{(f)} + \frac{4}{a} \right) \delta_{\alpha\beta}\delta_{ab}\delta_{n,m} \\ - \frac{1}{2a} \sum_{\mu=\pm1}^{\pm4} (1-\gamma_\mu)_{\alpha\beta} U_\mu(n)_{ab} \delta_{n+\hat{\mu},m} \Bigg] \psi^{(f)}(m) \end{aligned} \tag{3.22}$$

explicitly breaks chiral symmetry.

3.7.3 The Sheikholeslami-Wohlert (Clover) action

The "Sheikholeslami-Wohlert" or "clover" action [106]

$$S[\psi,\bar{\psi},U,M,c_{sw}] = S_{\text{Wilson}}[\psi,\bar{\psi},U,M] + c_{sw}a^5 \sum_{n\in\Lambda} \overline{\psi}(n) \sum_{\mu<\nu} \frac{i}{4} \sigma_{\mu\nu} \hat{F}_{\mu\nu} \psi(n) \tag{3.23}$$

is an improved Wilson fermionic action Eq. (3.22) in which discretization errors have been reduced from $\mathcal{O}(a)$ to $\mathcal{O}(a^2)$ by introducing the dimension-5 operator

$$S^{SW}[\psi,\bar{\psi},U] = \bar{\psi}\sigma_{\mu\nu}\hat{F}_{\mu\nu}\psi. \tag{3.24}$$

In Equations (3.23) and (3.24) c_{sw} is a real coefficient which has to be tuned nonperturbatively to remove $\mathcal{O}(a)$ errors in physical results, $\sigma_{\mu\nu} = (-i/2)[\gamma_\mu,\gamma_\nu]$ and the field strength tensor has the form

$$\hat{F}_{\mu\nu} = -\frac{1}{8a^2} \left(U_{\mu\nu}(n) + U_{\nu-\mu}(n) + U_{-\mu-\nu}(n) + U_{-\nu\mu}(n) \right) - (\mu \leftrightarrow \nu). \tag{3.25}$$

where $U_{\mu\nu}$ is the plaquette –c.f Equation (3.14)—. In this work we use an anisotropic version of the clover action to generate b quark propagators, this action is known as the Relativistic Heavy Quark action and will be introduced in section 3.7.5.

3.7.4 The Domain Wall Fermion (DWF) action

The construction of lattice actions is heavily constrained by the Nielsen-Ninomiya theorem [107], which states that no local action on an even number of dimensions can be constructed such that it does not contain doublers and which preserves chiral symmetry.

[3] $\gamma_{-\mu} \equiv \gamma_\mu$

In the statement of the Nielsen-Ninomiya theorem it is assumed that the Dirac operator anticommutes with γ_5, it was then shown by Ginsparg and Wilson [108] that the conclusion of the Nielsen-Ninomiya theorem can be avoided by changing the definition of chiral symmetry in the lattice to the following relation

$$\gamma^5 D(n|m) + D(n|m)\gamma^5 = aD(n|s)\gamma^5 D(s|m). \tag{3.26}$$

This equation know as the Ginsparg-Wilson relation allows for a definition of chiral symmetry on the lattice which corresponds to continuum chiral symmetry when the lattice spacing vanishes. It was shown in [13, 14, 109] that by introducing an unphysical fifth dimension an action can be constructed which solves the Ginsparg-Wilson relation in the limit of infinite fifth dimensional extent. This action is known as the Domain Wall Fermion action (DWF) and reads

$$S[\Psi, \bar{\Psi}, U] = \sum_{n,m\in\Lambda} \sum_{s,r=0}^{L_s-1} \bar{\Psi}(n,s) D^{\mathrm{dw}}(n,s|m,r)\Psi(m,r), \tag{3.27}$$

where the extent of the fifth dimension is denoted by L_s, Ψ are 5D fermionic fields, the gauge fields U are copied on each value of the 5-coordinate s, and

$$D^{\mathrm{dw}}(n,s|m,r) = \delta_{s,r} D(n|m) + \delta_{n,m} D_5^{\mathrm{dw}}(s|r). \tag{3.28}$$

The two operators on the right hand side of Eq. (3.28) are given by

$$D(n|m) = (4 - M_5)\delta_{n,m} - \frac{1}{2} \sum_{\mu=\pm1}^{\pm4} (1 - \gamma_\mu) U_\mu(n) \delta_{n+\hat{\mu},m}, \tag{3.29}$$

$$\begin{aligned} D_5^{\mathrm{dw}}(s|r) = {} & \delta_{s,r} - (1 - \delta_{s,N_5-1}) P_- \delta_{s+1,r} - (1 - \delta_{s,0}) P_+ \delta_{s-1,r} \\ & + M(P_- \delta_{s,N_5-1}\delta_{0,r} + P_+ \delta_{s,0}\delta_{N_5-1,r}) \end{aligned} \tag{3.30}$$

with chiral projectors $P_\pm = (1 \pm \gamma_5)/2$, quark mass M, and a 5D mass term M_5 whose domain is chosen so that doublers are removed and the positivity of the transfer matrix is guaranteed. Physical observables can then be constructed from the physical fields ψ and $\bar{\psi}$ which live on the 4D boundary of Λ_5,

$$\psi(n) = P_- \Psi(n,0) + P_+ \Psi(n, N_5 - 1), \tag{3.31}$$

$$\bar{\psi}(n) = \bar{\Psi}(n, N_5 - 1) P_- + \bar{\Psi}(n,0) P_+. \tag{3.32}$$

This mixing of left and right chiral modes is exponentially suppressed in L_s, meaning that exact chiral symmetry is recovered in the limit $L_s \to \infty$, but given that in the lattice L_s is finite there is a residual chiral symmetry breaking which can be measured by a residual mass of the quarks.

We end this section by noting that an alternative solution to the Ginsparg-Wilson relation is given by the overlap fermion action [110, 111] this action satisfies the Ginsparg-Wilson relation exactly but is computationally more expensive than the DWF action. Moreover, the DWF action becomes equivalent to the overlap fermion action as $L_s \to \infty$ [112].

3.7.5 The Relativistic Heavy Quark (RHQ) action

The fermionic actions discussed in the previous sections can be used to study hadrons containing light, strange and charm quarks for which discretization errors can be controlled with the currently accessible lattice spacings. This, however, is not the case for bottom quarks for which $m_b a \gg 1$. The study of hadrons containing b quarks requires the use of effective theories, such as heavy quark effective theory (HQET) [31–36], non-relativistic QCD (NRQCD) [37–39] or the relativistic heavy quark action (RHQ) [40–42]. In HQET the limit of infinite mass, i.e the static approximation, is discretized and $1/m_b$ corrections are treated as operator insertions. Because HQET relies on the static approximation it does not apply for heavy-heavy states. NRQCD is a discretization of a non-relativistic effective Lagrangian for heavy quarks in the continuum, it requires that the quarks have low velocities and its Lagrangian contains power-law divergences that blow up in the limit $m_b a \to 0$. The RHQ action can be used when the heavy quark states are at rest or have small spatial momenta and can be used to describe both heavy-light and heavy-heavy systems. It is based on the Fermilab method [40] which uses an anisotropic clover action (3.23) and extends Symanzik effective field theory [113, 114] to the regime $m_b a \not\ll 1$. In the Columbia formulation [42] the RHQ action takes the form

$$\begin{aligned} S[\psi, \bar{\psi}, U, M, c_{sw}, \zeta] = a^4 \sum_{n,m} \bar{\psi}(n) \Big[M + \gamma_0 D_0 + \zeta \vec{\gamma} \cdot \vec{D} - \frac{a}{2}(D_0)^2 - \frac{a}{2}(\vec{D})^2 \\ + c_p \sum_{\mu > \nu} \frac{ia}{4} \sigma_{\mu\nu} F_{\mu\nu} \Big] \psi(m) \end{aligned} \tag{3.33}$$

where

$$D_\mu \psi(n) = \frac{1}{2a} \Big[U_\mu(n) \psi(n+\mu) - U_\mu^\dagger(n-\mu) \psi(n-\mu) \Big], \tag{3.34}$$

$$D_\mu^2 \psi(n) = \frac{1}{a^2} \Big[U_\mu(n) \psi(n+\mu) + U_\mu^\dagger(n-\mu) \psi(n-\mu) - \psi(n) \Big], \tag{3.35}$$

$F_{\mu\nu}$ is defined in equation (3.25), and the three parameters, bare quark mass M, anisotropy parameter ζ and clover coefficient c_p are tuned non-perturbatively — c.f. Sec. 5.3.3.1 — so that all errors of $\mathcal{O}(|\vec{p}|a)$, $\mathcal{O}([Ma]^n)$ and $\mathcal{O}(|\vec{p}a|[Ma]^n)$ are removed from on-shell Green's functions.

3.8 Euclidean Correlators

In Euclidean space, the correlation function of two gauge invariant operators $O_1(\vec{0},0)$ and $O_2(\vec{x},t)$ is given by

$$\langle O_2(\vec{x},t)O_1(\vec{0},0)\rangle = \sum_n \frac{1}{Z_T}\langle m|e^{-(T-t)\hat{H}}\hat{O}_2(\vec{x},0)e^{-t\hat{H}}\hat{O}_1(\vec{0},0)|m\rangle \tag{3.36}$$

where $\hat{O}_1$ and $\hat{O}_2$ are operators that create and annihilate states, T denotes the extension of the lattice in the time direction, m are energy eigenstates and the normalization factor Z_T is given by

$$Z_T = \mathrm{Tr}\left[e^{-T\hat{H}}\right] = \sum_m \langle m|e^{-T\hat{H}}|m\rangle. \tag{3.37}$$

The Euclidean correlator can be evaluated by inserting the unit operator[4]

$$1 = \frac{1}{2E_n}\sum_n |n\rangle\langle n| \tag{3.38}$$

into (3.36) which then becomes

$$\begin{aligned}\langle O_2(\vec{x},t)O_1(\vec{0},0)\rangle &= \sum_{m,n}\frac{1}{2E_nZ_T}\langle m|e^{-(T-t)\hat{H}}\hat{O}_2(\vec{x},0)|n\rangle\langle n|e^{-t\hat{H}}\hat{O}_1(\vec{0},0)|m\rangle \\ &= \sum_{m,n}\frac{1}{2E_nZ_T}e^{-(T-t)E_m}\langle m|\hat{O}_2(\vec{x},0)|n\rangle e^{-tE_n}\langle n|\hat{O}_1(\vec{0},0)|m\rangle \\ &= \sum_{m,n}\frac{1}{2E_n}\frac{\langle m|\hat{O}_2(\vec{x},0)|n\rangle\langle n|\hat{O}_1(\vec{0},0)|m\rangle e^{-(T-t)\Delta E_m}e^{-t\Delta E_n}}{1+e^{-T\Delta E_1}+e^{-T\Delta E_2}+\cdots}\end{aligned} \tag{3.39}$$

where $|n\rangle$ are energy eigenstates and we defined

$$\Delta E_n = E_n - E_0. \tag{3.40}$$

where E_0 is the vacuum energy. In the limit $T\to\infty$

$$\lim_{T\to\infty}\langle O_2(\vec{x},t)O_1(\vec{0},0)\rangle = \sum_n \frac{1}{2E_n}\langle 0|\hat{O}_2(\vec{x},0)|n\rangle\langle n|\hat{O}_1(\vec{0},0)|0\rangle e^{-t\Delta E_n} \tag{3.41}$$

each of the exponentials corresponds to an energy level. These energies can be calculated by for instance choosing operators $\hat{O}_1 = \hat{O}_X^\dagger$ and $\hat{O}_2 = \hat{O}_X$ which create and annihilate a given state X from the vacuum, these states are described by a set of quantum numbers and hence the only matrix elements $\langle n|\hat{O}_1|0\rangle$ that will contribute are those for which $\langle n|$ has the same quantum numbers as X. If we now write $\langle n| = \langle x^{(0)}|$ for the ground state

[4] where we use the relativistic normalization of states

of X and $\langle x^{(1)}|$, $\langle x^{(2)}|, \cdots$ for subsequent excited states then we obtain from (3.41)

$$\lim_{T\to\infty} \langle O_X(\vec{x},t) O_X(\vec{0},0)^\dagger \rangle = \sum_n \frac{1}{2E_n} |\langle x^{(n)}|\hat{O}_X^\dagger|0\rangle|^2 e^{-t\Delta E_n - i\vec{x}\cdot\vec{p}_n}. \tag{3.42}$$

It follows that for sufficiently large t the sub-leading terms are strongly suppressed and so we can extract ΔE_1 from the exponential decay of the correlator. In this case we speak of single state dominance.

3.9 Discrete Symmetries

An understanding of discrete symmetries is necessary to construct meson interpolators that have the desired quantum numbers of physical states and to construct improved current operators. In the following we will discuss the discrete symmetries of charge conjugation, parity and time reversal, for quark bilinears involving a bottom quark b and a light or strange quark ψ.

3.9.1 Parity $\mathcal{P}$

The parity operator $\mathcal{P}$ performs a spatial inversion. Let $x_P = (x_0, -\vec{x})$ then quark and gauge fields transform as

$$\mathcal{P}: \quad \bar{\psi}(x) \to \bar{\psi}(x_P)\gamma_0 \tag{3.43}$$

$$b(x) \to \gamma_0 b(x_P) \tag{3.44}$$

$$\mathcal{P}: \quad U_0(x) \to U_0(x_P) \tag{3.45}$$

$$U_j(x) \to U_{-j}(x_P) \tag{3.46}$$

From which follows that derivatives acting on the heavy quark

$$\overrightarrow{D}_\mu b(x) = \frac{1}{2}\left[U_\mu(x) b(x+\hat{\mu}) - U_{-\mu}(x) b(x-\mu)\right] \tag{3.47}$$

will transform as:

$$\begin{aligned} \mathcal{P}: \quad \overrightarrow{D}_0 b(x) &\to \frac{1}{2}\left[U_0(x_P)\gamma_0 b(x_P+\hat{0}) - U_{-0}(x_P)\gamma_0 b(x_P-\hat{0})\right] \\ &= \gamma_0 \overrightarrow{D}_0 b(x_P) \\ \overrightarrow{D}_j b(x) &\to \frac{1}{2}\left[U_{-j}(x_P)\gamma_0 b(x_P+\hat{j}) - U_j(x_P)\gamma_0 b(x_P-\hat{j})\right] \\ &= -\gamma_0 \overrightarrow{D}_j b(x_P) \end{aligned} \tag{3.48}$$

and similarly derivatives acting on the light/strange/charm quark

$$\psi \overleftarrow{D}(x) = \frac{1}{2}\left[\bar{\psi}(x+\hat{\mu}) U_\mu^\dagger(x) - \psi(x-\mu) U_{-\mu}^\dagger\right] \tag{3.49}$$

will transform as

$$\bar{\psi}D_0(x) \to \bar{\psi}\overleftarrow{D}_0(x_P)\gamma_0 \qquad \text{and} \qquad \bar{\psi}\overleftarrow{D}_j(x) \to -\bar{\psi}\overleftarrow{D}_j(x_P)\gamma_0 \tag{3.50}$$

3.9.2 Time reversal $\mathcal{T}$

The time reversal operator $\mathcal{T}$ reverses the direction of the time axis. Let $x_T = (-x_0, \vec{x})$ then quark and gauge fields transform as

$$\mathcal{T}: \quad \bar{\psi}(x) \to \bar{\psi}(x_T)\gamma^5\gamma_0 \tag{3.51}$$
$$b(x) \to \gamma_0\gamma^5 b(x_T) \tag{3.52}$$
$$\mathcal{T}: \quad U_0(x) \to U_{-0}(x_T) \tag{3.53}$$
$$U_j(x) \to U_j(x_T) \tag{3.54}$$

from which follows that derivatives acting on the heavy quark will transform as:

$$\begin{aligned}\mathcal{T}: \quad \overrightarrow{D}_0 b(x) &\to \frac{1}{2}\left[U_0(x_T)\gamma_0\gamma^5 b(x_T+\hat{0}) - U_{-0}(x_T)\gamma_0\gamma^5 b(x_T-\hat{0})\right] \\ &= -\gamma_0\gamma^5\overrightarrow{D}_0 b(x_T) \qquad (3.55)\\ \overrightarrow{D}_j b(x) &\to \frac{1}{2}\left[U_j(x_T)\gamma_0\gamma^5 b(x_T+\hat{j}) - U_{-j}(x_T)\gamma_0\gamma^5 b(x_T-\hat{j})\right] \\ &= \gamma_0\gamma^5\overrightarrow{D}_0 b(x_T) \qquad (3.56)\end{aligned}$$

and similarly derivatives acting on the light/strange/charm quark will transform as:

$$\bar{\psi}(x)\overleftarrow{D}_0 \to -\bar{\psi}(x_T)\overleftarrow{D}_0\gamma^5\gamma_0 \qquad \text{and} \qquad \bar{\psi}(x)\overleftarrow{D}_j \to \bar{\psi}(x_T)\overleftarrow{D}_j\gamma^5\gamma_0 \tag{3.57}$$

3.9.3 Charge conjugation $\mathcal{C}$

The charge conjugation operator $\mathcal{C}$ transforms particles into antiparticles. Let C be the charge conjugation matrix with $C^{-1}\gamma^\mu C = -(\gamma^\mu)^T = -(\gamma^\mu)^*$ and $C^{-1}\gamma_5 C = (\gamma_5)^T = (\gamma_5)^*$ then quark and gauge fields transform as

$$\mathcal{C}: \quad \bar{\psi}(x) \to -\psi^T(x)C^{-1} \tag{3.58}$$
$$b(x) \to C\bar{b}^T(x) \tag{3.59}$$
$$\mathcal{C}: \quad U_0(x) \to U_{-0}(x) \tag{3.60}$$
$$U_j(x) \to U_j^*(x) \tag{3.61}$$

from which follows that derivatives acting on the heavy quark will transform as:

$$\begin{aligned}\mathcal{C}: \quad \overrightarrow{D}_\mu b(x) &\to \frac{1}{2}\left[U_\mu^*(x)C\bar{b}^T(x+\hat{\mu}) - U_{-\mu}^*(x)C\bar{b}^T(x-\hat{\mu})\right] \\ &= \frac{1}{2}C\left[U_\mu^{\dagger T}(x)\bar{b}^T(x+\hat{\mu}) - U_{-\mu}^{\dagger T}(x)\bar{b}^T(x-\hat{\mu})\right] \\ &= \frac{1}{2}C\left[\bar{b}(x+\hat{\mu})U_\mu^\dagger(x) - \bar{b}(x-\hat{\mu})U_{-\mu}^\dagger(x)\right]^T \\ &= C\left[\bar{b}(x)\overleftarrow{D}_\mu\right]^T\end{aligned} \tag{3.62}$$

and similarly derivatives acting on the light/strange/charm quark will transform as:

$$\bar{\psi}(x)\overleftarrow{D}_\mu \to -\left[\overrightarrow{D}_\mu\psi(x)\right]^T C^{-1} \tag{3.63}$$

3.10 Two-point functions

Meson interpolators are constructed out of quark fields such that they have the desired quantum numbers of the physical state, their general form is

$$\mathcal{O}(n) = \bar{\psi}^{(f_1)}(n)\Gamma\psi^{(f_2)}(n) \tag{3.64}$$

where Γ is a product of Gamma matrices — c.f Appendix A — and f_i are flavour indices. We can now define the fermionic part of the correlation function of two meson interpolators of the form $\mathcal{O} = \bar{d}(n)\Gamma u(n)$ as [96]

$$\begin{aligned}
\langle\mathcal{O}(n)\bar{\mathcal{O}}(m)\rangle &= \langle\bar{d}(n)\Gamma u(n)\bar{u}(m)\Gamma d(m)\rangle_F \\
&= \Gamma_{\alpha_1\beta_1}\Gamma_{\alpha_2\beta_2}\left\langle \bar{d}(n)^{\alpha_1}_{c_1} u(n)^{\beta_1}_{c_1} d(m)^{\alpha_2}_{c_2}\bar{u}(m)^{\beta_2}_{c_2}\right\rangle_F \\
&= -\Gamma_{\alpha_1\beta_1}\Gamma_{\alpha_2\beta_2}\left\langle u(n)^{\beta_1}_{c_1}\bar{u}(m)^{\alpha_2}_{c_2}\right\rangle_u \left\langle \bar{d}(n)^{\alpha_1}_{c_1} d(m)^{\beta_2}_{c_2}\right\rangle_d \\
&= -\Gamma_{\alpha_1\beta_1}\Gamma_{\alpha_2\beta_2} D_u^{-1}(n|m)^{\beta_1\alpha_2}_{c_1c_2} D_d^{-1}(n|m)^{\beta_2\alpha_1}_{c_2c_1} \\
&= -\operatorname{Tr}[\Gamma D_u^{-1}(n|m)\Gamma D_d^{-1}(m|n)]
\end{aligned} \tag{3.65}$$

In the third line of equation (3.65) Grassmann variables have been reordered and expectation values of the fermionic fields were factorized with respect to the flavours. This was followed by a Wick contraction [115] for each of the two flavours which results in the inverse Dirac operator $D^{-1}_{\psi^{(f_1)}}(n|m)$ which propagates a quark of flavour f_1 from space-time point n to the point m. We can now use (3.65) and the momentum projection of (3.41) to write two-point functions for pseudoscalar (P) and vector mesons (V) as

$$\begin{aligned}
C_{PP}(t,k) &= \sum_{\vec{x}}\langle\mathcal{O}_P(\vec{0},0)\mathcal{O}_P(\vec{x},t)^\dagger\rangle e^{-i\vec{k}\cdot\vec{x}} \\
&\xrightarrow{t\to\infty} \frac{|Z_P|^2}{2E_P}e^{-E_P t},
\end{aligned} \tag{3.66}$$

$$\begin{aligned}
C^{\mu\nu}_{VV}(t,k) &= \sum_{\vec{x}}\langle\mathcal{O}^\mu_V(\vec{0},0)\mathcal{O}^\nu_V(\vec{x},t)^\dagger\rangle e^{-i\vec{k}\cdot\vec{x}} \\
&\xrightarrow{t\to\infty} \sum_\lambda \epsilon^\mu(k,\lambda)\epsilon^{\nu*}(k,\lambda)\frac{|Z_V|^2}{2E_V}e^{-E_V t},
\end{aligned} \tag{3.67}$$

where $Z_P \equiv \langle P(\vec{k})|\bar{\psi}^{(f_1)}\gamma^5\psi^{(f_2)}|0\rangle$, $Z_V\epsilon^{\mu*}(\vec{k},\lambda) \equiv \langle V(\vec{k},\lambda)|\bar{\psi}^{(f_1)}\gamma^\mu\psi^{(f_2)}|0\rangle$ and $\varepsilon(\vec{k},\lambda)$ is the polarization vector of the vector meson with helicity λ. In (3.66) and (3.67)

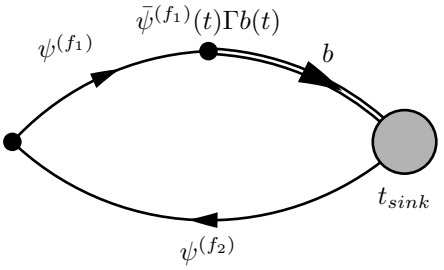

Figure 3.2: Three-point function with point source and smeared sink

we assume single state dominance — c.f section 3.8 — and we drop the 'around the world' contribution — i.e self interactions between particles at lattice site n and their counterpart across the boundary of the system —.

3.11 Quark Sources

3.11.1 Point Source

The lattice Dirac operator acts on the tensor product of the spin, color and lattice vector spaces making the computation of the complete propagator matrix, known as an all-to-all propagator, very expensive in terms of computer memory. The solution to this problem is given by a point-to-all propagator which corresponds to a single column of the inverse Dirac operator,

$$D^{-1}(n|m_0)_{\substack{\beta\alpha_0\\ba_0}} = \sum_{m,\alpha,a} D^{-1}(n|m_0)_{\substack{\beta\alpha\\ba}} S_0^{(m_0,\alpha_0,a_0)}(m)_{\substack{\alpha\\a}} \tag{3.68}$$

which is obtained by multiplying the full Dirac propagator by the point-source matrix

$$S_0^{(m_0,\alpha_0,a_0)}(m)_{\substack{\alpha\\a}} = \delta(m-m_0)\delta_{\alpha\alpha_0}\delta_{aa_0}. \tag{3.69}$$

3.11.2 Smeared Source

Point sources put the quark and anti-quark on the same lattice site making the overlap with the physical state small. To increase this overlap an extended source is used, meaning that the two quarks are placed on different spatial points but on the same time slice. A Gaussian smeared source [116–119] is obtained by multiplying the point source

(3.69) by the smearing operator M

$$S(n) = M(n,m)S_0(m) \tag{3.70}$$

where

$$M = \left(1 + \frac{\sigma^2}{4N}H\right) \tag{3.71}$$

$$H(\vec{n},\vec{m}) = \sum_{j=1}^{3}\left(U_j(\vec{n})\delta(\vec{n}+\hat{j},\vec{m}) + U_j(\vec{n}-\hat{j})^\dagger\delta(\vec{n}-\hat{j},\vec{m}) - 2\delta(\vec{n},\vec{m})\right)^N \tag{3.72}$$

here $\vec{n}$ and $\vec{m}$ are vectors containing the spatial coordinates of the lattice site. The number of smearing steps N and the smearing width σ are chosen to get the best possible overlap with the physical state. The Gaussian smeared source connects different sites of the time slice to the central site resulting on a more realistic wave function which can help to extract clear and strong correlation signals.

3.12 Three-point functions

So far we have discussed the propagation of two quarks of flavours f_1 and f_2 from space-time point m to point n, we also need to consider processes in which one of the quarks interacts with a flavour changing current

$$\mathcal{J}^\Gamma = \bar{\psi}^{(f_1)}\Gamma\psi^{(f_3)}. \tag{3.73}$$

When this is the case we talk about three-point functions schematically given in Figure 3.2. The three-point function for the decay of a B_s meson at rest into a pseudoscalar or vector meson is given by

$$\begin{aligned} C^\Gamma_{B_s\to P}(t,t_{\rm sink},\vec{k}) &= \sum_{\vec{x}\vec{y}}\langle\mathcal{O}_P(\vec{0},0)\mathcal{J}^\Gamma(\vec{y},t)\mathcal{O}^\dagger_{B_s}(\vec{x},t_{\rm sink})\rangle e^{-i\vec{k}\cdot\vec{x}} \\ &\xrightarrow{t,t_{\rm sink}\to\infty} \kappa\ \langle P(p)|\mathcal{J}^\Gamma(\vec{y},t)|B_s(p))\rangle e^{-E_P t - m_{B_s}(t_{\rm sink}-t)}, \end{aligned} \tag{3.74}$$

$$\begin{aligned} C^{\mu\Gamma}_{B_s\to V}(t,t_{\rm sink},\vec{k}) &= \sum_{\vec{x}\vec{y}}\langle\mathcal{O}^\mu_V(\vec{0},0)\mathcal{J}^\Gamma(\vec{y},t)\mathcal{O}^\dagger_{B_s}(\vec{x},t_{\rm sink})\rangle e^{-i\vec{k}\cdot\vec{x}} \\ &\xrightarrow{t,t_{\rm sink}\to\infty} \kappa\ \sum_\lambda \epsilon^\mu(k,\lambda)\langle V(k,\lambda)|\mathcal{J}^\Gamma(\vec{y},t)|B_s(p)\rangle e^{-E_V t - m_{B_s}(t_{\rm sink}-t)}, \end{aligned} \tag{3.75}$$

where single state dominance is assumed — c.f section 3.8 —, $\mathcal{O}_{B_s}$, $\mathcal{O}_P$ and $\mathcal{O}_V$ are annihilation operators for the B_s, pseudoscalar (P) and vector meson (V) respectively, $\kappa \equiv (Z^*_{P/V}Z_{B_s})/(4E_{P/V}m_{B_s})$ with $Z^*_{P/V}$ and Z_{B_s} as defined in section 3.10 and

$$\mathcal{O}_P(x) \equiv \bar{\psi}^{(f_1)}(x)\gamma^5\psi^{(f_2)}(x), \tag{3.76}$$

$$\mathcal{O}^\mu_V(x) \equiv \bar{\psi}^{(f_1)}(x)\gamma^\mu\psi^{(f_2)}(x), \tag{3.77}$$

$$\mathcal{O}_{B_s}(x) \equiv \bar{\psi}(x)\gamma^5 b(x), \tag{3.78}$$

$$\mathcal{J}^{\Gamma}(x) \equiv \bar{\psi}(x)\Gamma b(x). \tag{3.79}$$

3.13 Conclusion

In this chapter we have introduced the steps necessary to discretize QCD, we have discussed briefly different gauge and fermionic actions with particular emphasis on the actions that were used in our simulations, namely, Domain Wall fermion and the Relativistic Heavy quark action. We have introduced the discrete symmetries of time reversal, charge conjugation and parity which are necessary to obtain the $\mathcal{O}(a)$ improvement coefficients for the currents in section 4.3. Finally, we have discussed how to generate different quark sources, and how to construct two and three-point functions which are necessary for the extraction of form factors which is the subject of the next chapter.

Chapter 4

Lattice QCD for B-physics

4.1 Introduction

As discussed in section 2.8 the matrix elements for B_s decays to pseudoscalar or vector states can be expressed in terms of ten form factors which depend on the momentum transfer q^2 between the initial B_s meson and the final state meson. The matrix elements on Eqns. (2.68), (2.71)-(2.74) are isolated from lattice simulations by carefully choosing and computing ratios of 3-pt and 2-pt functions. These ratios are given in the B_s meson rest frame by [120]

$$\begin{aligned} R^{\Gamma}_{B_s\to P}(t,t_{\rm sink},k) &= \frac{C^{\Gamma}_{B_s\to P}(t,t_{\rm sink},\vec{k})}{\sqrt{C_{PP}(t,\vec{k})C_{B_sB_s}(t_{\rm sink}-t)}}\sqrt{\frac{4E_Pm_{B_s}}{e^{-E_Pt}e^{-m_{B_s}(t_{\rm sink}-t)}}} \\ &\xrightarrow{t,t_{\rm sink}\to\infty} \langle P(k)|\mathcal{J}^{\Gamma}|B_s(p)\rangle, \qquad (4.1) \\ R^{\alpha\Gamma}_{B_s\to\phi}(t,t_{\rm sink},k) &= \frac{C^{\alpha\Gamma}_{B_s\to\phi}(t,t_{\rm sink},\vec{k})}{\sqrt{\frac{1}{3}\sum_i C^{ii}_{\phi}(t,\vec{k})C_{B_s}(t_{\rm sink}-t)}}\sqrt{\frac{f(k,\lambda)E_{\phi}M_{B_s}}{e^{-E_{\phi}t}e^{-M_{B_s}(t_{\rm sink}-t)}}} \\ &\xrightarrow{t,t_{\rm sink}\to\infty} \sum_{\lambda}\varepsilon^{\alpha}(k,\lambda)\langle\phi(k,\lambda)|\mathcal{J}^{\Gamma}|B_s(p)\rangle, \qquad (4.2) \end{aligned}$$

where two-point C_{XX} and three-point functions $C^{X}_{B_s\to Y}$ are described in sections 3.10 and 3.12, α and Γ are the required combinations of Gamma matrices for the vector final state and the current, the polarization vector satisfies the relation

$$\sum_{\lambda}\epsilon^{\mu}(k,\lambda)\epsilon^{\nu *}(k,\lambda) = \frac{k^{\mu}k^{\nu}}{m_V^2} - g^{\mu\nu}, \qquad (4.3)$$

and $f(k,\lambda) \equiv \frac{4}{3}\sum_i\sum_{\lambda}\epsilon^i(k,\lambda)\epsilon^{i*}(k,\lambda)$.

4.2 Form factor extraction

In this section we will show the algebraic manipulations required to extract the full set of form factors $f_0, f_+, f_V, f_{A0}, f_{A1}, f_{A2}, f_{T1}, f_{T2}$ and f_{T3} from equations (2.68)-(2.74) using equations (4.1) and (4.2)

4.2.1 f_0 and f_+

The numerical analysis of the form factors f_+ and f_0 is performed by means of an alternative parametrization of (2.68) where the matrix element is written as:

$$\langle P(k)|i\bar{\psi}\gamma^\mu b|B_s(p)\rangle = \sqrt{2m_{B_s}}\left[v^\mu f_\parallel(q^2) + p_\perp^\mu f_\perp(q^2)\right] \tag{4.4}$$

where $v^\mu \equiv p^\mu/m_{B_s}$ is the four-velocity of the B_s meson, $p_\perp^\mu \equiv k^\mu - (k\cdot v)v^\mu$, and

$$f_\parallel(q^2) \equiv \frac{\langle P(k)|\bar{\psi}\gamma^0 b|B_s(p)\rangle}{\sqrt{2m_{B_s}}} = \frac{R^{\gamma^0}_{B_s\to P}(t, t_{\text{sink}}, k)}{\sqrt{2m_{B_s}}}, \tag{4.5}$$

$$f_\perp(q^2) \equiv \frac{\langle P(k)|\bar{\psi}\gamma^i b|B_s(p)\rangle}{k^i\sqrt{2m_{B_s}}} = \frac{R^{\gamma^i}_{B_s\to P}(t, t_{\text{sink}}, k)}{k^i\sqrt{2m_{B_s}}} \quad (\text{no } i \text{ sum}). \tag{4.6}$$

The form factor $f_\parallel$ and $f_\perp$ emerge directly from the lattice calculation, have a simple description in heavy-quark effective theory (HQET) [121] and also in heavy meson chiral perturbation theory (HMχPT) [122] making $f_\parallel$ and $f_\perp$ an ideal choice for lattice simulations. The form factors f_0 and f_+ can then be obtained from

$$f_0(q^2) = \frac{\sqrt{2m_{B_s}}}{m_{B_s}^2 - m_P^2}\left[(m_{B_s} - E_P)f_\parallel(q^2) + (E_P^2 - m_P^2)f_\perp(q^2)\right], \tag{4.7}$$

$$f_+(q^2) = \frac{1}{\sqrt{2m_{B_s}}}\left[f_\parallel(q^2) + (m_{B_s} - E_P)f_\perp(q^2)\right]. \tag{4.8}$$

4.2.2 f_V

Working in the B_s meson rest frame (2.71) simplifies to

$$\langle V(k,\lambda)|\bar{\psi}\gamma^i b|B_s(p)\rangle = -if_V(q^2)\frac{2m_{B_s}\epsilon^{0ijk}\epsilon_j^*(k,\lambda)k_k}{m_{B_s}+m_V}. \tag{4.9}$$

Contracting with the polarization vector $\epsilon^m(k,\lambda)$ and summing over polarization states it follows that

$$\begin{aligned}\sum_\lambda \epsilon^m(k,\lambda)\langle V(k,\lambda)|\bar{\psi}\gamma^i b|B_s(p)\rangle &= -if_V(q^2)\frac{2m_{B_s}\epsilon^{0ijk}k_k}{m_{B_s}+m_V}\sum_\lambda \epsilon^m(k,\lambda)\epsilon_j^*(k,\lambda)\\ &= -if_V(q^2)\frac{2m_{B_s}\epsilon^{0ijk}k_k}{m_{B_s}+m_V}\left(\frac{k^m k_j}{m_V^2} - g_j^m\right)\end{aligned}$$

$$= i f_V(q^2) \frac{2 m_{B_s} \epsilon^{0imk} k_k}{m_{B_s} + m_V} \tag{4.10}$$

which can then be evaluated using (4.2)

$$f_V(q^2) = -i R^{\gamma^m \gamma^i}_{B_s \to V}(t, t_{\text{sink}}, k) \frac{(m_{B_s} + m_V)}{2 m_{B_s} \epsilon_{0ijk} k^k} \quad (\text{no } i,j \text{ sum}). \tag{4.11}$$

4.2.3 f_{A_0}

Terms containing the form factors f_{A_1} and f_{A_2} can be removed from (2.72) by contracting with the momentum transfer vector q. The resulting equation reads:

$$\begin{aligned} q_\mu \sum_\lambda \epsilon^i(k,\lambda) \langle V(k,\lambda) | \bar{\psi} \gamma^\mu \gamma^5 b | B_s(p) \rangle &= 2 f_{A_0}(q^2) \left(\frac{k \cdot q}{m_v^2} k^i - q^i \right) \\ &= 2 f_{A_0}(q^2) \frac{k^i E_V m_{B_s}}{m_V}. \end{aligned} \tag{4.12}$$

Equation (4.12) can then be used together with (4.2) to obtain the form factor f_{A_0}

$$f_{A_0}(q^2) = \frac{m_V}{2 k^i E_V m_{B_s}} q_\mu R^{\gamma^i \gamma^{\mu 5}}_{B_s \to V}(t, t_{\text{sink}}, k) \quad (\text{no } i \text{ sum}) \tag{4.13}$$

where $\gamma^{\mu 5} \equiv \gamma^\mu \gamma^5$.

4.2.4 f_{A_1}

Contracting (2.72) with the vector $\eta = (0, \delta_{1j}, \delta_{2j}, \delta_{3j})$ and setting $k_j = 0$ ($q_j = 0$) we obtain:

$$\sum_\lambda \epsilon^i(k,\lambda) \langle V(k,\lambda) | \bar{\psi} \gamma^\mu \gamma^5 b | B_s(p) \rangle = -f_{A_1}(q^2)(m_{B_s} + m_V) g^{i\mu}. \tag{4.14}$$

which can then be used together with (4.2) to obtain the form factor f_{A_1}

$$f_{A_1}(q^2) = R^{\gamma^j \gamma^{i5}}_{B_s \to V}(t, t_{\text{sink}}, k) \frac{1}{m_{B_s} + m_V} \quad (k^i = 0) \quad (\text{no } i \text{ sum}). \tag{4.15}$$

4.2.5 f_{A_2}

The contraction of (2.72) with a vector η such that $\eta \cdot q = 0$ yields a simplified expression from which the form factor f_{A_2} can be extracted:

$$\begin{aligned} \eta_\mu \sum_\lambda \epsilon^i(k,\lambda) \langle V(k,\lambda) | \bar{\psi} \gamma^\mu \gamma^5 b | B_s(p) \rangle &= f_{A_1}(q^2)(m_{B_s} + m_V) \left(\frac{k \cdot \eta}{m_V^2} k^i - \eta^i \right) \\ &\quad - f_{A_2}(q^2) \frac{\eta \cdot (k+p)}{m_{B_s} + m_V} \left(\frac{k \cdot q}{m_V^2} k^i - q^i \right). \end{aligned} \tag{4.16}$$

Given that $q = (m_{B_s} - E_v, -\vec{k})$ a possible choice of η is given by $\eta = (k_1/(m_{B_s} - E_v), -1, 0, 0)$. With this choice (4.16) yields

$$\begin{aligned}\eta_\mu \sum_\lambda \epsilon^i(k,\lambda)\langle V(k,\lambda)|\bar{\psi}\gamma^\mu\gamma^5 b|B_s(p)\rangle &= f_{A_1}(q^2)(m_{B_s}+m_V)\left(\frac{k_1 m_{B_s}}{m_V^2}k^i - \delta^{1i}\right)\\ &\quad - f_{A_2}(q^2)\frac{2m_{B_s}^2 E_V}{m_V^2(m_{B_s}-E_V)}k_1 k^i\\ &= f_{A_1}(q^2)(m_{B_s}+m_V)\left(\frac{m_{B_s}}{m_V^2} - \frac{\delta^{1i}}{k_1 k^i}\right)k_1 k^i\\ &\quad - f_{A_2}(q^2)\frac{2m_{B_s}^2 E_V}{m_V^2(m_{B_s}-E_V)}k_1 k^i \qquad (4.17)\end{aligned}$$

together with (4.2) and using $k_i = -k^i$ results in:

$$\begin{aligned}-\frac{R^{\gamma^i\gamma^{05}}_{B_s\to V}(t,t_{\text{sink}},k)}{k_i(m_{B_s}-E_V)} - \frac{R^{\gamma^i\gamma^{15}}_{B_s\to V}(t,t_{\text{sink}},k)}{k_1 k_i} &= f_{A_1}(q^2)(m_{B_s}+m_V)\left(\frac{m_{B_s}}{m_V^2} + \frac{\delta^{1i}}{k_1 k_i}\right)\\ &\quad - f_{A_2}(q^2)\frac{2m_{B_s}^2 E_V}{m_V^2(m_{B_s}-E_V)}. \qquad (4.18)\end{aligned}$$

4.2.6 f_{T_1}

In the B_s meson rest frame (2.73) simplifies to

$$q_\nu\langle V(k,\lambda)|\bar{\psi}\sigma^{\nu i}b|B_s(p)\rangle = -f_{T_1}(q^2)2m_{B_s}\epsilon^{0ijk}\epsilon_j^*(k,\lambda)k_k \qquad (4.19)$$

which can be contracted with the polarization vector $\epsilon^m(k,\lambda)$ and summed over polarization states

$$\begin{aligned}q_\nu \sum_\lambda \epsilon^m\langle V(k,\lambda)|\bar{\psi}\sigma^{\nu i}b|B_s(p)\rangle &= -2m_{B_s}f_{T_1}(q^2)\epsilon^{0ijk}\sum_\lambda \epsilon^m(k,\lambda)\epsilon_j^*(k,\lambda)k_k\\ &= -2m_{B_s}f_{T_1}(q^2)\epsilon^{0ijk}\left(\frac{k^m k_j}{m_V^2} - g_j^m\right)k_k\\ &= 2m_{B_s}f_{T_1}(q^2)\epsilon^{0imk}k_k. \qquad (4.20)\end{aligned}$$

This expression can then be evaluated using (4.2)

$$\begin{aligned}f_{T_1}(q^2) &= R^{\gamma^m\sigma^{\nu i}}_{B_s\to V}(t,t_{\text{sink}},k)\frac{q_\nu}{4m_{B_s}\epsilon^{0imk}k_k}\\ &= \frac{1}{2m_{B_s}\epsilon^{0imk}k_k}\Big((m_{B_s}-E_V)R^{\gamma^m\sigma^{0i}}_{B_s\to V}(t,t_{\text{sink}},k)\\ &\quad + k_l R^{\gamma^m\sigma^{li}}_{B_s\to V}(t,t_{\text{sink}},k)\Big) \quad (\text{no } i,m \text{ sum}). \qquad (4.21)\end{aligned}$$

4.2.7 f_{T_2} and f_{T_3}

Contracting (2.74) with the polarization vector $\epsilon^m(k,\lambda)$ and summing over polarization states we obtain

$$\begin{aligned}
&q_\nu \sum_\lambda \epsilon^i(k,\lambda)\langle V(k,\lambda)|\bar{\psi}\sigma^{\nu\mu}\gamma^5 b|B(p)\rangle \\
&= if_{T_2}(q^2)\left[\sum_\lambda \epsilon^i(k,\lambda)\epsilon^{\mu *}(k,\lambda)(m_{B_s}^2 - m_V^2) - \sum_\lambda \epsilon^i(k,\lambda)\epsilon^{\rho *}(k,\lambda)q_\rho(p+k)^\mu\right] \\
&+ if_{T_3}(q^2)\sum_\lambda \epsilon^i(k,\lambda)\epsilon^{\rho *}(k,\lambda)q_\rho\left[q^\mu - \frac{q^2}{m_{B_s}^2 - m_V^2}(p+k)^\mu\right] \\
&= if_{T_2}(q^2)\left[\left(\frac{k^i k^\mu}{m_V^2} - g^{i\mu}\right)(m_{B_s}^2 - m_V^2) - \left(\frac{k^i k^\rho}{m_V^2} - g^{i\rho}\right)q_\rho(p+k)^\mu\right] \\
&+ if_{T_3}(q^2)\left(\frac{k^i k^\rho}{m_V^2} - g^{i\rho}\right)q_\rho\left[q^\mu - \frac{q^2}{m_{B_s}^2 - m_V^2}(p+k)^\mu\right] \\
&= if_{T_2}(q^2)\left[\left(\frac{k^i k^\mu}{m_V^2} - g^{i\mu}\right)(m_{B_s}^2 - m_V^2) - \left(\frac{k\cdot q}{m_V^2}k^i - q^i\right)(p+k)^\mu\right] \\
&+ if_{T_3}(q^2)\left(\frac{k\cdot q}{m_V^2}k^i - q^i\right)\left[q^\mu - \frac{q^2}{m_{B_s}^2 - m_V^2}(p+k)^\mu\right]. \qquad (4.22)
\end{aligned}$$

Terms including $\epsilon\cdot q$ can be removed from (4.22) by setting $k^i = 0$ ($q^i = 0$). The resulting expression can then be evaluated with (4.2) from which follows

$$\begin{aligned}
f_{T_2}(q^2) &= \frac{-i}{(m_{B_s}^2 - m_V^2)}q_\nu(k)R_{B_s\to V}^{\gamma^i\sigma^{[\nu i]5}}(t,t_{\text{sink}},k) \\
&= \frac{-i}{(m_{B_s}^2 - m_V^2)}\Big[(m_{B_s} - E_V)R_{B_s\to V}^{\gamma^i\sigma^{[0i]5}}(t,t_{\text{sink}},k) \\
&+ k_j R_{B_s\to V}^{\gamma^i\sigma^{[ji]5}}(t,t_{\text{sink}},k)\Big] \qquad (4.23)
\end{aligned}$$

where $\sigma^{[\mu\nu]5} \equiv \sigma^{\mu\nu}\gamma^5$. The form factor f_{T_3} can then be obtained from (4.22) by setting $\mu = 0$:

$$\begin{aligned}
&q_\nu \sum_\lambda \epsilon^i(k,\lambda)\langle V(k,\lambda)|\bar{\psi}\sigma^{\nu 0}\gamma^5 b|B(p)\rangle \\
&= if_{T_2}(q^2)\left[\frac{E_V}{m_V^2}(m_{B_s}^2 - m_V^2) - \left(\frac{k\cdot q}{m_V^2} + 1\right)(m_{B_s} + E_V)\right]k^i \\
&+ if_{T_3}(q^2)\left(\frac{k\cdot q}{m_V^2} + 1\right)\left[(m_{B_s} - E_V) - \frac{q^2}{m_{B_s}^2 - m_V^2}(m_{B_s} + E_V)\right]k^i. \qquad (4.24)
\end{aligned}$$

4.3 Operator renormalization and improvement

In lattice QCD, the lattice spacing a provides an ultraviolet cut-off, making Lattice QCD a regularized field theory. To complete the renormalization process lattice results must be identified to the continuum theory. In the case of matrix elements this identification can be achieved by multiplying lattice results with the vector current renormalization constant Z^{hl}

$$\langle P/\phi|J|B_s\rangle_{\text{continuum}} = Z^{hl}_{\gamma_\mu}\langle P/\phi|\mathcal{J}|B_s\rangle_{\text{lattice}} \tag{4.25}$$

where continuum and lattice currents are denoted by J and $\mathcal{J}$, respectively, and $P = \{K, D_s\}$. The uncertainty in the determination of $Z^{hl}_{\gamma_\mu}$ due to one-loop corrections can be reduced by writing [123–125]

$$Z^{hl}_{\gamma_\mu} = \rho_{\gamma_\mu}\sqrt{Z^{hh}_{\gamma_\mu}Z^{ll}_{\gamma_\mu}} \tag{4.26}$$

where the heavy light renormalization factor Z^{hl}_Γ has been decomposed into the product of the coefficient ρ_Γ and the flavour conserving nonperturbative renormalization constants of the heavy-heavy and light-light vector currents

$$Z^{hh}_{\gamma_0} = \frac{\sum_{\vec{x}}\langle B_s(\vec{x},t')B_s(\vec{0},0)\rangle}{\sum_{\vec{x},\vec{y}}\langle B_s(\vec{x},t')J_0(\vec{y},t)B_s(\vec{0},0)\rangle} \tag{4.27}$$

$$Z^{ll}_{\gamma_i} = \frac{\sum_{\vec{x}}\sum_{i=1}^{3}\langle \mathcal{V}_i(\vec{x},t)V_i(\vec{0},0)\rangle}{\sum_{\vec{x}}\sum_{i=1}^{3}\langle V_i(\vec{x},t)V_i(\vec{0},0)\rangle}, \tag{4.28}$$

where $B_s = \bar{s}\gamma_5 b$, $J_0 = \bar{b}\gamma_0 b$, and the local (V) and conserved ($\mathcal{V}$) vector currents are defined for Domain Wall Fermions as [14]

$$V_i(n) = \bar{q}(n)\gamma_i q(n) \tag{4.29}$$

$$\begin{aligned}\mathcal{V}_\mu(n) = \sum_{s=0}^{L_s-1}\frac{1}{2}\Big[&\bar{q}(n+\hat{\mu},s)(1+\gamma_\mu)U^\dagger_{n\mu}q(n,s)\\ &-\bar{q}(n,s)(1-\gamma_\mu)U_{n\mu}q(n+\hat{\mu},s)\Big].\end{aligned} \tag{4.30}$$

Here, L_s is the extent of the unphysical fifth dimension, n are lattice sites, $\hat{\mu}$ is a unit vector in the μ direction, s is the value of the coordinate in the fifth dimension, and $U_{n\mu}$ are link variables. The bulk of the renormalization of $Z^{hl}_{\gamma_\mu}$ is contained in the flavour conserving factors $Z^{ll}_{\gamma_\mu}$ and $Z^{bb}_{\gamma_\mu}$, resulting in a much improved convergence of perturbation theory for the residual matching factor ρ_{γ_μ}. This perturbative factor is expected to be close to unity because most of the radiative corrections cancel in the ratio $Z^{hl}_{\gamma_\mu}/\sqrt{Z^{hh}_{\gamma_\mu}Z^{ll}_{\gamma_\mu}}$ [126].

The heavy-light current can be improved to $\mathcal{O}(a)$ by adding to it terms containing a single covariant derivative (that is, of one higher mass dimension) with appropriate coefficients.

These improvement terms must satisfy symmetry and dimensional considerations and for vector and axial vector currents are given by [126]:

$$V_\mu^1 = \bar{\psi}\overrightarrow{D}_\mu b, \tag{4.31}$$
$$V_\mu^2 = \bar{\psi}\overleftarrow{D}_\mu b, \tag{4.32}$$
$$V_\mu^3 = \bar{\psi}\gamma_\mu\gamma_i\overrightarrow{D}_i b, \tag{4.33}$$
$$V_\mu^4 = \bar{\psi}\gamma_\mu\gamma_i\overleftarrow{D}_i b, \tag{4.34}$$
$$A_\mu^1 = \bar{\psi}\gamma_5\overrightarrow{D}_\mu b, \tag{4.35}$$
$$A_\mu^2 = \bar{\psi}\gamma_5\overleftarrow{D}_\mu b, \tag{4.36}$$
$$A_\mu^3 = \bar{\psi}\gamma_5\gamma_\mu\gamma_i\overrightarrow{D}_i b, \tag{4.37}$$
$$A_\mu^4 = \bar{\psi}\gamma_5\gamma_\mu\gamma_i\overleftarrow{D}_i b. \tag{4.38}$$

These improvement terms can then be used together with temporal ($c^n_{\gamma_0}$, $c^n_{\gamma_5\gamma_0}$) and spatial matching factors ($c^n_{\gamma_i}$, $c^n_{\gamma_5\gamma_i}$) calculated to one loop in lattice perturbation theory to obtain the $\mathcal{O}(\alpha_s a)$ renormalized currents [127]

$$V_0(x) = \rho_{\gamma_0}\sqrt{Z_V^{ll}Z_V^{hh}}\left[V_0^0(x) + c^3_{\gamma_0}V_0^3(x) + c^4_{\gamma_0}V_0^4(x)\right], \tag{4.39}$$
$$V_i(x) = \rho_{\gamma_i}\sqrt{Z_V^{ll}Z_V^{hh}}\left[V_i^0(x) + c^1_{\gamma_i}V_i^1(x) + c^2_{\gamma_i}V_i^2(x) + c^3_{\gamma_i}V_i^3(x) + c^4_{\gamma_i}V_i^4(x)\right]. \tag{4.40}$$
$$A_0(x) = \rho_{\gamma_5\gamma_0}\sqrt{Z_A^{ll}Z_A^{hh}}\left[A_0^0(x) + c^3_{\gamma_5\gamma_0}A_0^3(x) + c^4_{\gamma_5\gamma_0}A_0^4(x)\right], \tag{4.41}$$
$$\begin{aligned} A_i(x) = \rho_{\gamma_5\gamma_i}\sqrt{Z_A^{ll}Z_A^{hh}}\big[&A_i^0(x) + c^1_{\gamma_5\gamma_i}A_i^1(x) + c^2_{\gamma_5\gamma_i}A_i^2(x) \\ &+c^3_{\gamma_5\gamma_i}A_i^3(x) + c^4_{\gamma_5\gamma_i}A_i^4(x)\big]. \end{aligned} \tag{4.42}$$

In Section 6.3.1 we will present our results for the matching coefficients. In the case of tensor and pseudotensor currents the operators needed for $\mathcal{O}(a)$ improvement have not been published [128], but they can be obtained by studying how tensors and pseudotensors transform under discrete symmetries. In the next sections we present the steps we followed for our independent calculation of the $\mathcal{O}(a)$ improvement terms for tensor and pseudotensor currents.

4.3.1 Transformation of unimproved Tensor and Pseudotensor currents

Having introduced the discrete symmetries of parity, charge conjugation and time reversal in section 3.9, we can now see how tensorial currents, that is, how operators of the form $\mathcal{J} = \bar{\psi}\sigma_{\mu\nu}b$ transform under these symmetries

$$\begin{aligned} \mathcal{P}: \quad J^{j0} &\to \bar{\psi}(x_P)\gamma^0\sigma^{j0}\gamma^0 b(x_P) \\ &= -J^{j0}(x_P) \\ J^{jk} &\to \bar{\psi}(x_P)\gamma^0\sigma^{jk}\gamma^0 b(x_P) \\ &= J^{jk}(x_P) \\ \mathcal{T}: \quad J^{j0} &\to \bar{\psi}(x_T)\gamma^5\gamma^0\sigma^{j0}\gamma^0\gamma^5 b(x_T) \\ &= -J^{j0}(x_T) \end{aligned} \tag{4.43}$$

$$
\begin{aligned}
J^{jk} &\to \bar{\psi}(x_T)\gamma^5\gamma^0\sigma^{jk}\gamma^0\gamma^5 b(x_T) \\
&= J^{jk}(x_T) \qquad (4.44)\\
\mathcal{C}: \quad J^{\mu\nu} &\to -\psi^T(x)C^{-1}\sigma^{\mu\nu}C\bar{b}^T(x_T) \\
&= -\psi^T(x)(\sigma^{\nu\mu})^T\bar{b}^T(x_T) \\
&= \psi^T(x)(\sigma^{\mu\nu})^T\bar{b}^T(x_T) \\
&= -\left[\bar{b}(x)(\sigma^{\mu\nu})\psi(x)\right]^T \\
&= -\left[J^{\mu\nu}(x)\right]^T_{b\leftrightarrow\psi} \qquad (4.45)
\end{aligned}
$$

Similarly, we can study how pseudotensors, that is, how operators of the form $\mathcal{J} = \bar{\psi}\gamma_5\sigma_{\mu\nu}b$ transform under discrete symmetries

$$
\begin{aligned}
\mathcal{P}: \mathcal{J}^{j0} &\to \mathcal{J}^{j0}(x_P) \\
\mathcal{J}^{jk} &\to -\mathcal{J}^{jk}(x_P) \\
\mathcal{T}: \mathcal{J}^{j0} &\to \bar{\psi}(x_T)\gamma^5\gamma^0\gamma^5\sigma^{j0}\gamma^0\gamma^5 b(x_T) \\
&= \mathcal{J}^{j0}(x_T) \\
\mathcal{J}^{jk} &\to -\mathcal{J}^{jk}(x_T) \\
\mathcal{C}: \quad \mathcal{J}^{\mu\nu} &\to \left[\mathcal{J}^{\mu\nu}(x)\right]^T_{b\leftrightarrow\psi}\,. \qquad (4.46)
\end{aligned}
$$

4.3.2 $\mathcal{O}(a)$ improvement terms for tensor and pseudotensor currents

Having introduced the transformation properties of tensor and pseudotensor currents under discrete symmetries, we can now work out the $\mathcal{O}(a)$ improvement terms. We start by writing down all possible combinations of gamma matrices and a single covariant derivative which have two antisymmetric free indices. Furthermore, because we are interested in the RHQ action (3.33) which is anisotropic we write separately terms that have only spatial indices and those that involve a temporal index. We arrive at the following preliminary list of improvement terms

$$
\begin{aligned}
O^{\mu\nu}_{1,R_t} &= \bar{\psi}(x)g^{0\mu}\gamma^0\overrightarrow{D}^\nu b(x) - (\mu \leftrightarrow \nu) && (4.47)\\
O^{\mu\nu}_{1,R_x} &= \bar{\psi}(x)g^{i\mu}\gamma^i\overrightarrow{D}^\nu b(x) - (\mu \leftrightarrow \nu) && (4.48)\\
O^{\mu\nu}_{2,R_t} &= \bar{\psi}(x)\sigma^{\mu\nu}\gamma^0\overrightarrow{D}^0 b(x) && (4.49)\\
O^{\mu\nu}_{2,R_x} &= \bar{\psi}(x)\sigma^{\mu\nu}\gamma^i\overrightarrow{D}^i b(x) && (4.50)\\
O^{\mu\nu}_{3,R_t} &= \bar{\psi}(x)\epsilon^{0i\mu\nu}\gamma^0\overrightarrow{D}^i b(x) && (4.51)\\
O^{\mu\nu}_{3,R_x} &= \bar{\psi}(x)\epsilon^{i0\mu\nu}\gamma^i\overrightarrow{D}^0 b(x) && (4.52)\\
O^{\mu\nu}_{4,R_t} &= \bar{\psi}(x)\epsilon^{0i\mu\nu}\gamma^0\gamma^i\gamma^\rho\overrightarrow{D}^\rho b(x) && (4.53)\\
O^{\mu\nu}_{4,R_x} &= \bar{\psi}(x)\epsilon^{i0\mu\nu}\gamma^i\gamma^0\gamma^\rho\overrightarrow{D}^\rho b(x) && (4.54)\\
O^{\mu\nu}_{5,R_t} &= \bar{\psi}(x)g^{0\mu}\gamma^0\gamma^5\overrightarrow{D}^\nu b(x) - (\mu \leftrightarrow \nu) && (4.55)
\end{aligned}
$$

$$O^{\mu\nu}_{5,R_x} = \bar{\psi}(x) g^{i\mu} \gamma^i \gamma^5 \overrightarrow{D}^\nu b(x) - (\mu \leftrightarrow \nu) \tag{4.56}$$
$$O^{\mu\nu}_{6,R_t} = \bar{\psi}(x) \sigma^{\mu\nu} \gamma^0 \gamma^5 \overrightarrow{D}^0 b(x) \tag{4.57}$$
$$O^{\mu\nu}_{6,R_x} = \bar{\psi}(x) \sigma^{\mu\nu} \gamma^i \gamma^5 \overrightarrow{D}^i b(x) \tag{4.58}$$
$$O^{\mu\nu}_{7,R_t} = \bar{\psi}(x) \epsilon^{0i\mu\nu} \gamma^i \gamma^5 \overrightarrow{D}^0 b(x) \tag{4.59}$$
$$O^{\mu\nu}_{7,R_x} = \bar{\psi}(x) \epsilon^{i0\mu\nu} \gamma^0 \gamma^5 \overrightarrow{D}^i b(x) \tag{4.60}$$
$$O^{\mu\nu}_{8,R_t} = \bar{\psi}(x) \epsilon^{0i\mu\nu} \gamma^0 \gamma^i \gamma^\rho \gamma^5 \overrightarrow{D}^\rho b(x) \tag{4.61}$$
$$O^{\mu\nu}_{8,R_x} = \bar{\psi}(x) \epsilon^{i0\mu\nu} \gamma^i \gamma^0 \gamma^\rho \gamma^5 \overrightarrow{D}^\rho b(x) \tag{4.62}$$
$$O^{\mu\nu}_{9,R_t} = \bar{\psi}(x) g^{0\mu} \overrightarrow{D}^\nu b(x) - (\mu \leftrightarrow \nu) \tag{4.63}$$
$$O^{\mu\nu}_{9,R_x} = \bar{\psi}(x) g^{i\mu} \overrightarrow{D}^\nu b(x) - (\mu \leftrightarrow \nu) \tag{4.64}$$
$$O^{\mu\nu}_{10,R_t} = \bar{\psi}(x) \sigma^{0\mu} \overrightarrow{D}^\nu b(x) - (\mu \leftrightarrow \nu) \tag{4.65}$$
$$O^{\mu\nu}_{10,R_x} = \bar{\psi}(x) \sigma^{i\mu} \overrightarrow{D}^\nu b(x) - (\mu \leftrightarrow \nu) \tag{4.66}$$
$$O^{\mu\nu}_{11,R_t} = \bar{\psi}(x) g^{0\mu} \sigma^{\nu\lambda} \overrightarrow{D}^\lambda b(x) - (\mu \leftrightarrow \nu) \tag{4.67}$$
$$O^{\mu\nu}_{11,R_x} = \bar{\psi}(x) g^{i\mu} \sigma^{\nu\lambda} \overrightarrow{D}^\lambda b(x) - (\mu \leftrightarrow \nu) \tag{4.68}$$
$$O^{\mu\nu}_{12,R_t} = \bar{\psi}(x) g^{0\mu} \gamma^5 \overrightarrow{D}^\nu b(x) - (\mu \leftrightarrow \nu) \tag{4.69}$$
$$O^{\mu\nu}_{12,R_x} = \bar{\psi}(x) g^{i\mu} \gamma^5 \overrightarrow{D}^\nu b(x) - (\mu \leftrightarrow \nu) \tag{4.70}$$
$$O^{\mu\nu}_{13,R_t} = \bar{\psi}(x) \sigma^{0\mu} \gamma^5 \overrightarrow{D}^\nu b(x) - (\mu \leftrightarrow \nu) \tag{4.71}$$
$$O^{\mu\nu}_{13,R_x} = \bar{\psi}(x) \sigma^{i\mu} \gamma^5 \overrightarrow{D}^\nu b(x) - (\mu \leftrightarrow \nu) \tag{4.72}$$
$$O^{\mu\nu}_{14,R_t} = \bar{\psi}(x) g^{0\mu} \sigma^{\nu\lambda} \gamma^5 \overrightarrow{D}^\lambda b(x) - (\mu \leftrightarrow \nu) \tag{4.73}$$
$$O^{\mu\nu}_{14,R_x} = \bar{\psi}(x) g^{i\mu} \sigma^{\nu\lambda} \gamma^5 \overrightarrow{D}^\lambda b(x) - (\mu \leftrightarrow \nu) \tag{4.74}$$

This list can be reduced by noticing that some terms are identical up to a sign —e.g. (4.61) and (4.62)—, others have uncontracted Latin indices and hence violate rotational symmetry —e.g (4.72)— and others do not transform under discrete symmetries as tensors nor as pseudotensors -e.g (4.73). The list can also be reduced by means of the equations of motion, which for on-shell states read

$$\left[m_0^{(b)} + \gamma^0 \overrightarrow{D}^0 + \zeta \boldsymbol{\gamma} \cdot \overrightarrow{\boldsymbol{D}} + \mathcal{O}(a) \right] b = 0 \tag{4.75}$$
$$\bar{\psi} \left[m_0^{(q)} - \gamma^0 \overleftarrow{D}^0 - \overleftarrow{\boldsymbol{D}} \cdot \boldsymbol{\gamma} + \mathcal{O}(a^2) \right] = 0 \tag{4.76}$$

and hence

$$\overrightarrow{D}^0 b = -m_0^{(b)} \gamma^0 b - \zeta \gamma^0 \boldsymbol{\gamma} \cdot \overrightarrow{\boldsymbol{D}} b + \mathcal{O}(a) \tag{4.77}$$
$$\bar{\psi} \overleftarrow{D} = m_0^{(q)} \bar{\psi} \gamma^0 - \bar{\psi} \overleftarrow{\boldsymbol{D}} \cdot \boldsymbol{\gamma} \gamma^0 + \mathcal{O}(a^2) \tag{4.78}$$

Equations (4.77) and (4.78) can then be used to show that terms involving temporal derivatives are redundant, e.g

$$\begin{aligned}
O^{\mu\nu}_{2,R_t} &= \bar{\psi}(x)\sigma^{\mu\nu}\gamma^0\overrightarrow{D}^0 b(x) \\
&= \bar{\psi}\sigma^{\mu\nu}\left[-m_0^{(b)}b(x) - \zeta\boldsymbol{\gamma}\cdot\boldsymbol{D}b(x)\right] \\
&= -m_0^{(b)}J^{\mu\nu} - \zeta O^{\mu\nu}_{2,R_x} \\
O^{jk}_{7,R_t} &= \bar{\psi}(x)\epsilon^{0ijk}\gamma^i\gamma^5\overrightarrow{D}^0 b(x) \\
&= \bar{\psi}(x)\epsilon^{0ijk}\gamma^i\gamma^5\left[-m_0^{(b)}\gamma^0 b(x) - \zeta\gamma^0\boldsymbol{\gamma}\cdot\boldsymbol{D}b(x)\right] \\
&= \frac{i}{4}\bar{\psi}(x)\epsilon^{0ijk}\gamma^i\epsilon_{\mu\nu\alpha\beta}\gamma^\mu\gamma^\nu\gamma^\alpha\gamma^\beta\left[-m_0^{(b)}\gamma^0 b(x) - \zeta\gamma^0\boldsymbol{\gamma}\cdot\overrightarrow{\boldsymbol{D}}b(x)\right] \\
&= \frac{i}{4}\bar{\psi}(x)\gamma^i\delta^{0ijk}_{\mu\nu\alpha\beta}\gamma^\mu\gamma^\nu\gamma^\alpha\gamma^\beta\left[-m_0^{(b)}\gamma^0 b(x) - \zeta\gamma^0\boldsymbol{\gamma}\cdot\overrightarrow{\boldsymbol{D}}b(x)\right] \\
&= \pm\frac{i}{4}\bar{\psi}(x)\gamma^i\gamma^0\gamma^i\gamma^j\gamma^k\left[-m_0^{(b)}\gamma^0 b(x) - \zeta\gamma^0\boldsymbol{\gamma}\cdot\overrightarrow{\boldsymbol{D}}b(x)\right] \\
&= \pm\frac{i}{4}\bar{\psi}(x)\sigma^{jk}\left[-m_0^{(b)}b(x) - \zeta\boldsymbol{\gamma}\cdot\overrightarrow{\boldsymbol{D}}b(x)\right] \\
&= \pm\frac{i}{4}\bar{\psi}(x)\left[m_0^{(b)}\frac{1}{2}J^{jk} + \zeta O^{jk}_{2,Rx}\right]b(x)
\end{aligned} \tag{4.79}$$

Finally, given that $\gamma^\alpha\gamma^\beta\gamma^\rho = g^{\alpha\beta}\gamma^\rho - g^{\alpha\rho}\gamma^\beta + g^{\beta\rho}\gamma^\alpha - i\epsilon_{\mu\alpha\beta\rho}\gamma^\mu\gamma^5$ we have that

$$\begin{aligned}
O^{jk}_{8,R_t} &= \bar{\psi}(x)\epsilon^{0ijk}\gamma^0\gamma^i\gamma^m\gamma^5\overrightarrow{D}^m b(x) \\
&= -i\bar{\psi}(x)\epsilon^{0ijk}\epsilon^{\mu 0im}\gamma^\mu\gamma^5\gamma^5\overrightarrow{D}^m b(x) \\
&= -i\delta^{0ijk}_{\mu 0im}O^{\mu m}_{1,R_x}
\end{aligned} \tag{4.80}$$

and similarly $O^{jk}_{4,R_t} = -i\delta^{0ijk}_{\mu 0im}O^{\mu m}_{5,R_x}$. It can be concluded that the full list of $\mathcal{O}(a)$ improvement terms classified in terms of operators which transform just like the unimproved tensor and pseudotensor currents is given by[1]:

1. Tensor

$$O^{0j}_{1,R_t} + O^{0j}_{1,L_t} = [\bar{\psi}(x)\gamma^0\overrightarrow{D}^j b(x) + \bar{\psi}(x)\overleftarrow{D}^j\gamma^0 b(x)] - (0 \leftrightarrow j) \tag{4.81}$$

$$O^{ij}_{1,R_x} + O^{ij}_{1,L_x} = [\bar{\psi}(x)\gamma^i\overrightarrow{D}^j b(x) + \bar{\psi}(x)\overleftarrow{D}^j\gamma^i b(x)] - (i \leftrightarrow j) \tag{4.82}$$

$$O^{ij}_{2,R_x} - O^{ij}_{2,L_x} = \bar{\psi}(x)\sigma^{ij}\boldsymbol{\gamma}\cdot\overrightarrow{\boldsymbol{D}}b(x) - \bar{\psi}(x)\overleftarrow{\boldsymbol{D}}\cdot\boldsymbol{\gamma}\sigma^{ij}b(x) \tag{4.83}$$

$$O^{i0}_{2,R_t} - O^{i0}_{2,L_t} = \bar{\psi}(x)\sigma^{i0}\boldsymbol{\gamma}\cdot\overrightarrow{\boldsymbol{D}}b(x) - \bar{\psi}(x)\overleftarrow{\boldsymbol{D}}\cdot\boldsymbol{\gamma}\sigma^{i0}b(x) \tag{4.84}$$

$$O^{ij}_{7,R_x} + O^{ij}_{7,L_x} = \bar{\psi}(x)\epsilon^{0lij}\gamma^0\gamma^5\overrightarrow{D}^l b(x) + \bar{\psi}(x)\overleftarrow{D}^l\gamma^5\gamma^0\epsilon^{0lij}b(x) \tag{4.85}$$

2. Pseudotensor

$$O^{ij}_{3,R_x} + O^{ij}_{3,L_x} = \bar{\psi}(x)\epsilon^{l0ij}\gamma^0\overrightarrow{D}^l b(x) + \bar{\psi}(x)\overleftarrow{D}^l\gamma^0\epsilon^{l0ij}b(x) \tag{4.86}$$

[1] where O_L denotes operators in which the derivative acts on the left, that is it acts on the ligth quark, e.g if $O^{0j}_{1,R_t} = [\bar{\psi}(x)\gamma^0\overrightarrow{D}^j b(x) - (0 \leftrightarrow j)]$ then $O^{0j}_{1,L_t} = [\bar{\psi}(x)\overleftarrow{D}^j\gamma^0 b(x) - (0 \leftrightarrow j)]$

$$O^{0j}_{5,R_t} + O^{0j}_{5,L_t} = \bar{\psi}(x)\gamma^0\gamma^5\overrightarrow{D}^j b(x) + \bar{\psi}(x)\overleftarrow{D}^j\gamma^5\gamma^0 b(x) \tag{4.87}$$

$$O^{ij}_{5,R_x} + O^{ij}_{5,L_x} = [\bar{\psi}(x)\gamma^i\gamma^5\overrightarrow{D}^j b(x) + \bar{\psi}(x)\overleftarrow{D}^j\gamma^5\gamma^i b(x)] - (i \leftrightarrow j) \tag{4.88}$$

$$O^{i0}_{6,R_t} - O^{i0}_{6,L_t} = \bar{\psi}(x)\sigma^{i0}\gamma^5\boldsymbol{\gamma}\cdot\overrightarrow{\boldsymbol{D}} b(x) - \bar{\psi}(x)\overleftarrow{\boldsymbol{D}}\cdot\boldsymbol{\gamma}\gamma^5\sigma^{i0} b(x) \tag{4.89}$$

$$O^{ij}_{6,R_x} - O^{i0}_{6,L_t} = \bar{\psi}(x)\sigma^{ij}\gamma^5\boldsymbol{\gamma}\cdot\overrightarrow{\boldsymbol{D}} b(x) - \bar{\psi}(x)\overleftarrow{\boldsymbol{D}}\cdot\boldsymbol{\gamma}\gamma^5\sigma^{ij} b(x) \tag{4.90}$$

These operators are in agreements with those obtained in [128].

4.4 Conclusion

In this chapter we have discussed the steps necessary to extract the form factors involved in the decays of pseudoscalar mesons to pseudoscalar or vector meson final states, namely, $f_\parallel$, $f_\perp$, f_V, f_{A_0}, f_{A_1}, $f_{A_{12}}$, f_{T_1}, f_{T_2} and $f_{T_{23}}$ from lattice simulations. We followed this with a brief discussion on operator renormalization and improvement. We performed an independent calculation of the $\mathcal{O}(a)$ improvement terms for tensor and pseudotensor currents which provides a check on the results obtained in [128]. Once perturbative calculations of the matching coefficients for the improvement operators of tensor and pseudotensor currents become available a full calculation to $\mathcal{O}(\alpha_s a)$ will become possible.

Chapter 5

Data generation and processing

5.1 Introduction

In this chapter we discuss the setup used on our simulations and the statistical methods used to study our results. In Section 5.2 we give an overview of the gauge field ensembles we used as the starting point of our numerical simulations, this is followed in Section 5.3 by the technicalities involved in the generation of the quark propagators and the RHQ action tuning. We then discuss in Section 5.4 the steps followed to obtain the best possible signal from our two-point and three-point functions. Finally in Section 5.5 we discuss the jackknife and super-jackknife methods which will be used to determine the statistical errors from our results.

5.2 Gauge Fields

Our simulations are based on RBC-UKQCD's set of 2+1 flavour gauge field configurations [7, 10–12] generated with the Iwasaki gauge action [43]

$$S_G[U] = -\frac{2}{g^2}\left[(1-8c_1)\sum_{n\in\Lambda}\sum_{\mu<\nu}\mathrm{Re}\,\mathrm{Tr}[U_{\mu\nu}(n)] + c_1\sum_{n\in\Lambda}\sum_{\mu\neq\nu}\mathrm{Re}\,\mathrm{Tr}[U^R_{\mu\nu}(n)]\right] \tag{5.1}$$

where $U_{\mu\nu}(n)$ is the plaquette Eq.(3.14) and $U^R_{\mu\nu}(n)$ is the path ordered product of link variables around the 1×2 rectangle in the μ, ν plane at the point n,

$$U^R_{\mu\nu}(n) = U_\mu(n)U_\nu(n+2\hat{\mu})U_{-\mu}(n+2\hat{\mu}+\hat{\nu})U_{-\nu}(n+\hat{\nu}). \tag{5.2}$$

We use the Iwasaki gauge action since it produces smoother gauge fields which reduce the residual chiral symmetry breaking for Domain Wall Fermions (DWF) at finite L_s — c.f Section 3.7.4 —. We use the DWF action [13, 14, 44] for the light quarks and work

$L^3 \times T$	L_s	a^{-1} [GeV]	am_l^{sea}	am_h^{sea}	am_s^{phys}	M_π [MeV]	# configs	# time sources
$24^3 \times 64$	16	1.785(5)	0.005	0.040	0.03224(18)	337(1)	1636	1
$24^3 \times 64$	16	1.785(5)	0.010	0.040	0.03224(18)	356(1)	1419	1
$32^3 \times 64$	16	2.383(9)	0.004	0.030	0.02477(18)	302(2)	628	2
$32^3 \times 64$	16	2.383(9)	0.006	0.030	0.02477(18)	363(2)	889	2
$32^3 \times 64$	16	2.383(9)	0.008	0.030	0.02477(18)	411(2)	544	2

Table 5.1: Overview of the gauge field ensembles. The ensembles were generated by the RBC and UKQCD collaborations [7, 10–12] using 2+1 flavour domain-wall fermions and Iwasaki gauge actions. The domain-wall height for light and strange quarks is $M_5 = 1.8$. The 24^3 and 32^3 ensembles are generated using the Shamir domain-wall kernel [13, 14]. Values for the inverse lattice spacing and the quark and meson masses are taken from the refined analysis [11] and updated to include the finer $a^{-1} = 2.77$ GeV ensemble [12]. The light sea-quark mass is labelled am_l, the heavy sea-quark mass am_h, and am_s^{phys} is the mass of the physical strange quark mass. The valence strange quark masses used in our simulations on 24^3 and 32^3 ensembles are $am_s^{\text{sim}} = 0.03224$ and $am_s^{\text{sim}} = 0.025$, respectively.

on five ensembles featuring unitary pion masses down to ∼300 MeV, at inverse lattice spacings of 1.785(5) and 2.383(9) GeV. These lattice spacings were determined from a global fit that included the ensembles of Table 5.1 and the physical point ensembles with lattice sizes $48^3 \times 96$ and $64^3 \times 128$ [7, 10–12] by adjusting the masses of light and strange quarks until the ratios M_π/M_Ω and M_K/M_Ω had their physical values and taking ratios such as

$$a^{-1} = (M_\Omega)_{\text{phys}}/(aM_\Omega)_{\text{lat}}. \tag{5.3}$$

On all our ensembles $M_\pi L$ is greater than 3.8 and the spatial box sizes are at least 2.6 fm, meaning that finite volume corrections which are $\mathcal{O}(\exp(-M_\pi L))$ [129] are therefore $\approx$ 2%. Details of the configurations as well as the number of gauge field configurations and sources per configuration are summarized in Tab. 5.1. In order to reduce autocorrelations between ensembles, we perform a random 4-vector shift of the gauge field prior to starting the generation of quark propagators.

5.3 Quark propagators

5.3.1 Light and strange quark propagators

We generate light and strange quark domain-wall propagators with periodic boundary conditions in space and antiperiodic in time, using a point source —c.f Section 3.11.1—, domain-wall height $M_5 = 1.8$ and fifth dimension extent $L_s = 16$.

$L^3 \times T$	a^{-1}[GeV]	am_l	am_h	am_c^{sim}	$M_{D_s}^{\text{sim}}$[GeV]
$24^3 \times 64$	1.785(5)	0.005	0.040	0.30, 0.35, 0.40	1.5654(8), 1.6981(9), 1.8244(10)
$24^3 \times 64$	1.785(5)	0.010	0.040	0.30, 0.35, 0.40	1.5707(9), 1.7037(10), 1.8304(11)
$32^3 \times 64$	2.383(9)	0.004	0.030	0.28, 0.34	1.8300(12), 2.0367(14)
$32^3 \times 64$	2.383(9)	0.006	0.030	0.28, 0.34	1.8340(10), 2.0406(11) 3.059(11)
$32^3 \times 64$	2.383(9)	0.008	0.030	0.28, 0.34	1.8351(13), 2.0420(15)

Table 5.2: Simulated charm-like bare input quark masses am_c^{sim} and the corresponding values of the D_s^{sim} meson masses in GeV for our 24^3 and 32^3 ensembles. The physical D_s mass is $M_{D_s} = 1.969(14)$ GeV [6].

5.3.2 Charm quark propagators

Given that the mass of the charm quark ($m_c^{\overline{\text{MS}}}(\mu = m_c) = 1.28 \pm 0.03$ GeV [6]) is less than our smallest cut-off ($a^{-1} = 1.785(5)$ GeV), the simulation of charm quarks can proceed either by means of the RHQ action or through a fully relativistic formulation based on the DWF action. While the RHQ action is numerically cheaper, simulating charm quarks using the DWF action has the advantage that we match the action used for light and strange quarks, and there is no need to tune the three parameters of the RHQ action for the charm quark. We therefore simulate charm quarks based on the recent work featuring the optimized Möbius DWF action [12, 130–132] with domain-wall height $M_5 = 1.6$, extent of the fifth dimension $L_s = 12$ and Möbius parameters $b = 1.5$ and $c = 0.5$. With this set-up and the use of bare quark masses below $am_q \lesssim 0.4$ discretization errors have been shown to remain small for physical quantities such as decay constants and meson masses [131]. Thus on our coarse ensembles ($a^{-1} = 1.785(5)$ GeV), we cannot directly simulate charm quarks but expect a linear extrapolation to be benign [12, 132]. We simulate 2—3 charm-like quark masses and subsequently extra-/interpolate to the physical charm quark mass. The bare charm quark masses used in our simulations as well as the D_s masses relevant for the extra-/interpolation are listed in Table 5.2.

5.3.3 Bottom quark propagators

We simulate the heavy b-quarks using the RHQ action [42, 133] discussed in Section 3.7.5 with Gaussian smeared sources [119] to reduce excited state contamination — c.f Section 3.11.2 —, the smearing parameters for the $a^{-1} = 1.785(5)$ GeV ensemble are $\sigma = 7.86$ and $N = 100$, and for the $a^{-1} = 2.383(9)$ GeV ensemble $\sigma = 10.36$ and $N = 170$.

5.3.3.1 RHQ action tuning

We performed the non-perturbative tuning of the three RHQ parameters m_0a, c_p and ζ following the prescription of Ref. [134]. In this prescription the RHQ parameters are determined by requiring that the B_s meson lattice dispersion relation

$$\begin{aligned}(aE(\vec{p}))^2 &= \left(\frac{M_1}{M_2}\right)(a\vec{p})^2 + (aM_1)^2 + \mathcal{O}([a\vec{p}]^4) \\ M_1 &= E(\vec{p}^{\,2} = 0) \\ M_2 &= M_1 \times \left(\frac{\partial E^2}{\partial p_i^2}\right)^{-1}_{\vec{p}=0}\end{aligned} \tag{5.4}$$

is equivalent to the continuum one to $\mathcal{O}([a\vec{p}]^4)$, that is, we require $M_1 = M_2$. We also require that the calculation of the spin-averaged B_s meson mass

$$\bar{M}_{B_s} = \frac{1}{4}\left(M_{B_s} + 3M_{B_s^*}\right), \tag{5.5}$$

and the hyperfine splitting

$$\Delta M_{B_s} = M_{B_s^*} - M_{B_s} \tag{5.6}$$

obtained with the RHQ action correctly reproduce the experimentally measured results $\Delta M_{B_s} = 49.0(1.6)$ MeV and $\bar{M}_{B_s} = 5.404(1)$ GeV [6]. The bottom strange system is chosen since discretization and chiral perturbation errors are expected to be small. The tuning is carried out in a region of parameter space close enough to the true parameters such that the linear relation

$$\begin{bmatrix} \overline{M}_{B_s} \\ \Delta M_{B_s} \\ \frac{M_1}{M_2} \end{bmatrix} = J \begin{bmatrix} m_0a \\ c_p \\ \zeta \end{bmatrix} + A \tag{5.7}$$

holds. In Eq. (5.7) J is a 3×3 matrix of coefficients and A is a 3-element constant column vector. We determine seven sets of parameters $\{m_0a, c_p, \zeta\}$, $\{m_0a \pm \sigma_{m_0a}, c_p, \zeta\}$, $\{m_0a, c_p \pm \sigma_{c_p}, \zeta\}$ and $\{m_0a, c_p, \zeta \pm \sigma_\zeta\}$ where σ_X is a chosen uncertainty of the parameter X, and check whether the region bounded by them is in the region for which Eq. (5.7) holds. If this is the case then the matrix J and the vector A are computed

$$J = \left[\frac{Y_3 - Y_2}{2\sigma_{m_0a}}, \frac{Y_5 - Y_4}{2\sigma_{c_p}}, \frac{Y_7 - Y_6}{2\sigma_\zeta}\right], \tag{5.8}$$

$$A = Y_1 - J \times [m_0a, c_p, \zeta]^T, \tag{5.9}$$

$$Y_i = \left[\overline{M}_{b_s}, \Delta M_{B_s}, M_1/M_2\right]_i^T \tag{5.10}$$

a^{-1} [GeV]	$m_0 a$	c_P	ζ
1.785(5)	7.471(51)(75)(82)(45)	4.92(13)(28)(07)(24)	2.929(63)(100)(15)(03)
2.383(9)	3.485(25)(38)(45)(31)	3.06(07)(18)(05)(15)	1.760(30)(58)(07)(02)

Table 5.3: Tuned RHQ parameters on the 24^3 and 32^3 ensembles. Errors listed for $m_0 a$, c_P, and ζ are, from left to right: statistics, heavy-quark discretization errors, the lattice scale uncertainty, and the uncertainty due to the experimental measurement of the B_s meson hyperfine splitting, respectively.

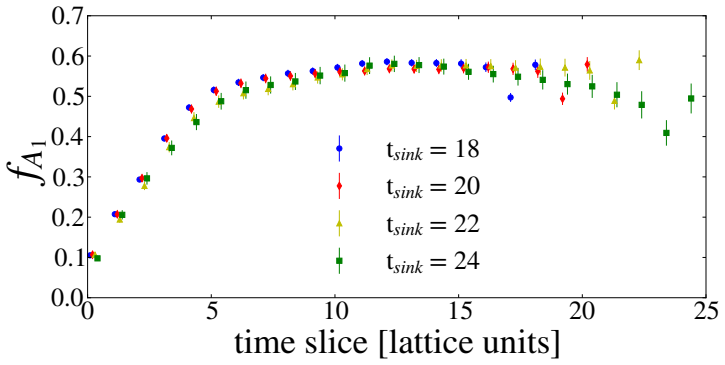

Figure 5.1: Unimproved form factor f_{A_1} for the $B_s \to \phi \ell^+ \ell^-$ decay at zero momentum for four different source-sink separations on the coarse $a^{-1} = 1.785(5)$ GeV ensemble with $am_l = 0.005$.

where i denotes the i^{th} parameter set. The RHQ parameters are then determined from

$$\begin{bmatrix} m_0 a \\ c_p \\ \zeta \end{bmatrix}^{RHQ} = J^{-1} \times \left(\begin{bmatrix} \overline{M}_{B_s} \\ \Delta M_{B_s} \\ \frac{M_1}{M_2} \end{bmatrix} - A \right) \tag{5.11}$$

The RHQ parameters are considered tuned when the values obtained from Eq. (5.11) are within the box defined by the seven sets of parameters. If this is not the case the box is re-centered at the result of Eq. (5.11) and another iteration is performed. The results of the tuning are presented in Table 5.3.

5.4 Two point and three point functions

As discussed in Section 4.1 the extraction of matrix elements requires the calculation of two-point and three-point functions. In this Section we discuss the steps that we followed to obtain the best possible signal.

5.4.1 Source-sink separation

In order to optimise the signal obtained from 3-point correlators, we study four different source-sink separations seeking the choice which results in the longest plateau and small

statistical errors. We compare the results obtained for a given decay at zero momentum using $\Delta t \equiv t_{\text{sink}} - t_{\text{source}} = 18, 20, 22, 24$, we present an example of the resulting plot in figure 5.1. Within statistical uncertainties, all choices for t_{sink} agree. We found that for all 3-point correlators the best signal is obtained for $t_{\text{sink}} - t_{\text{source}} = 20$ confirming the choice made in reference [135] for semileptonic charged currents. Scaling with the lattice spacing we obtain $t_{\text{sink}} - t_{\text{source}} = 26$ as the optimal source sink separation for the ensembles with $a^{-1} = 2.383(9)$ GeV.

5.4.2 Smearing of Charm-strange 2-point functions

We investigated Gaussian smeared sources for the charm quarks with different widths σ following a similar procedure to the one presented in [134]. We generate c-quark propagators with a gauge invariant Gaussian source for the spatial wave function (3.70) where we use the criterion $N > 3\sigma^2/2$ for the number of iterations N so that the source is spatially smooth and a good approximation to a Gaussian [134]. We study the effect that combinations of $(\sigma, N) = \{(1.39, 5),(1.97, 10), (2.78, 15), (3.93, 30), (7.86, 100), (11.79, 215)\}$ have on the effective mass of the D_s and D_s^* mesons. We show the results of our study on the coarse ensemble 24^3 with $am_l = 0.005$ in Figure 5.2. As can be seen in the plots, the green data corresponding to a width $\sigma = 7.86$ and $N = 100$ smearing iterations result in the earliest onset of the plateau which also extends over many time slices. This is the same outcome as found in the study of bottom quarks in reference [134].

5.5 Statistical Analysis

The data presented in the following chapter was analyzed using single elimination jackknife re-sampling after first averaging correlators computed with different sources on the same gauge field configuration. For functions of several observables computed on different ensembles we use the super jackknife method introduced in [136] and discussed in more detail in [137]. The jackknife and super jackknife methods can be used to study both simple averages and quantities that are obtained from a fit [96, 138, 139], hence we will use these two methods to determine the errors for fitted quantities in a simple straightforward way.

5.5.1 Jackknife method

The single elimination jackknife method [140] estimates the bias of an estimator $\hat{\theta}$ for the parameter θ of a data set of size N, by removing the nth entry of the original data set $(n = 1, \cdots, N)$ and recalculating the estimator based on the rest of the data. Let $\hat{\theta}$ be

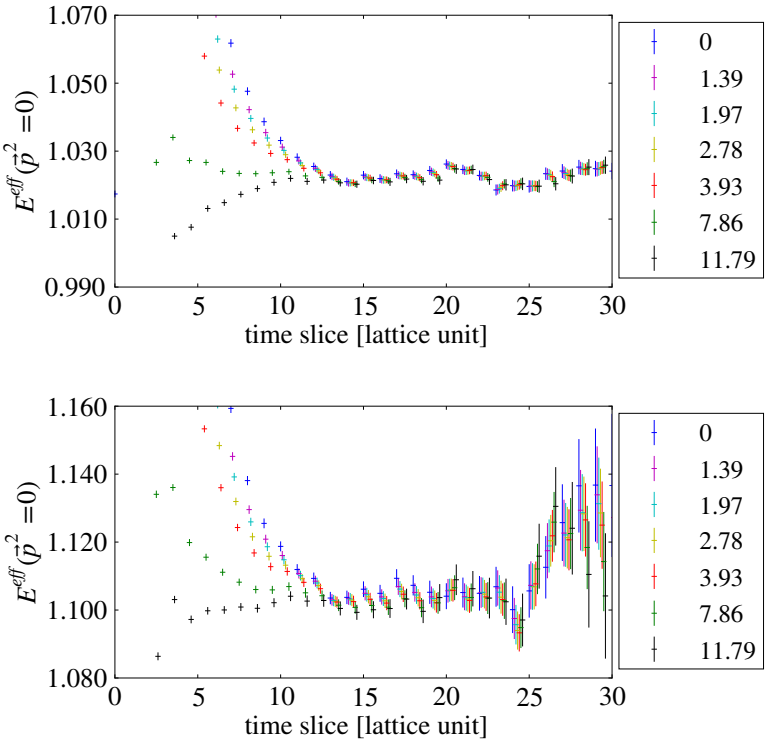

Figure 5.2: Exploring different widths σ of the Gaussian source used to generate charm quarks by comparing effective masses for the D_s-like meson on the top and the D_s^*-like meson on the bottom. Strange quarks are generated with a point source and both propagators are contracted with a point sink. The data are obtained on the coarse 24^3 ensemble with $am_l = 0.005$ using $am_s^{\text{sim}} = 0.03224$ and $am_c^{\text{sim}} = 0.400$.

the estimator of the unknown parameter θ obtained using all available observations $X = \{X_1, X_2, \cdots, X_N\}$, let θ_i be the given statistic but based on the subset of observations $\{X_1, \cdots, X_{i-1}, X_{i+1}, \cdots, X_N\}$ then the jackknife bias estimator is given by

$$b_{\text{jack}} = (N-1)\left(\frac{1}{N}\sum_{i=1}^{N}\theta_i - \hat{\theta}\right) \tag{5.12}$$

which leads to the bias reduced jackknife estimator of θ

$$\tilde{\theta}_{\text{jack}} = \hat{\theta} - b_{\text{jack}} = N\hat{\theta} - \frac{N-1}{N}\sum_{i=1}^{N}\theta_i = \frac{1}{N}\sum_{i=1}^{N}\Big(N\hat{\theta} - (N-1)\theta_i\Big) = \frac{1}{N}\sum_{i=1}^{N}\tilde{\theta}_i \tag{5.13}$$

which defines $\tilde{\theta}_i$. Tukey [141] conjectured that $\tilde{\theta}_i$, $i = 1, \cdots, N$ may be treated as though they were independently and identically distributed and that their variance can be used to estimate the variance of the original estimator. The jackknife variance estimator is

then given by

$$\sigma^2 \equiv \frac{N-1}{N}\sum_{i=1}^{N}\left(\theta_i - \frac{1}{N}\sum_{j=1}^{N}\theta_j\right)^2 \tag{5.14}$$

The results presented in the following chapter are quoted using $\langle\theta\rangle = \hat{\theta} \pm \sigma$

5.5.2 Super Jackknife method

The Super Jackknife method [137, 142] starts with M distinct uncorrelated ensembles, we denote by $\hat{\theta}^k$ the central value and by θ_n^k with $n = 1, \cdots, N_k$ the jackknife samples of the observable θ on the k^{th} ensemble of size N_k. We now construct $N = \sum_{k=1}^{M} N_k$ super jackknife samples of which the first N_1 are given by the columns of the following matrix:

$$\begin{bmatrix} \hat{\theta}^1 & \theta_1^1 & \theta_2^1 & \cdots & \theta_{N_1-1}^1 & \theta_{N_1}^1 \\ \hat{\theta}^2 & \hat{\theta}^2 & \hat{\theta}^2 & \cdots & \cdots & \hat{\theta}^2 \\ \hat{\theta}^3 & \hat{\theta}^3 & \hat{\theta}^3 & \cdots & \cdots & \hat{\theta}^3 \\ \vdots & \vdots & \vdots & \vdots & \ddots & \vdots \\ \hat{\theta}^{M-1} & \hat{\theta}^{M-1} & \hat{\theta}^{M-1} & \cdots & \cdots & \hat{\theta}^{M-1} \\ \hat{\theta}^M & \hat{\theta}^M & \hat{\theta}^M & \cdots & \cdots & \hat{\theta}^M \end{bmatrix}, \tag{5.15}$$

the next N_2 are the columns of

$$\begin{bmatrix} \hat{\theta}^1 & \hat{\theta}^1 & \hat{\theta}^1 & \cdots & \cdots & \hat{\theta}^1 \\ \hat{\theta}^2 & \theta_1^2 & \theta_2^2 & \cdots & \theta_{N_2-1}^2 & \theta_{N_2}^2 \\ \hat{\theta}^3 & \hat{\theta}^3 & \hat{\theta}^3 & \cdots & \cdots & \hat{\theta}^3 \\ \vdots & \vdots & \vdots & \vdots & \ddots & \vdots \\ \hat{\theta}^{M-1} & \hat{\theta}^{M-1} & \hat{\theta}^{M-1} & \cdots & \cdots & \hat{\theta}^{M-1} \\ \hat{\theta}^M & \hat{\theta}^M & \hat{\theta}^M & \cdots & \cdots & \hat{\theta}^M \end{bmatrix}, \tag{5.16}$$

and in general we will get the k^{th} set of super jackknife samples from the columns of

$$\begin{bmatrix} \hat{\theta}^1 & \hat{\theta}^1 & \hat{\theta}^1 & \cdots & \cdots & \hat{\theta}^1 \\ \hat{\theta}^2 & \hat{\theta}^2 & \hat{\theta}^2 & \cdots & \cdots & \hat{\theta}^2 \\ \vdots & \vdots & \vdots & \vdots & \ddots & \vdots \\ \hat{\theta}^{k-1} & \hat{\theta}^{k-1} & \hat{\theta}^{k-1} & \cdots & \cdots & \hat{\theta}^{k-1} \\ \hat{\theta}^k & \theta_1^k & \theta_2^k & \cdots & \theta_{N_k-1}^k & \theta_{N_k}^k \\ \hat{\theta}^{k+1} & \hat{\theta}^{k+1} & \hat{\theta}^{k+1} & \cdots & \cdots & \hat{\theta}^{k+1} \\ \vdots & \vdots & \vdots & \vdots & \ddots & \vdots \\ \hat{\theta}^{M-1} & \hat{\theta}^{M-1} & \hat{\theta}^{M-1} & \cdots & \cdots & \hat{\theta}^{M-1} \\ \hat{\theta}^M & \hat{\theta}^M & \hat{\theta}^M & \cdots & \cdots & \hat{\theta}^M \end{bmatrix}. \tag{5.17}$$

That is, if there are two ensembles A and B of size $N_A = 100$ and $N_B = 20$, respectively, then the jth superjackknife block for $j < 100$ is built using the jth sample of ensemble A and the central value of B, if $j > 100$ then the super jackknife block is constructed using the central value of A and the jackknife sample j-100 of ensemble B. If the super jackknife blocks, $\tilde{a}$, are used for a fitting procedure then one minimizes the function

$$\begin{aligned}\chi^2_j = &\sum_{\alpha=1}^{N_A}\sum_{\beta=1}^{N_A}(y(\{x\}^A)_\alpha - \tilde{a}^A_{\alpha,j})(y(\{x\}^A)_\beta - \tilde{a}^A_{\beta,j})(C^A)^{-1}_{\alpha\beta} \\ &+ \sum_{\alpha=1}^{N_B}\sum_{\beta=1}^{N_B}(y(\{x\}^B)_\alpha - \tilde{a}^B_{\alpha,j})(y(\{x\}^B)_\beta - \tilde{a}^B_{\beta,j})(C^B)^{-1}_{\alpha\beta}\end{aligned} \tag{5.18}$$

where $y(\{x\})$ is a model function with parameters $\{x\}$ which might be ensemble dependent, the index j denotes the number of the super jackknife block and the covariance matrix is defined as

$$C^A_{\alpha\beta} = \frac{1}{N_A - 1}\langle(\tilde{a}^A_{\alpha,j} - \langle\tilde{a}^A_\alpha\rangle)(\tilde{a}^A_{\beta,j} - \langle\tilde{a}^A_\beta\rangle)\rangle. \tag{5.19}$$

The super jackknife method takes the correlations within each ensemble correctly into account, and implicitly sets correlations amongst different ensembles to zero. In the limit case in which $M = 1$ it reduces to the regular jackknife method discussed in the previous section.

5.6 Conclusion

In this chapter we have introduced the setup that we used for the generation of two- and three-point functions necessary for the extraction of form factors using the ratio method discussed in Section 4.1. We have also discussed the statistical methods that will be central for our data analysis and the extraction of results on Chapter 6.

Chapter 6

Results

6.1 Introduction

In this chapter we present our final results. We begin in section 6.2 by determining the effective masses of the B_s, D_s, K and ϕ mesons. We then divide the rest of this chapter into two main sections which discuss our results for the Standard Model tree-level decays $B_s \to K\ell\nu$ and $B_s \to D_s\ell\nu$, section 6.3, and the rare decay $B_s \to \phi\ell^+\ell^-$, section 6.4. These two sections have the same structure, we begin by determining the flavour conserving renormalization factor Z_V^{bb}, we then use this result to renormalise our improved vector and tensor currents. Then we discuss the process to perform the chiral-continuum extrapolation of our results and finally we introduce the z-expansion which we use to extrapolate our continuum results to $q^2 = 0$.

6.2 Effective Mass fits

In section 4.1 we have shown that in order to extract the form factors f_0, f_+, f_V, f_{A_0}, f_{A_1}, f_{A_2}, f_{T_1}, f_{T_2} and f_{T_3} we need to compute ratios of two point and three point functions (4.1) and (4.2). Given that these ratios involve meson masses and energies, we will start by computing these values for all the mesons involved in the decays we are interested in, namely, $B_s \to K\ell\nu$, $B_s \to D_s\ell\nu$ and $B_s \to \phi\ell^+\ell^-$. At sufficiently large lattice times the effective mass ($\vec{p} = 0$) and energies ($\vec{p} \neq 0$) for meson X can be extracted from its two-point function C_{XX} (3.65) using the formula

$$E(t,\vec{p}) = \cosh^{-1}\left[\frac{C_{XX}(t,\vec{p}) + C_{XX}(t+2,\vec{p})}{2C_{XX}(t+1,\vec{p})}\right]. \tag{6.1}$$

The result of applying (6.1) yields a value for the effective mass/energy for each time slice, we then perform correlated, constant in time fits minimizing

$$\chi^2 = (E(\Delta t, \vec{p})_\alpha - E_{\text{fit}}) C^{-1}_{\alpha\beta} (E(\Delta t, \vec{p})_\beta - E_{\text{fit}}). \tag{6.2}$$

where $E(\Delta t, \vec{p})$ means that we are summing terms $E(t, \vec{p})$ in the range Δt. The fitting range Δt is chosen so that there is no visible excited state contamination and where we obtain acceptable χ^2 per degree of freedom and p values, the exceptions are the B_s and ϕ meson masses on the $am_l = 0.004$ where p values of 6% and 1.06% were obtained respectively. We keep these values since we impose the same fit ranges for all ensembles with the same lattice spacing. Fitting ranges for the 32^3 ensembles are obtained by scaling our choices on 24^3 using the ratio of the lattice spacings. In Figure 6.1 we show results for effective mass fits on the $a^{-1} = 1.785(5)$ GeV ensemble with $am_l = 0.005$ together with the dependence of the effective mass on the starting time slice used for the fit. Numerical results for all other ensembles are given in Tables 6.1—6.3. Where available our results fully agree with previous published RBC/UKQCD results [135]. In lattice simulations the quality of the signal is reduced as the momentum of the meson is increased, it is convenient then to use either the continuum dispersion relation

$$E^2 = m^2 + |\vec{p}|^2 \tag{6.3}$$

or the lattice dispersion relation

$$E = 2a^{-1} \sinh^{-1} \sqrt{\sinh^2\left(\frac{am}{2}\right) + \sum_{i=1}^{3} \sin^2\left(\frac{ap_i}{2}\right)} \tag{6.4}$$

together with the effective mass obtained from (6.1) and (6.2) to extract effective energies. In figure 6.2 we show a comparison of the pion, kaon, ϕ and D_s meson energies with continuum-limit expectations, we see deviations from continuum-limit expectations for the D_s meson, but the lattice dispersion relation gives a good description of all the meson energies studied. Residual cutoff effects will vanish once we extrapolate to the continuum limit.

	Kaon				ϕ meson			
am_l	$[t_{min}, t_{max}]$	aM_K	χ^2/dof	p	$[t_{min}, t_{max}]$	aM_ϕ	χ^2/dof	p
0.005	[12, 23]	0.30576(45)	1.35	19%	[12, 22]	0.5914(28)	1.27	24%
0.010	[12, 23]	0.32670(43)	0.80	63%	[12, 22]	0.6079(29)	0.36	97%
0.004	[16, 29]	0.22419(45)	1.22	25%	[16, 29]	0.4412(24)	2.11	1%
0.006	[16, 29]	0.23412(34)	0.58	89%	[16, 29]	0.4508(22)	0.40	97%
0.008	[16, 29]	0.24089(42)	1.13	32%	[16, 29]	0.4486(27)	0.84	62%

Table 6.1: Kaon and ϕ meson masses on all ensembles

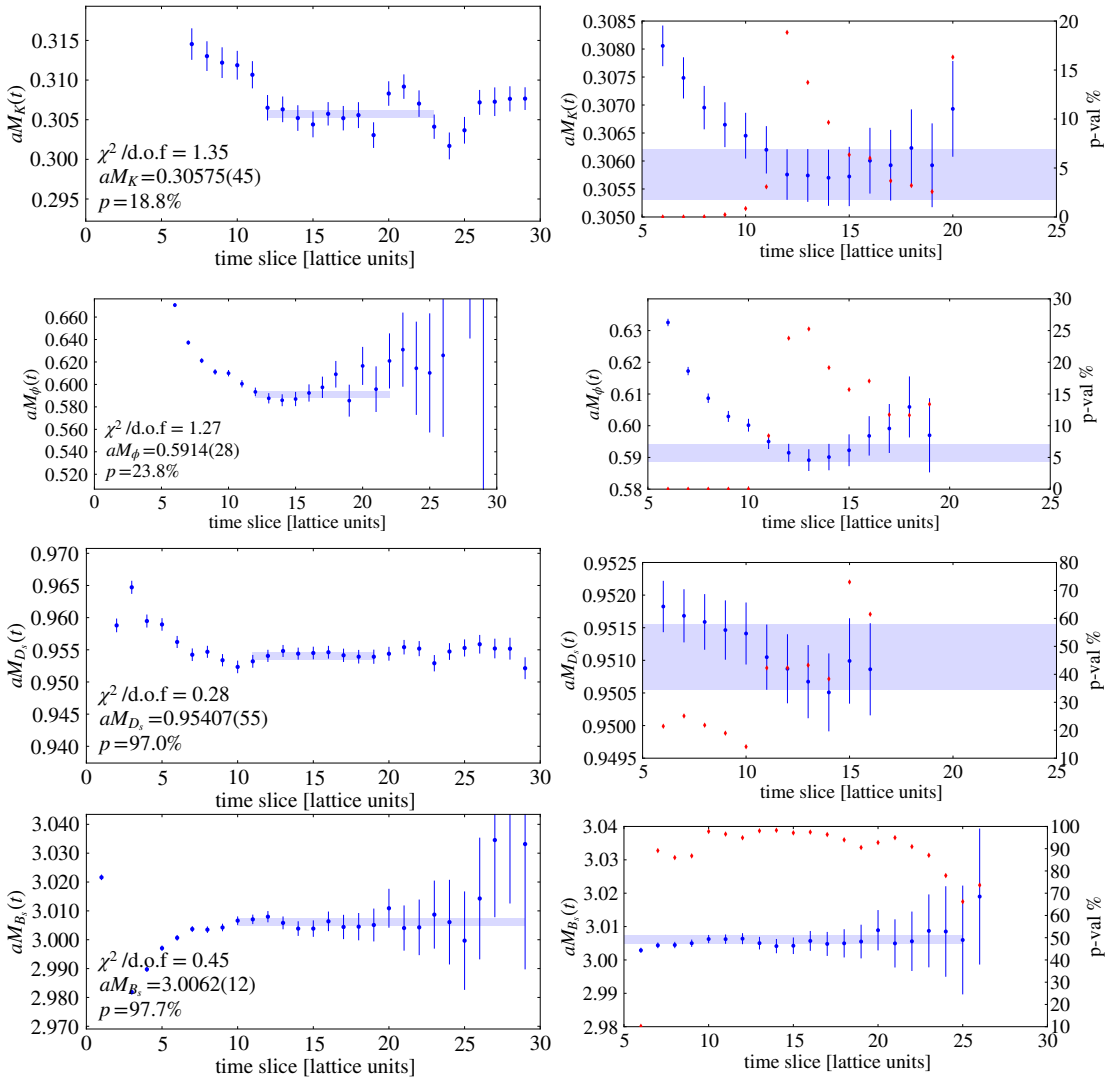

Figure 6.1: From top to bottom: (left) effective mass plots for the kaon, ϕ meson , D_s meson (with unphysical $am_c = 0.350$) and B_s meson on the $a^{-1} = 1.785$GeV ensemble with $am_l = 0.005$, (right) dependence of the effective mass on the starting time slice with a fixed final time, the shaded band indicates the preferred fit, red diamonds indicate p-value.

6.3 Semileptonic decays $B_s \to D_s \ell\nu$ and $B_s \to K\ell\nu$

6.3.1 Operator renormalization and improvement

As discussed in Section 4.3 operator renormalization requires the determination of the perturbative coefficient ρ (4.26), and the flavour-conserving renormalization factors Z^{ll} (4.28) and Z^{bb} (4.27). The flavour conserving renormalization factor Z^{ll} is taken from [11] and we determine Z^{bb} from the matrix element of the $b \to b$ vector current between two B_s mesons following [143]. We reduce discretization errors in the heavy-light/charm vector current by improving it through $\mathcal{O}(\alpha_s a)$. The temporal and spatial $\mathcal{O}(a)$ vector

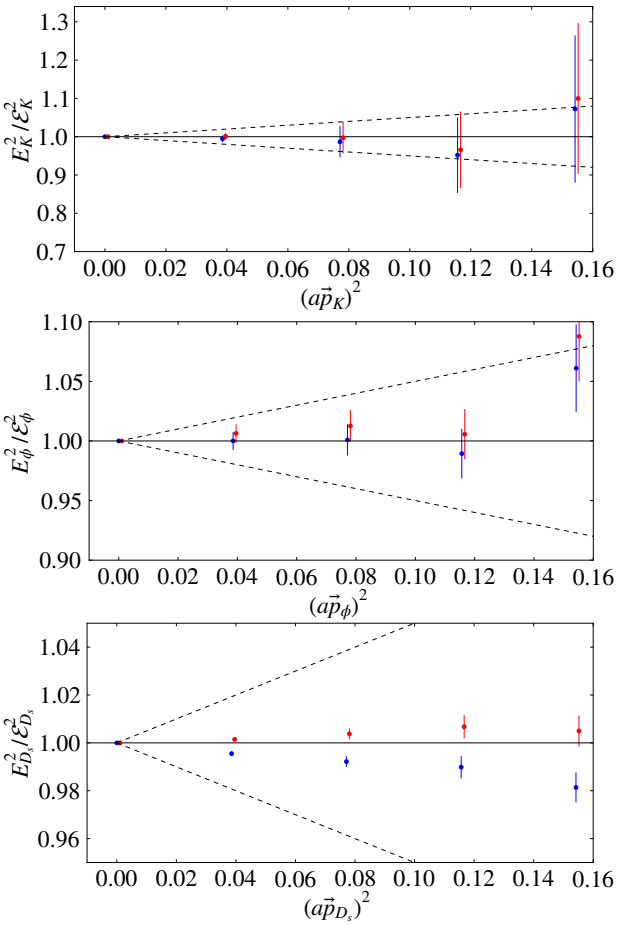

Figure 6.2: From top to bottom: Comparison of the kaon, ϕ and D_s $am_c = 0.280$ meson energies with continuum-limit and lattice dispersion relation expectations on the $a^{-1} = 2.383(9)$ GeV ensemble with $am_l = 0.004$. E indicates energy from fit to (6.2) and $\mathcal{E}$ indicates energy using the dispersion relation. Blue points are obtained using the continuum dispersion relation (6.3) and red points using the lattice dispersion relation (6.4). The dashed lines show a power counting estimate of the leading order $\mathcal{O}((a\vec{p})^2)$ momentum dependent discretization errors.

current operators needed are given by the following sums [135]

$$V_0^{\text{imp}}(x) = V_0^0(x) + c_t^3 V_0^3(x) + c_t^4 V_0^4(x), \tag{6.5}$$

$$V_i^{\text{imp}}(x) = V_i^0(x) + c_s^1 V_i^1(x) + c_s^2 V_i^2(x) + c_s^3 V_i^3(x) + c_s^4 V_i^4(x). \tag{6.6}$$

We obtain the values of the coefficients c_t^n and c_s^n at one loop using mean-field improved lattice perturbation theory [15] evaluated at the $\overline{\text{MS}}$ coupling $\alpha_s^{\overline{\text{MS}}}(a^{-1})$. Results for operator renormalization factors and the improvement coefficients are shown in Tables 6.5, 6.4, respectively.

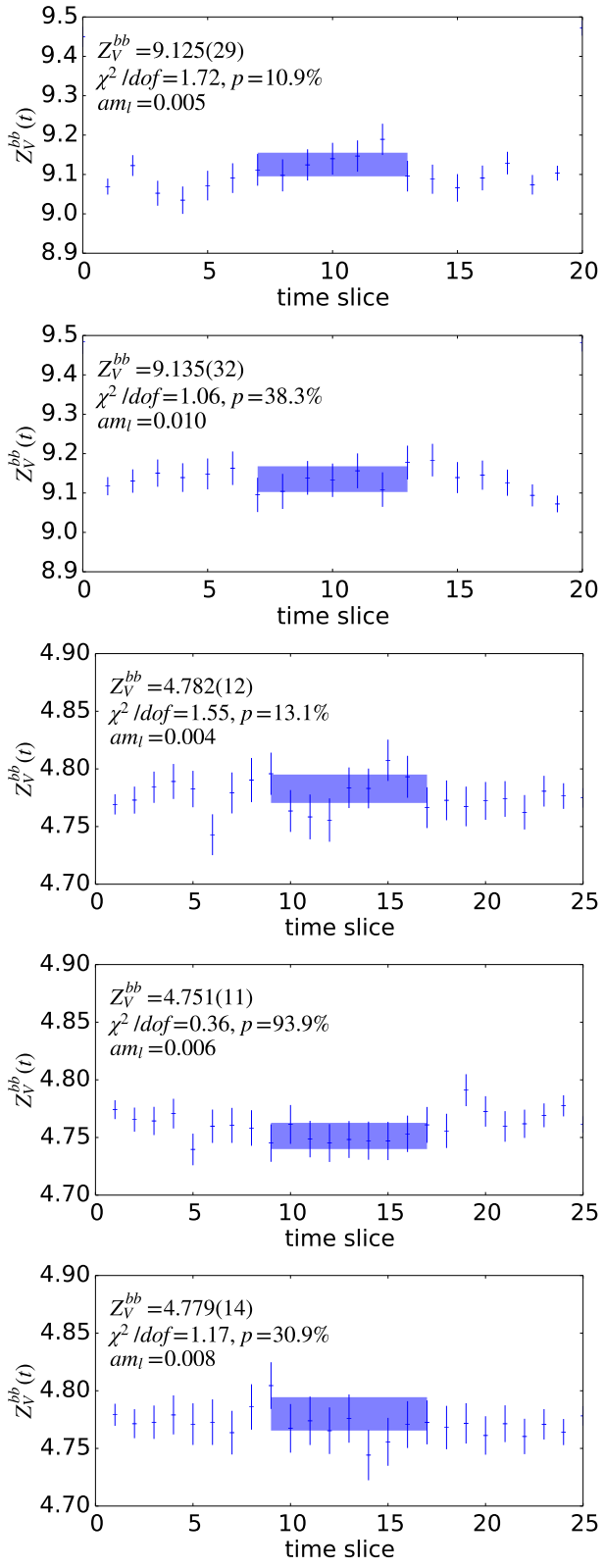

Figure 6.3: Determination of Z^{bb} from correlated constant in time fits to the ratio (4.27).

a^{-1}[GeV]	am_l	am_c	$[t_{min}, t_{max}]$	aM_{D_s}	χ^2/dof	p
1.785	0.005	0.30	[11, 19]	0.87681(44)	1.07	38%
		0.35	[11, 19]	0.95105(50)	1.01	42%
		0.40	[11, 19]	1.02188(54)	0.92	49%
1.785	0.010	0.30	[11, 19]	0.87957(51)	0.34	95%
		0.35	[11, 19]	0.95407(55)	0.28	97%
		0.40	[11, 19]	1.02505(60)	0.26	97%
2.383	0.004	0.28	[15, 25]	0.76789(51)	1.24	25%
		0.34	[15, 25]	0.85462(57)	1.25	25%
2.383	0.006	0.28	[15, 25]	0.76941(41)	1.00	43%
		0.34	[15, 25]	0.85611(46)	0.90	53%
2.383	0.008	0.28	[15, 25]	0.77010(57)	0.44	93%
		0.34	[15, 25]	0.85689(64)	0.48	90%

Table 6.2: D_s meson masses on all ensembles

	B_s			
am_l	$[t_{min}, t_{max}]$	aM_{B_s}	χ^2/dof	p
0.005	[10, 29]	3.0062(12)	0.45	98%
0.010	[10, 29]	3.0072(14)	1.11	33%
0.004	[13, 29]	2.2515(11)	1.58	6%
0.006	[13, 29]	2.25274(95)	0.55	92%
0.008	[13, 29]	2.2541(13)	0.95	51%

Table 6.3: B_s meson masses on all ensembles

Table 6.4: Operator renormalization factors. The flavour conserving factor Z_V^{ll} was obtained non-perturbatively in [11]. We determine Z_V^{bb} from a weighted average of the result of correlated fits to (4.27) on our ensembles —c.f Figure 6.3—. We compute the ρ factor at one loop in mean-field improved lattice perturbation theory using $\alpha_s^{\overline{MS}}(a^{-1})$ [15].

a^{-1} [GeV]	Z_V^{ll}	Z_V^{bb}	$\alpha_s^{\overline{\text{MS}}}(a^{-1})$	ρ_{V_0}	ρ_{V_i}
1.785(5)	0.71273(26)	9.130(21)	0.23	1.02518	0.99653
2.383(9)	0.74404(181)	4.768(11)	0.22	1.01535	0.99358

Table 6.5: Improvement coefficients. We compute the matching coefficients c_i^n at one loop in mean-field improved lattice perturbation theory using $\alpha_s^{\overline{MS}}(a^{-1})$ [15].

a^{-1} [GeV]	$\alpha_s^{\overline{\text{MS}}}(a^{-1})$	c_t^3	c_t^4	c_s^1	c_s^2	c_s^3	c_s^4
1.785(5)	0.23	0.0562	−0.010	−0.00088	0.0017	0.0489	−0.0031
2.383(9)	0.22	0.0545	−0.0094	−0.0013	0.00031	0.0479	−0.0019

6.3.2 The form factors $f_\parallel$ and $f_\perp$ at finite lattice spacing

Having extracted the effective masses and energies of the Kaon, D_s and B_s mesons, we can now use (4.5) and (4.6) to obtain the form factors $f_\parallel$ and $f_\perp$, respectively. We

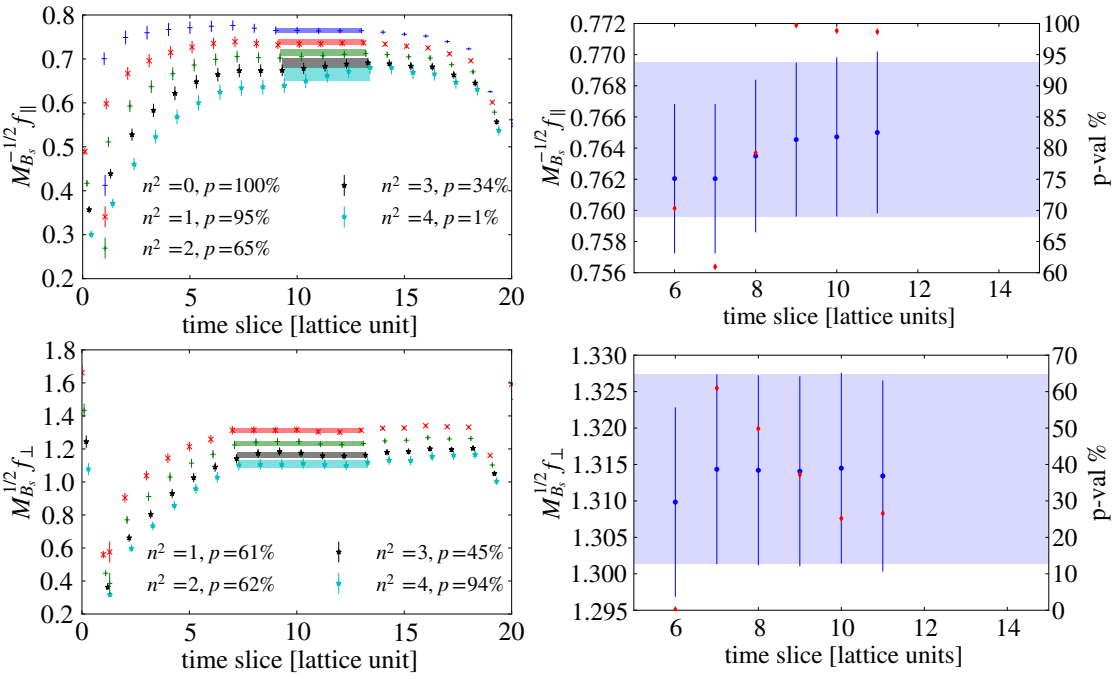

Figure 6.4: From top to bottom $B_s \to D_s \ell\nu$ form factors $f_{\parallel}$ and $f_{\perp}$, (left) form factors as a function of time on the $a^{-1} = 1.785(5)$ GeV ensemble with $am_l = 0.005$ and $am_c = 0.300$. (right) dependence of the form factor on the starting time slice with a fixed final time $t = 13$ at the smallest momentum $f_{\parallel} : n = 0$, $f_{\perp} : n = 1$. The shaded band indicates the preferred fit with error, red diamonds indicate p-value.

present the results of performing correlated, constant in time fits to (4.5) and (4.6) in Figure 6.4, and Tables B.1—B.3. We choose our fitting range for a given form factor on the $a^{-1} = 1.785(5)$ GeV ensembles using the following procedure: for the smallest allowed momentum we pick the right most time slice we consider unaffected by excited state contamination and then we analyse how the p-value is affected by varying the initial time slice included in the fit. Our goal is to choose the largest possible plateau with a sensible p-value. Having determined the best fitting range for a given form factor at the smallest momentum we apply this same range for all momenta removing the bias that will rise if the fitting range for each momentum is found by visual inspection. Within our fitting ranges contamination from excited states is not visible. Fitting ranges for the 32^3 ensembles are obtained by scaling our choices on 24^3 using the ratio of the lattice spacings. These procedure returns p values in the range $[20\%, 100\%]$ on 80% of the fitted quantities.

6.3.2.1 Charm mass extrapolation

As discussed in section 5.3.2 the results of our simulation of $B_s \to D_s \ell\nu$ decays are two-point and three-point functions obtained with unphysical charm like quark masses —c.f. Table 5.2 for the details—, meaning that we must extra-/interpolate the form factors

Table 6.6: Fits to the non-perturbative flavour-conserving factor Z_V^{bb} on all ensembles

a^{-1}[GeV]	m_l	Z_v^{bb}	χ^2/dof	p
1.785(5)	0.005	9.152(29)	1.72	10.9%
1.785(5)	0.010	9.135(32)	1.06	38.3%
2.383(9)	0.004	4.782(12)	1.55	13.1%
2.383(9)	0.006	4.751(11)	0.36	93.9%
2.383(9)	0.008	4.779(14)	1.17	30.9%

obtained in the previous section to the physical charm mass $M_{D_s} = 1.969(14)$ GeV. We begin by plotting the form factors as a function of the corresponding unphysical D_s mass and units of momentum squared $n^2 = (\vec{p}L/(2\pi))^2$ —c.f Fig. 6.5— The points look close to being on a plane; hence we try a first order expansion in the D_s mass and momentum

$$\begin{aligned} f(q^2(M_{D_s}+\delta M_{D_s}, |\vec{p}|^2+\delta|\vec{p}|^2); M_{D_s}+\delta M_{D_s}) = f(q^2(M_{D_s}+|\vec{p}|^2), M_{D_s}) \\ + \frac{\partial f}{\partial q^2}\left(\frac{\partial q^2}{\partial M_{D_s}}\delta M_{D_s} + \frac{\partial q^2}{\partial |\vec{p}|^2}\delta|\vec{p}|^2\right) \\ + \frac{\partial f}{\partial M_{D_s}}\delta M_{D_s} \end{aligned} \tag{6.7}$$

where $|\vec{p}| = 2\pi n/L$, L is the lattice size and n are units of momentum. From the above discussion our first fit ansatz is given by the function:

$$f(M_{D_s}, n^2) = c_0 + c_1 M_{D_s} + c_2 n^2 \quad \text{Type I} \tag{6.8}$$

where we have absorbed a factor of $(2\pi/L)^2$ in c_2. We also perform the following fits to study systematic effects due to our choice of expansion

$$f(M_{D_s}, n^2) = c_0 + c_1 M_{D_s} + c_2 n^2 + c_3 M_{D_s} n^2 \quad \text{Type II} \tag{6.9}$$

$$f(M_{D_s}, n^2) = c_0 + c_1 M_{D_s} + c_2 n^2 + c_3 (n^2)^2 \quad \text{Type III} \tag{6.10}$$

$$f(M_{D_s}, n^2) = c_0 + c_1 M_{D_s} + c_2 n^2 + c_3 M_{D_s} n^2 + c_4 (n^2)^2 \quad \text{Type IV} \tag{6.11}$$

The results for fits of Type I, II, III and IV for improved form factors are shown in Tables B.7 and B.8 , given that the smallest χ^2/dof is obtained for type IV (6.11) fits we extrapolate to physical charm using this fit and use types I, II and III to estimate the systematics due to the charm extrapolation.

6.3.3 $B_s \to K\ell\nu$ form factors chiral-continuum extrapolation

As discussed in section 2.5 chiral symmetry undergoes an explicit breaking due to the nonzero mass of light and strange quarks giving rise to the pseudo-Goldstone bosons

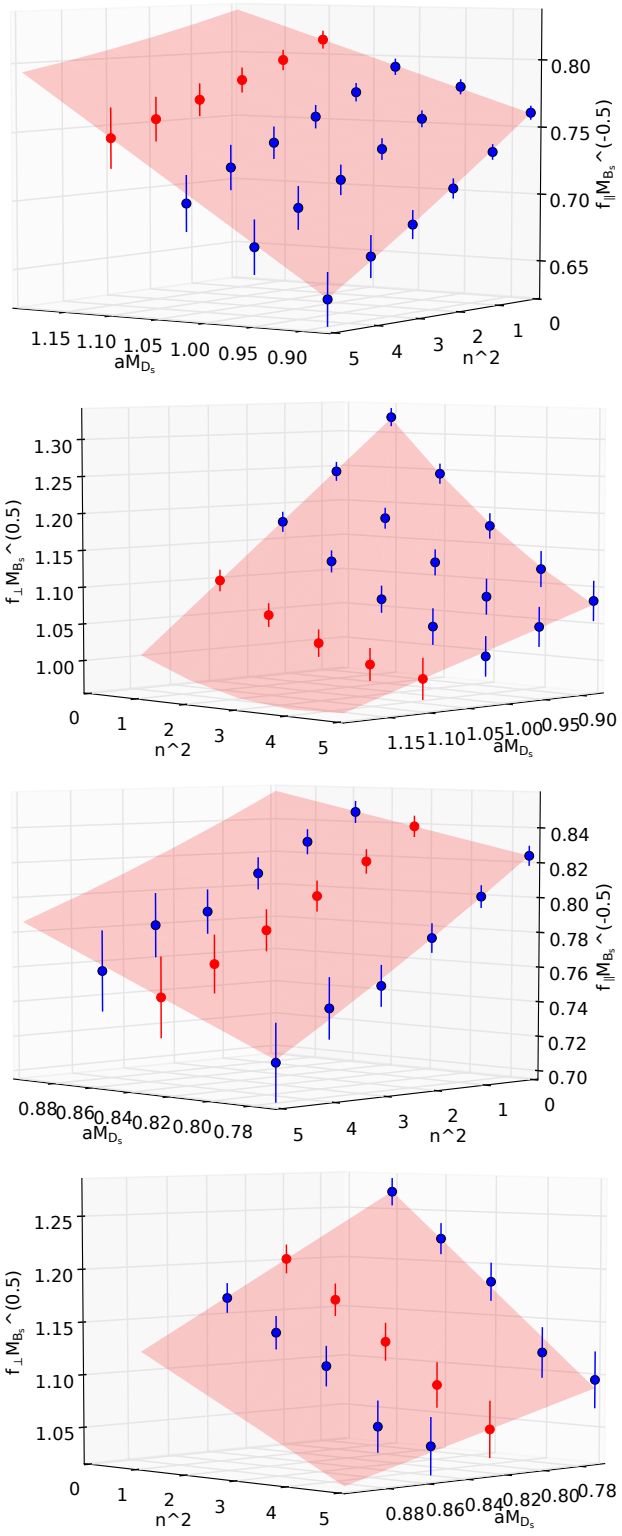

Figure 6.5: Form factors $f_{\|}$ and $f_{\perp}$ as a function of the mass of the D_s meson and units of momentum squared n^2, the top two plots are for the $a^{-1} = 1.785(5)$ GeV ensemble with $am_l = 0.005$ and the bottom two plots are for the $a^{-1} = 2.383(9)$ GeV ensemble with $am_l = 0.006$. The shaded surface indicates our chosen fit function (6.11)

$\pi^{\pm}$, π^0, $K^{\pm}$, K^0, $\bar{K}^0$ and η. The low-momentum strong interactions of these pseudo-Goldstone bosons are described by the effective Lagrangian [52]

$$\mathcal{L} = \frac{f_\pi^2}{8} \operatorname{Tr}\left[\partial^\mu \Sigma \partial_\mu \Sigma^\dagger\right] + v \operatorname{Tr}\left[\Sigma^\dagger \mathcal{M} + \mathcal{M}^\dagger \Sigma\right] \tag{6.12}$$

where v is an independent coefficient

$$\mathcal{M} = \operatorname{diag}(m_u, m_d, m_s), \tag{6.13}$$

Σ is given in (2.42) and f_π is the pion decay constant. The inclusion of heavy-light mesons in chiral perturbation theory requires the inclusion of heavy quark spin symmetry. This is achieved by introducing the field [144–146]

$$H_a(v) = \frac{1+\not{v}}{2}\left[B_\mu^{*a}(v)\gamma_\mu - B^a(v)\gamma_5\right], \tag{6.14}$$

where B^a and B_μ^{*a} are pseudoscalar and vector heavy-light mesons, a indicates the flavour of the light quark and the factor $(1+\not{v})/2$ projects out the particle component of the heavy quark only. The heavy meson superfield (6.14) transforms as $H_a \to S H_a$ and $H_a \to H_b U_{ba}^\dagger$ under $SU(2)$ spin transformations S and $SU(3)$ flavour transformations U. We can now write the HMχPT Lagrangian to lowest order in the chiral and $1/M_B$ expansion as [144–146]

$$\begin{aligned}\mathcal{L} = &-i \operatorname{Tr}\left(\bar{H}_a v_\mu \partial^\mu H_a\right) + \frac{i}{2}\operatorname{Tr}\left(\bar{H}_a v_\mu [\xi^\dagger \partial^\mu \xi + \xi \partial^\mu \xi^\dagger]_{ab} H_b\right) \\ &+ \frac{ig}{2}\operatorname{Tr}\left(\bar{H}_a \gamma_\mu \gamma_5 [\xi^\dagger \partial^\mu \xi - \xi \partial^\mu \xi^\dagger]_{ab} H_b\right)\end{aligned} \tag{6.15}$$

where the traces are on Dirac space, $\xi = \sqrt{\Sigma}$, v is the four velocity of the heavy meson, $\bar{H}_a(v) = \gamma_0 H_a^\dagger(v)\gamma_0$, and g is the coupling of the heavy meson to the Goldstone boson. The HMχPT Lagrangian (6.15) contains both heavy meson superfields and pseudo-Goldstone bosons, coupled together in an $SU(3)_L \times SU(3)_R$ invariant way [147]. This Lagrangian can then be used to determine the one loop chiral correction for $B_s \to K\ell\nu$ form factors which take the form

$$\delta f = -\frac{3}{4} M_\pi^2 \log\left(\frac{M_\pi^2}{\Lambda^2}\right) \tag{6.16}$$

while this chiral logarithm is dominant in the limit of very small light quark masses it is unlikely that for physical Kaons this is the case, it may however give an indication of the magnitude of $SU(3)$ violation [147]. The NLO SU(2) hard-kaon HMχPT expression that we will use to extrapolate the renormalized lattice form factors to the physical light

Table 6.7: Coefficients for the chiral-continuum extrapolation of the form factors $f_\parallel$ and $f_\perp$ for the $B_s \to K\ell\nu$ decay obtained from correlated fits to (6.17).

	c_0	c_1	c_2	c_3	c_4	χ^2/dof	p
$M_{B_s}^{-1/2} f_\parallel$	0.929(62)	0.692(251)	0.587(224)	-0.331(161)	-0.007(3)	1.19	25%
$M_{B_s}^{1/2} f_\perp$	0.941(140)	0.181(199)	-0.358(318)	0.011(220)	-0.0020(28)	0.72	77%

quark mass and interpolate in the Kaon energy is given by [148, 149]

$$f_i^{B_s\to K}(M_\pi, E_K, a^2) = \frac{1}{E_K + \Delta_i} c_0 \left[1 + \left(\frac{\delta f}{(4\pi f)^2} + c_1 \frac{M_\pi^2}{\Lambda^2} + c_2 \frac{E_K}{\Lambda} + c_3 \frac{E_K^2}{\Lambda^2} + c_4 \frac{a^2}{\Lambda^2 a_{32}^4}\right)\right] \tag{6.17}$$

where $i = \{\parallel, \perp\}$ and the effects of resonances below the B_sK production threshold are accounted for by the inclusion of the poles $\Delta_\parallel = M_{B_s} - M_{B^*}(0^+)$ and $\Delta_\perp = M_{B_s} - M_{B^*}(1^-)$ where the $B^*(J^P)$ resonance corresponds to a state with flavour $b\bar{u}$ and quantum numbers $J^P = 0^+$ and 1^- for $f_\parallel$ and $f_\perp$, respectively. $\Delta_\parallel = 263$ MeV from the model estimate in [150] and $\Delta_\perp = -41.6$ MeV from experiment [151]. The pion decay constant has the value $f_\pi = 130.4$ MeV [151], $\Lambda = 1$ GeV is the scale associated with chiral symmetry breaking and the term proportional to a^2 in 6.17 accounts for the dominant lattice spacing dependence. Cut-off effects from Domain Wall Fermions and the Iwasaki action are $\mathcal{O}(a\Lambda_{QCD})^2$ using $\Lambda_{QCD} = 500$ MeV we estimate this to be $\sim 5\%$. The results of the chiral-continuum extrapolation are shown in Figure 6.6 and the fitting coefficients are given in Table 6.7. We also show in Figure 6.8 and discuss in section 6.3.5.1 the effect that different fits have on the central value of the chiral continuum extrapolation.

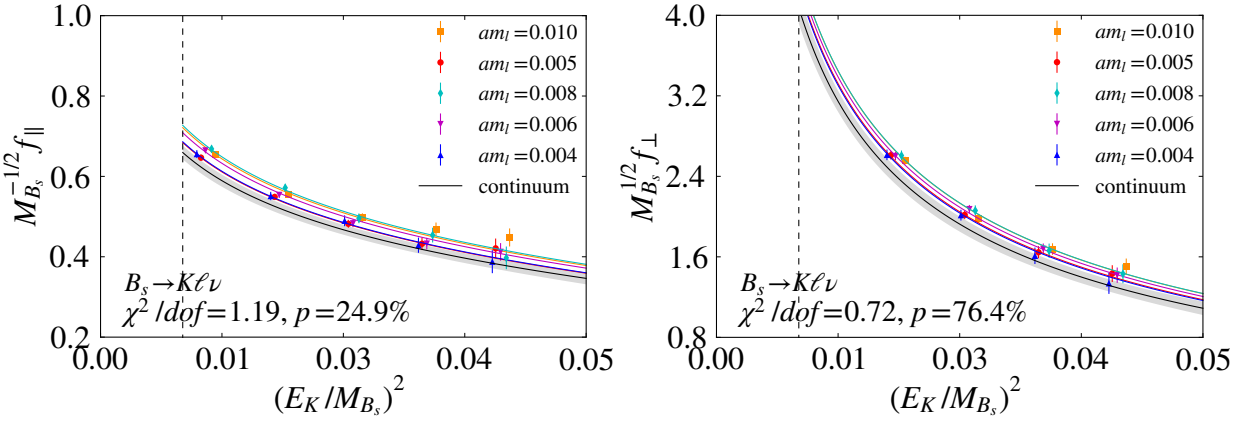

Figure 6.6: Chiral-continuum extrapolation of the $B_s \to K\ell\nu$ form factors — $f_\parallel$ (left) and $f_\perp$ (right)— from correlated fits using NLO SU(2) hard-Kaon HMχPT. The shaded band indicates statistical errors, the vertical dashed line on the left-hand side of each plot indicates where $E_{K_s} = M_{K_s}$.

Table 6.8: Coefficients for the continuum extrapolation of the form factors $f_\parallel$ and $f_\perp$ for the $B_s \to D_s \ell\nu$ decay obtained from an uncorrelated fit to (6.18).

	c_0	c_1	c_2	c_3	χ^2/dof
$M_{B_s}^{-1/2} f_\parallel$	0.516(81)	1.22(1.31)	1.48(34)	-8(5)	0.354
$M_{B_s}^{1/2} f_\perp$	0.694(91)	0.31(1.46)	1.77(27)	-6(4)	0.539

6.3.4 $B_s \to D_s \ell\nu$ form factors chiral continuum extrapolation

Having performed the extra-/interpolation to the physical charm individually on each ensemble, we now proceed to obtain the form factor shape using pole dominance, our ansatz is

$$f_i(q,a) = \frac{c_0 + c_1(\Lambda_{\rm QCD} a)^2}{1 - \left(c_2 + c_3 \Lambda_{QCD}^2 a^2\right) q^2 / M_{B_c^{(*)}}^2} \tag{6.18}$$

where $\Lambda_{\rm QCD} = 500$ MeV, $M_{B_c}^* = 6.330(9)$ GeV [152] and $M_{B_c} = 6.42(10)$ GeV [9]. Although the data obtained from the extra-/interpolation on a given ensemble is highly correlated, the correlation matrices have large condition numbers preventing their use in correlated fits. As a result we perform uncorrelated fits for the continuum extrapolation of the form factors $f_\parallel$ and $f_\perp$. Moreover, to improve the quality of the fit we have removed the ensemble with $am_l = 0.004$ from the fits of $B_s \to D_s \ell\nu$ form factors as this ensemble has shown behaviour which is not in line with that of the other two ensembles with $a^{-1} = 2.384(9)$ GeV. The resulting plots are shown in Figure 6.7 and the fitting coefficients are given in Table 6.8, we see a $> 6\%$ lattice spacing dependence at lowest momentum. Variation to our fitting ansatz are explained in section 6.3.5.1 and their effect on the central value of the fit are shown in Figure 6.9

6.3.5 Systematics

In this section we present the sources of systematic errors on the determination of the form factors of the $B_s \to K \ell\nu$ and $B_s \to D_s \ell\nu$ decays.

6.3.5.1 Chiral-continuum extrapolation

The systematic uncertainty due to the chiral-continuum extrapolation of the $B_s \to K$ form factors is obtained by applying the following changes to the chiral-continuum fit ansatz (6.17)

1. omitting the term proportional to a^2
2. omitting the term proportional to M_π^2
3. omitting terms proportional to a^2 and M_π^2

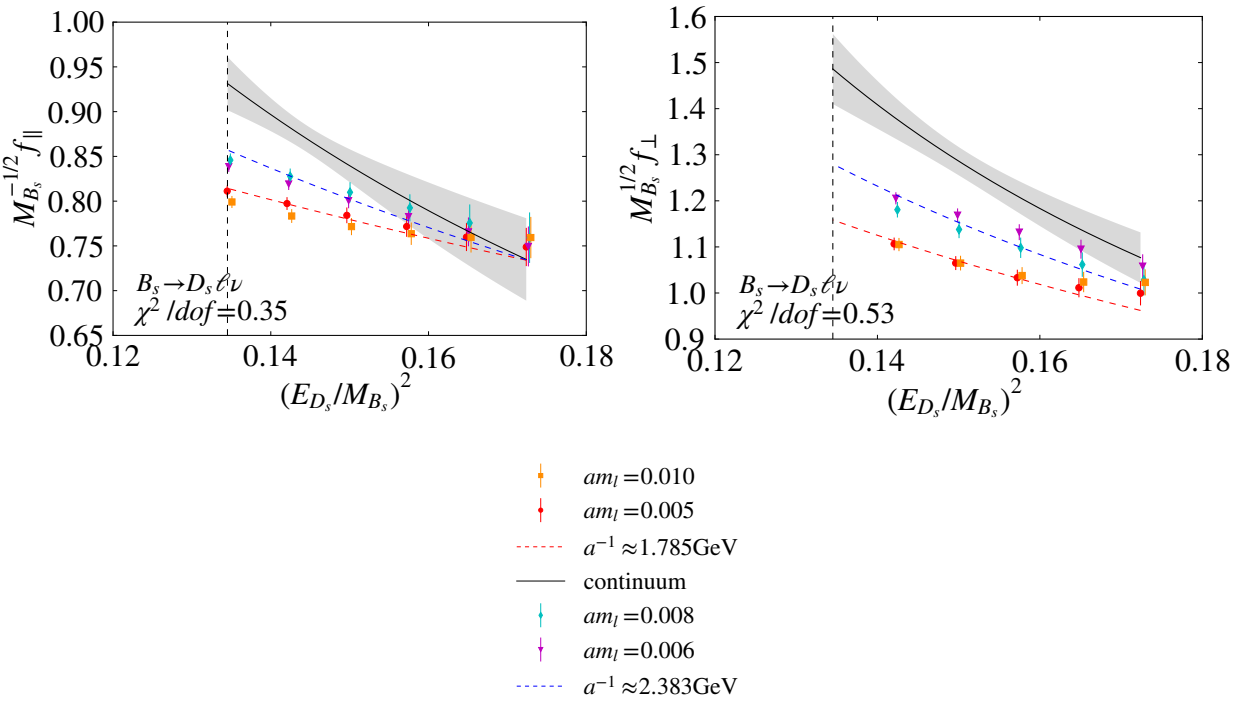

Figure 6.7: Continuum extrapolation using (6.18) and the main diagonal of the covariance matrix for the form factors $f_\parallel$ and $f_\perp$ of the $B_s \to D_s \ell\nu$ decay. The shaded band indicates statistical errors, the vertical dashed line on the left-hand side of each plot indicates where $E_{D_s} = M_{D_s}$.

4. analytic fits omitting the chiral logarithms
5. analytic fits omitting the chiral logarithms and the term proportional to a^2
6. varying the value of f_π in the coefficients of the chiral logarithms from f_0= 112 MeV [7] in the chiral limit to $f_K = 155.5$ MeV [151]
7. varying the scalar pole mass $M_{B^*}(0^+) = 5.63$ GeV in $f_0^{B_s K}$ by plus/minus 100 MeV
8. omitting the data point at zero momentum
9. omitting the data point at the highest momentum $\vec{p} = 2\pi/L(2,0,0)$
10. excluding ensembles with pion masses $M_\pi \gtrsim 400$ MeV.

For the $B_s \to D_s$ form factors we apply the following changes to (6.18)

1. replacing type IV charm extrapolation by types I, II and III (6.9)
2. omitting the data point at zero momentum
3. omitting the data point at the highest momentum $\vec{p} = 2\pi/L(2,0,0)$
4. including a term proportional to M_π^2 in the numerator of (6.18)

Figures 6.8 and 6.9 shows the relative changes of the form-factor central values under each fit variation

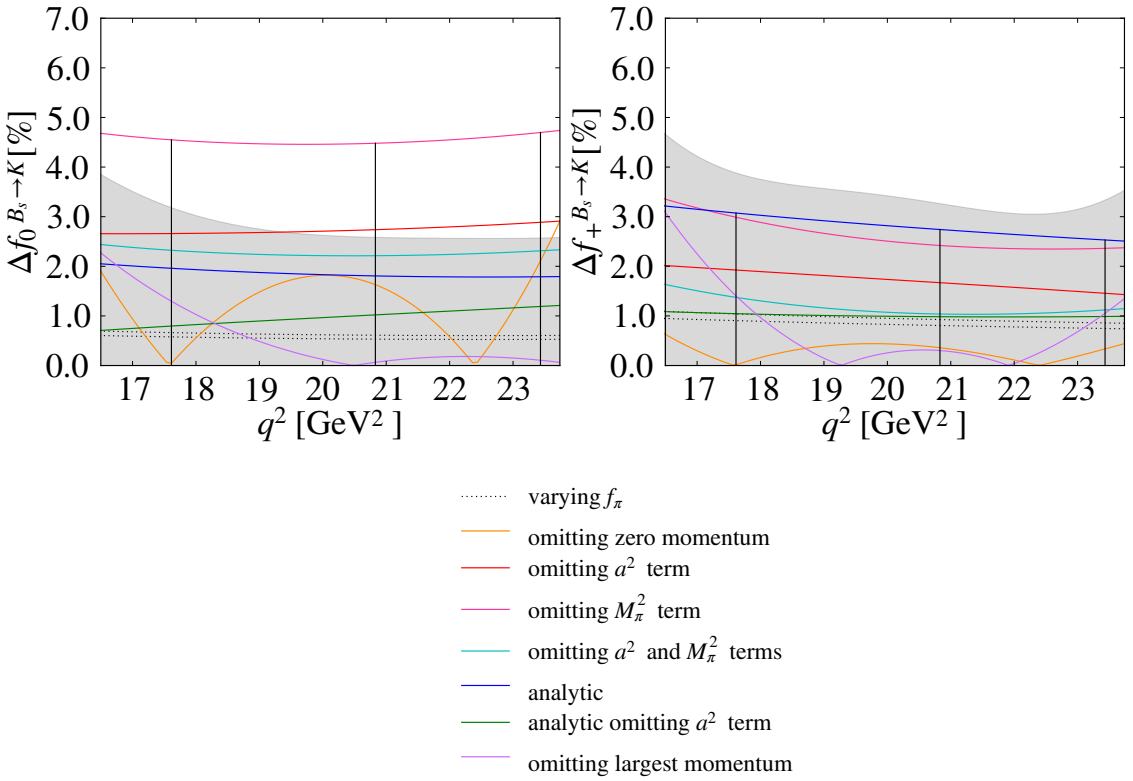

Figure 6.8: Relative change of the form-factor central value under the considered fit variations for $B_s \to K\ell\nu$. In each plot, the shaded band shows the statistical uncertainty of the preferred fit. The three vertical lines show the location of the synthetic data points used in the subsequent extrapolation to $q^2 = 0$.

$$\Delta f_i = |f_i^{\text{pref.}} - f_i^{\text{alt.}}|/f_i^{\text{pref.}}\,, \tag{6.19}$$

where $i = \{0, +\}$. For $B_s \to K$ decays the largest difference between our preferred fit and the alternative fits is obtained when the term proportional to M_π^2 is removed to (6.17) it accounts for a $\sim 5\%$ change for f_0 and $\sim 3\%$ for f_+. Omitting the chiral logarithms has an effect $\sim 2\%$ and $\sim 3\%$ for f_0 and f_+, respectively. Removing the a^2 term from (6.17) changes the central value of the f_0 and f_+ fits by $\sim 3\%$ and $\sim 2\%$. For $B_s \to D_s\ell\nu$ decays the largest difference between our preferred fit and alternative fits is obtained when the term proportional to M_π^2 is added to (6.18) and when we use as input for our fits Type III charm extrapolation (6.10). Given that there is no light valence quark content variation in the decay $B_s \to D_s\ell\nu$ it is not clear why adding a term proportional to M_π^2 would result in the largest systematic for this decay. Whether the observed change is due to a real effect such as a one-loop vertex correction, simulation noise, or a combination of these two factors requires further study and is beyond the scope of this work. We take the largest difference between our preferred fits (6.17) and

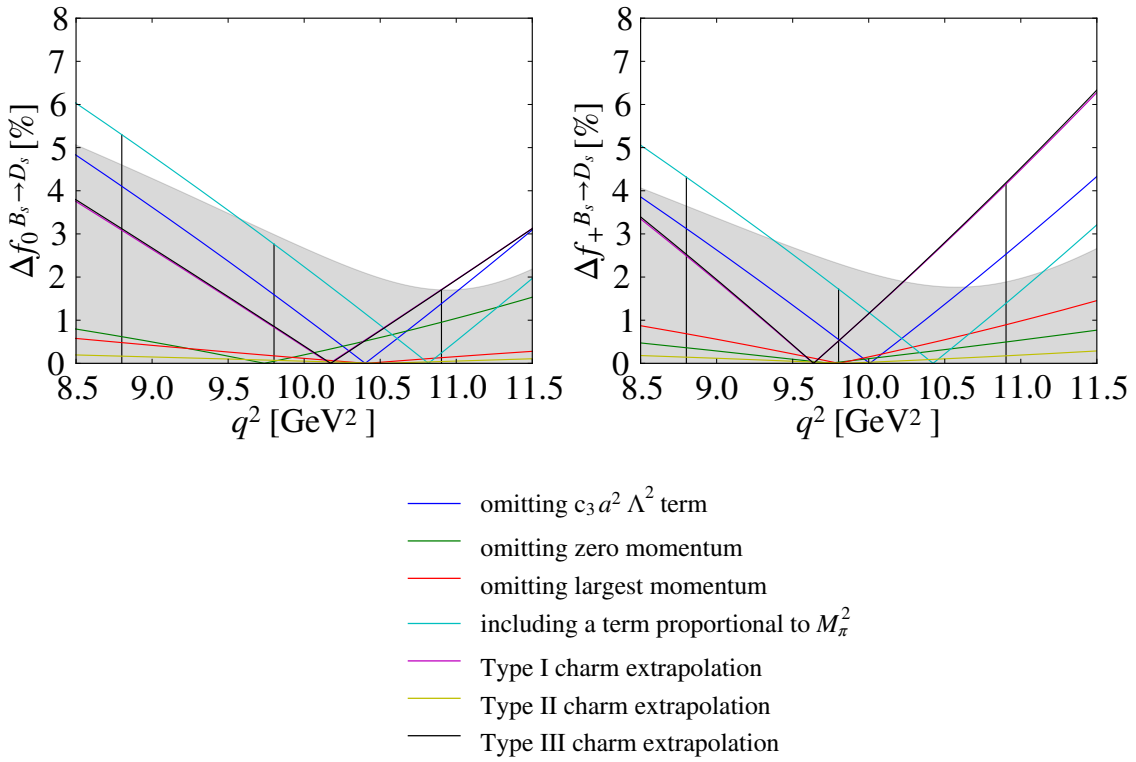

Figure 6.9: Relative change of the form-factor central value under the considered fit variations for $B_s \to D_s \ell\nu$. In each plot, the shaded band shows the statistical uncertainty of the preferred fit. The three vertical lines show the location of the synthetic data points used in the subsequent extrapolation to $q^2 = 0$.

$\{m_0 a, c_p, \zeta\}$	$\{7.420, 4.860, 2.920\}$
$\{m_0 a \pm \sigma_{m_0 a}, c_p, \zeta\}$	$\{7.420 \pm 0.180, 4.860, 2.920\}$
$\{m_0 a, c_p \pm \sigma_{c_p}, \zeta\}$	$\{7.420, 4.860 \pm 0.420, 2.920\}$
$\{m_0 a, c_p, \zeta \pm \sigma_\zeta\}$	$\{7.420, 4.860, 2.920 \pm 0.210\}$

Table 6.9: Seven sets of parameters used to estimate the systematic errors due to the implicit dependence of the RHQ parameters on the lattice spacing

(6.18) and any of the alternate fits as systematic uncertainty due to the chiral-continuum extrapolation.

6.3.5.2 Lattice-scale uncertainty

The implicit dependence on the lattice spacing through the parameters of the RHQ action $m_0 a, c_p, \zeta$ is estimated by computing the form factors $f_\parallel$ and $f_\perp$ for the seven sets of parameters shown in Table 6.9. We then perform uncorrelated two parameter fits to obtain the slopes $\Delta f/\Delta m_0 a$, $\Delta f/\Delta c_p$,$\Delta f/\Delta\zeta$. These slopes are then multiplied by the uncertainty in the corresponding RHQ parameter due to the lattice spacing in Table 5.3. We add the individual contributions from the three RHQ parameters in quadrature to obtain the total systematic error due to the lattice spacing. We obtain that the error

Table 6.10: Systematic error results due to the valence strange-quark mass dependence of the $B_s \to K\ell\nu$ and $B_s \to D_s\ell\nu$ form factors $f_\parallel$ and $f_\perp$ on the $a^{-1} = 1.785(5)$ GeV ensemble with $am_l = 0.005$, $\tilde{m}_s = m_s + m_{\rm res}$. Results are shown for final meson momenta $\vec{p}^2 = (2\pi\vec{n}/L)^2$.

	$B_s \to K\ell\nu$		$B_s \to D_s\ell\nu$	
n^2	$f_\parallel$	$f_\perp$	$f_\parallel$	$f_\perp$
0	0.00%		0.01%	
1	0.00%	0.05%	0.00%	0.00%
2	0.01%	0.04%	0.00%	0.00%
3	0.02%	0.04%	0.00%	0.00%
4	0.01%	0.03%	0.00%	0.01%

due to the lattice spacing for the $B_s \to K\ell\nu$ form factors is 1% both for $f_\parallel$ and $f_\perp$, and for the $B_s \to D_s\ell\nu$ form factor is 0.8% and 1.6% for $f_\parallel$ and $f_\perp$, respectively.

6.3.5.3 u/d - quark mass uncertainty

We estimate the error in the $B_s \to K\ell\nu$ form factors due to the u/d-quark mass uncertainty by varying $am_{u/d}$ by plus/minus one sigma. We observe a central value shift for f_0 and f_+ of 0.1%. For $B_s \to D_s\ell\nu$ form factors we estimate that the error due to the mass uncertainty of u/d-quark is negligible.

6.3.5.4 Valence strange-quark mass dependence

The strange quark masses employed in our simulations correspond to a mass at or near its physical value. To study the valence strange-quark mass dependence, we calculated the $B_s \to K\ell\nu$, $B_s \to D_s\ell\nu$ form factors on the $a^{-1} = 1.785(5)$ GeV, $am_l = 0.005$ ensemble with two additional spectator-quark masses of $am_s = 0.03$ and 0.04. Figure 6.10 shows the valence-quark mass dependence of the $B_s \to K\ell\nu$ and $B_s \to D_s\ell\nu$ form factors. We observe that all errors are below percent level —c.f Table 6.10— and hence negligible.

6.3.5.5 Heavy-quark discretization errors

In the region $m_0 a \sim 1$, the RHQ action leads to a nontrivial lattice-spacing dependence of physical quantities. We estimate the discretization errors of the heavy sector using HQET power counting. The $\mathcal{O}(a^2)$ errors from the action are obtained from the mismatch coefficients — i.e. coefficients needed so that lattice matrix element match their continuum counterpart — of the dimension 6 bilinears $\bar{b}\{\gamma \cdot \mathbf{D}, \alpha \cdot \mathbf{E}\}b$ and $\bar{b}\gamma_4(\mathbf{D} \cdot \mathbf{E} - \mathbf{E} \cdot \mathbf{D})b$ [143, 153]:

$$f_E(m_0, c_p, \zeta) = \frac{1}{8m_E^2 a^2} - \frac{1}{8m_2^2 a^2}, \tag{6.20}$$

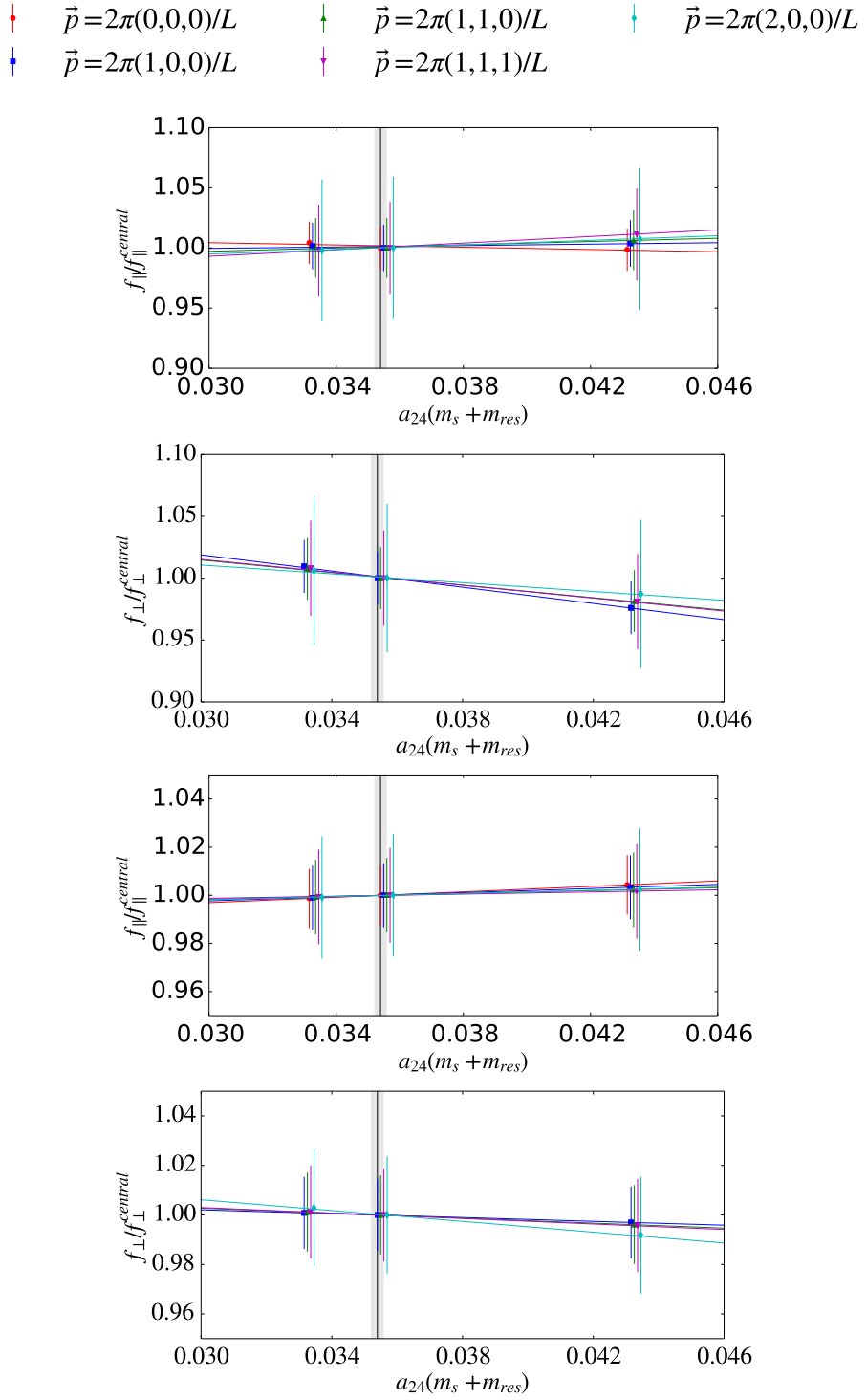

Figure 6.10: Valence strange-quark mass dependence of the $B_s \to K$ (top two panels) and $B_s \to D_s$ (bottom two panels) form factors $f_\parallel$ and $f_\perp$ on the $a^{-1} = 1.785(5)$ GeV ensemble with $am_l = 0.005$. The slopes are normalized by the form factors obtained with the strange-quark mass used in our production simulations. The colored lines show the results of a linear fit to the three data points at each momentum. The black vertical line with error band shows the total (statistical plus systematic) uncertainty in the physical strange-quark mass [7]. For clarity, data points at equal strange-quark masses are plotted with a slight horizontal off-set.

where

$$\frac{1}{m_2 a} = \frac{2\zeta^2}{m_0 a(2+m_0 a)} + \frac{\zeta}{1+m_0 a}, \tag{6.21}$$

$$\frac{1}{4m_E^2 a} = \frac{\zeta^2}{[m_0 a(2+m_0 a)]^2} + \frac{\zeta_{c_P}}{m_0 a(2+m_0 a)}. \tag{6.22}$$

$$\tag{6.23}$$

The tree-level coefficients for the $\mathcal{O}(a^2)$ improved heavy-light electroweak operators $\bar{b}\Gamma\mathbf{D}^2 q$, $\bar{q}\Gamma i\mathbf{\Sigma}\cdot\mathbf{B}b$ and $\bar{q}\Gamma\alpha\cdot\mathbf{E}b$, are given in [40], and are used in [143] to obtain the mismatch functions

$$f_{X_1}(m_0 a, c_p, \zeta) = -\frac{1}{2}\left[d_1^2 - \frac{\zeta}{2(1+m_0 a)}\right], \tag{6.24}$$

$$f_{X_2}(m_0 a, c_p, \zeta) = -\frac{1}{2}\left[d_1^2 - \frac{c_p}{2(1+m_0 a)}\right], \tag{6.25}$$

$$f_Y(m_0 a, c_p, \zeta) = -\frac{1}{2}\left[\frac{(\zeta - c_p)(1+m_0 a)}{m_0 a(2+m_0 a)} - \frac{d_1}{m_2 a}\right], \tag{6.26}$$

$$d_1 = \frac{\zeta(1+m_0 a)}{m_0 a(2+m_0 a)} - \frac{1}{2m_2 a}. \tag{6.27}$$

We estimate the $\mathcal{O}(\alpha_s^2 a, a^2)$ error from the current using the function [143]

$$f_3(m_0 a, c_p, \zeta) = \alpha_s^2 \zeta \frac{2}{(2+m_0 a)} \tag{6.28}$$

and obtain the size of the relative error from $f_E, f_{X_1}, f_{X_2}, f_Y$ and f_3 using

$$\text{error}_n \sim f_n(m_0 a, c_P, \zeta)(a\Lambda_{\text{QCD}})^k, \tag{6.29}$$

where $n = \{E, X_1, X_2, Y, 3\}$ and $k = 2$ for all functions except for f_3 for which it takes the value $k = 1$. We present in Table 6.11 the estimates of heavy-quark discretization errors from the five different operators in the action and the current. We take the size of the heavy-quark discretization errors to be the estimate on our finer $a^{-1} = 2.383(9)$ GeV lattices, which is 1.55% for $f_\parallel$ and 1.81% for $f_\perp$.

6.3.5.6 RHQ parameter uncertainties

As discussed in section 5.3.3 our b-quark propagators are obtained using the non-perturbatively tuned RHQ action (3.33). The tuned parameters $m_0 a, c_p$ and ζ given in Table 5.3 have four significant sources of uncertainty: lattice-scale, statistics, heavy-quark discretization errors and experimental inputs. We present in Figures 6.11 and 6.12 the RHQ parameter dependence of the $B_s \to K\ell\nu$ and $B_s \to D_s\ell\nu$ form factors $f_\parallel$ and $f_\perp$. We estimate the systematics due to the RHQ parameter uncertainties by multiplying the slopes shown in this plots $\Delta f/\Delta m_0 a$, $\Delta f/\Delta c_p$, $\Delta f/\Delta\zeta$ by the uncertainty

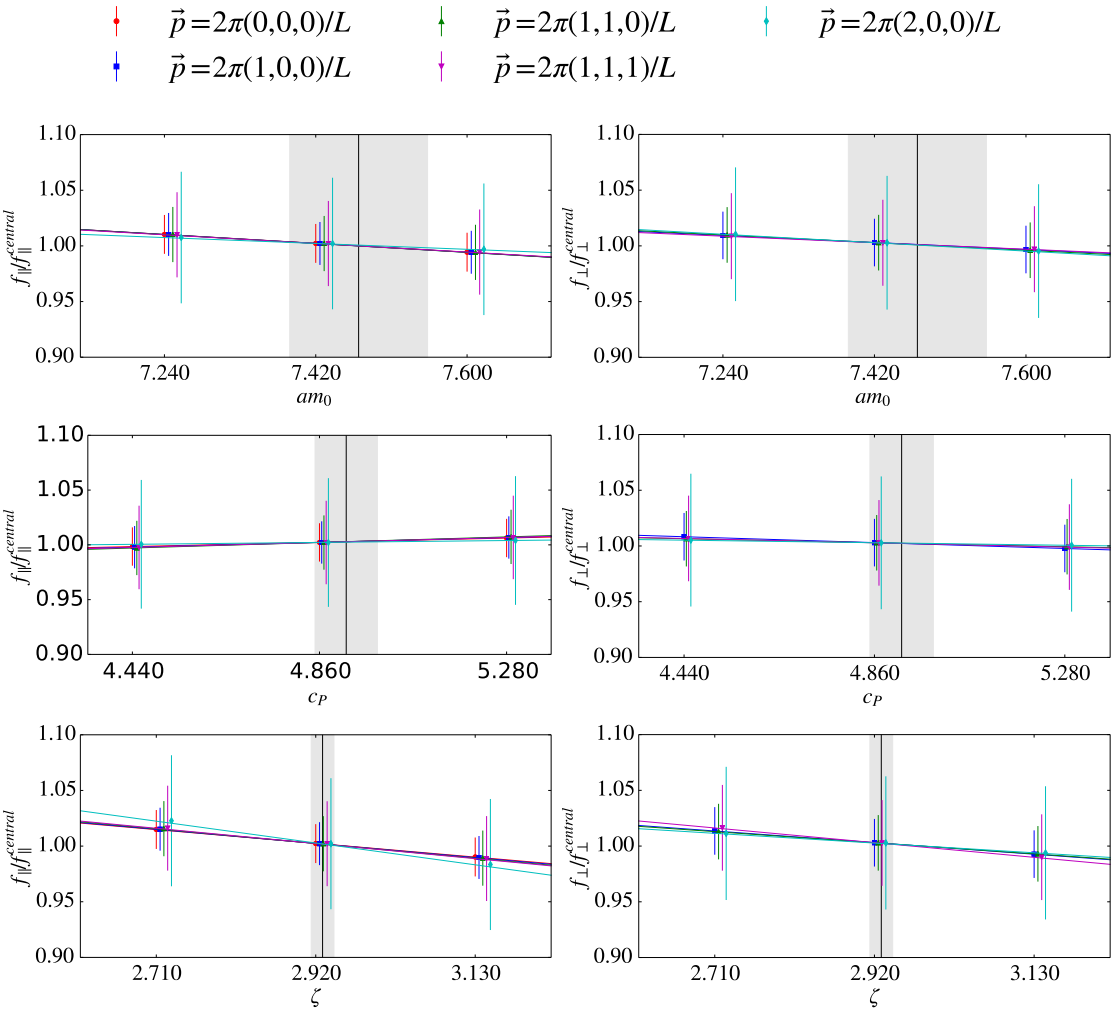

Figure 6.11: RHQ parameter dependence of the $B_s \to K$ form factors $f_\parallel$ (left) and $f_\perp$ (right) on the 24^3 ensembles with $am_l = 0.005$ using the unimproved heavy-light vector current in Eq. (4.4). The slopes are normalized using the form factors obtained at the central set of RHQ parameters. From top to bottom, the plots show the dependence on $m_0 a$, c_P, and ζ. The colored lines show the results of a linear fit to the three data points at each momentum. The black vertical lines indicate the tuned values of the RHQ parameters. The shaded vertical bands indicate the systematic errors in the RHQ parameters due to the lattice-scale uncertainty. For clarity, data points at equal RHQ parameter values are plotted with a slight horizontal off-set.

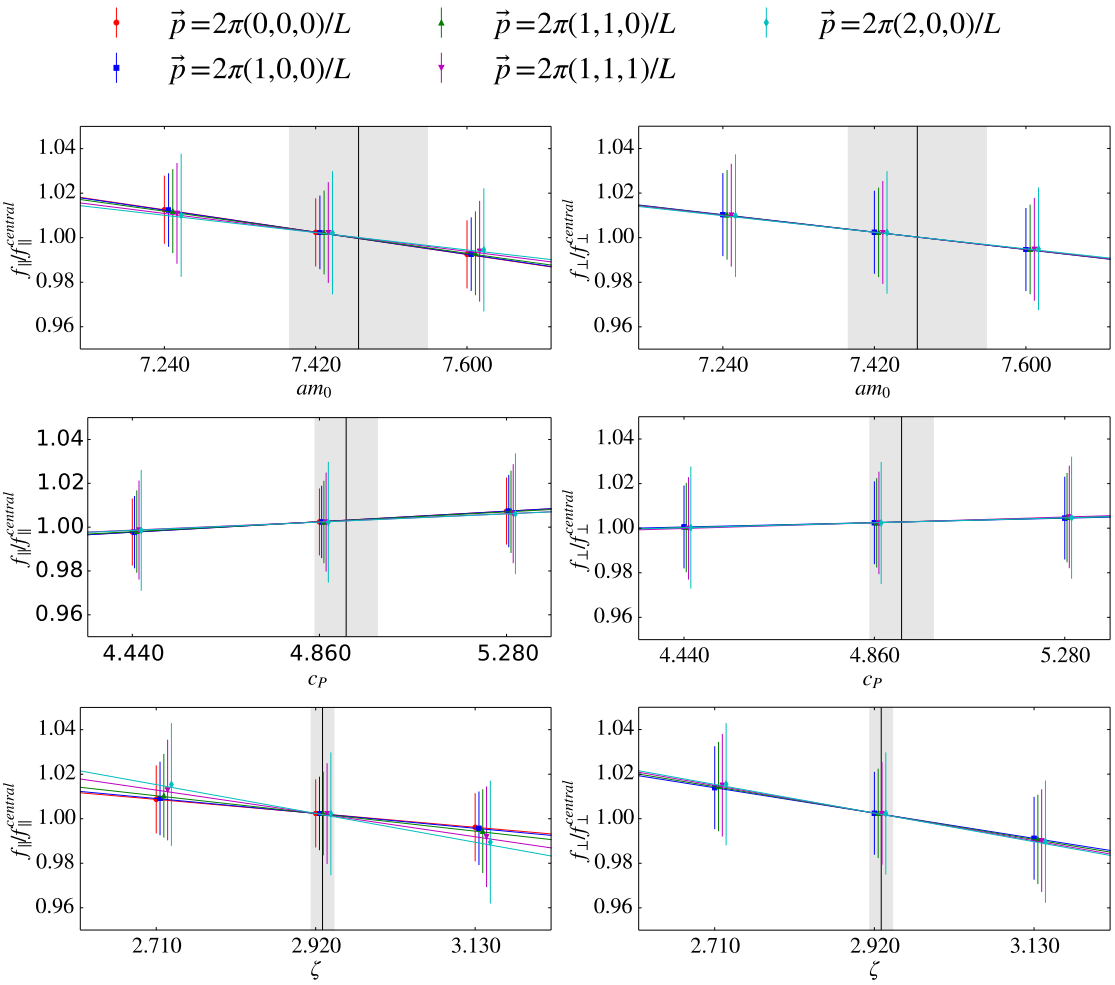

Figure 6.12: RHQ parameter dependence of the $B_s \to D_s$ form factors $f_\parallel$ (left) and $f_\perp$ (right) on the 24^3 ensembles with $am_l = 0.005$ using the unimproved heavy-light vector current in Eq. (4.4). The slopes are normalized using the form factors obtained at the central set of RHQ parameters. From top to bottom, the plots show the dependence on $m_0 a$, c_P, and ζ. The colored lines show the results of a linear fit to the three data points at each momentum. The black vertical lines indicate the tuned values of the RHQ parameters. The shaded vertical bands indicate the systematic errors in the RHQ parameters due to the lattice-scale uncertainty. For clarity, data points at equal RHQ parameter values are plotted with a slight horizontal off-set.

Table 6.11: Percentage errors from mismatches in the action and current for the bottom quark on the 24^3 and 32^3 ensembles. For this estimate, we calculate the mismatch functions for the non-perturbatively-tuned parameters of the RHQ action from Table 5.3. We estimate the size of operators using HQET power counting with $\Lambda_{\rm QCD} = 500$ MeV and the coupling constant $\alpha_s^{\bar{\rm MS}}(1/a) = 1/3$ on the 24^3 ensemble and 0.22 on the 32^3 ensembles. To obtain the total, we add the individual errors in quadrature, including each contribution the number of times that operator occurs. Contribution E is counted twice, and 3 is counted twice for $f_\parallel$ and four times for $f_\perp$.

	$\mathcal{O}(a^2)$ error from action	$\mathcal{O}(a^2)$ errors from current			$\mathcal{O}(\alpha_s^2 a)$ error from current	Total (%)	
	E	X_1	X_2	Y	3	$f_\parallel$	$f_\perp$
$a^{-1} = 1.785(5)$ GeV	0.47	0.67	1.13	1.07	1.93	3.27	4.26
$a^{-1} = 2.383(9)$ GeV	0.36	0.43	0.75	0.76	0.65	1.55	1.81

in the corresponding RHQ parameter due to heavy quark discretization errors and experimental inputs — c.f. Table 5.3—, and adding the individual contributions from the three RHQ parameters and the two uncertainty sources in quadrature. We obtain that the error due to the lattice spacing for the $B_s \to K\ell\nu$ form factors is 1% both for $f_\parallel$ and $f_\perp$, and for the $B_s \to D_s\ell\nu$ form factor is 0.8% and 1.6% for $f_\parallel$ and $f_\perp$, respectively.

6.3.5.7 Light/charm-quark discretization errors

The action and the heavy-light/charm vector currents are the dominant sources of discretization errors from the light/charm quark and gluon sector. These discretization errors are $\mathcal{O}((a\Lambda_{\rm QCD})^2)$ from the action and $\mathcal{O}(\alpha_s a\tilde{m}_q, (a\tilde{m}_q)^2, \alpha_s^2 a\Lambda_{\rm QCD}, (ap)^2)$ from the heavy-light vector currents, where $a\tilde{m}_q = am_q + am_{\rm res} = \{a\tilde{m}_{ud} = 0.00102(5), a\tilde{m}_c = 0.540(13)\}$ [6, 7, 10] is the bare quark mass. We do not observe any evidence of sizeable momentum dependent discretization errors in our data. As shown in Figure 6.2 the Kaon and D_s meson energies are consistent with continuum expectations, and smaller than power-counting estimates of $\mathcal{O}((ap)^2)$. Hence we do not include momentum dependent discretization errors in our systematics. We remove the dominant error coming from the action by the inclusion of a term proportional to a^2 in the chiral-continuum extrapolation (6.17), and give estimates of the discretization errors from the heavy-light/charm vector currents on the $a^{-1} = 2.384$ GeV ensembles on Table 6.12

6.3.5.8 Renormalization factor

We have presented in section 4.3 our renormalization procedure. We will now consider the uncertainties from the three parameters entering (4.26) separately and then add them in quadrature to obtain the total error. The statistical uncertainty of the flavour

Table 6.12: Heavy-light/charm vector current discretization errors for the $B_s \to K\ell\nu$ and $B_s \to D_s\ell\nu$ decays with $\Lambda_{\rm QCD} = 500$ MeV and $\alpha_s = 0.22$. As shown in Figure 6.2 the Kaon and D_s meson energies are consistent with continuum expectations, and smaller than power-counting estimates of $\mathcal{O}((ap)^2)$. Hence momentum dependent discretization errors in our systematics are taken to be 0%.

	$B_s \to K\ell\nu$	$B_s \to D_s\ell\nu$
$\mathcal{O}(\alpha_s a\tilde{m}_q)$	$\sim 0.7\%$	$\sim 12\%$
$\mathcal{O}((a\tilde{m}_q)^2)$	$> 0.1\%$	$\sim 29\%$
$\mathcal{O}(\alpha_s^2 a\Lambda_{\rm QCD})$	$\sim 1\%$	$\sim 1\%$
$\mathcal{O}((ap)^2)$	0%	0%

conserving factors Z^{ll} (4.28) and Z^{bb} (4.27) is in both cases 0.2% —c.f. Table (6.4)—. We estimate the perturbative truncation error to be the full size of the 1-loop correction in the $a^{-1} = 2.384$ GeV ensemble, this leads to an error for ρ_{V^0} and ρ_{V_i} to be 1.6% and 0.6%, respectively. Errors of $\mathcal{O}(\alpha_s a\tilde{m}_q)$ and $\mathcal{O}((a\tilde{m}_q)^2)$ due to quark mass dependent errors in ρ_{V^μ} have already been accounted for in the previous section, so we don't count them again. Our final estimate for the systematic uncertainty due to the renormalization factor is 1.7% for $f_\parallel$ and 0.7% for $f_\perp$.

6.3.5.9 Electromagnetic and Isospin breaking

The leading quark-mass contribution to the isospin breaking from the valence quark masses is of $\mathcal{O}((m_d - m_u)/\Lambda_{\rm QCD}) \sim 0.5\%$, which is obtained using the light quark masses $m_u = 2.40(23)$ MeV and $m_d = 4.80(23)$ MeV from [154] and $\Lambda_{\rm QCD} = 500$ MeV. The electromagnetic contribution to the isospin breaking is expected to be $\mathcal{O}(\alpha_s) \sim 1/137 \sim 0.7\%$ which is the typical size of 1-loop QED corrections.

6.3.6 Error budget

We present in Tables 6.13 and 6.14 our complete error budget on the determination of $B_s \to K\ell\nu$ and $B_s \to D_s\ell\nu$ form factors at three representative q^2 values within the range of simulated lattice momenta — c.f Section 6.3.7 —. We find that the largest source of uncertainty for $B_s \to K\ell\nu$ form factors comes from statistical errors, followed closely by the systematic errors due to the chiral continuum extrapolation. We calculate a total uncertainty of $\sim 5\%$ for $f_+^{B_s\to K}$ and $\sim 6\%$ for $f_0^{B_s\to K}$. This values indicate a reduction in the total uncertainty $\sim 1\%$ compared with [135]. The largest source of uncertainty for $B_s \to D_s\ell\nu$ form factors comes from light quark and gluon discretization errors and calculate a total uncertainty of $\sim 16\%$ for both the $f_+^{B_s\to D_s}$ and $f_0^{B_s\to D_s}$ form factors.

	$f_+^{B_s\to K}$			$f_0^{B_s\to K}$		
E_P [GeV]	0.85	0.50	0.27	0.85	0.50	0.27
q^2 [GeV^2]	17.6	20.8	23.4	17.6	20.8	23.4
$f(q^2)$	0.99	1.64	2.77	0.99	1.64	2.77
Statistics	3.9	3.3	3.3	3.2	2.6	2.6
Chiral-continuum extrapolation	3.1	2.8	2.5	4.6	4.5	4.7
Light-quark mass m_{ud}	0.1	0.1	0.1	0.1	0.1	0.1
Strange-quark mass m_s	0.1	0.1	0.1	0.0	0.0	0.0
Lattice-scale uncertainty	1.6	1.6	1.6	1.5	1.5	1.5
RHQ parameter tuning	1.0	1.0	1.0	1.0	1.0	1.0
Renormalization factor	1.0	0.9	0.9	1.6	1.6	1.7
Heavy-quark discretization errors	1.8	1.8	1.8	1.6	1.6	1.6
Light-quark & gluon discretization errors	1.2	1.2	1.2	1.2	1.2	1.2
Isospin breaking	0.7	0.7	0.7	0.7	0.7	0.7
Total (%)	5.2	4.6	4.7	6.5	6.1	6.3

Table 6.13: Error budget for the $B_s \to K\ell\nu$ form factors at three representative q^2 values in the range of simulated lattice momenta. For convenience, we also show the corresponding Kaon and D_s meson energy, E_P. Errors are given in %. The total error is obtained by adding the individual errors in quadrature.

6.3.7 Synthetic data points

The continuum physical quark-mass $f_+(q^2)$ and $f_0(q^2)$ form factors are obtained from the chiral-continuum extrapolation of the form factors $f_\parallel$ and $f_\perp$, equations (6.17) and (6.18), by performing the linear combinations

$$f_+(q^2) = \frac{1}{\sqrt{2M_{B_s}}}[f_\parallel(E_{D_s}) + (M_{B_s} - E_{D_s})f_\perp(E_{D_s})] \tag{6.30}$$

$$f_0(q^2) = \frac{\sqrt{2M_{B_s}}}{M_{B_s}^2 - M_{D_s}^2}[(M_{B_s} - E_{D_s})f_\parallel(E_{D_s}) + (E_{D_s}^2 - M_{D_s}^2)f_\perp(E_{D_s})] \tag{6.31}$$

Now that we have taken into account lattice effects, we generate three synthetic data points in the q^2 region in which our lattice simulations were performed. These synthetic data points are given in Table 6.13 and are used to extrapolate to $q^2 = 0$ using the z-expansion [155, 156].

6.3.8 z-expansion

To obtain results over the full kinematical range we use our synthetic data points together with their correlations, and rely on the analyticity of the form factors as a function of the momentum transfer q^2 and the z-variable [155, 156]

$$z(q^2, t_0) = \frac{\sqrt{1 - q^2/t_+} - \sqrt{1 - t_0/t_+}}{\sqrt{1 - q^2/t_+} + \sqrt{1 - t_0/t_+}}. \tag{6.32}$$

	$f_+^{B_s\to D_s}$			$f_0^{B_s\to D_s}$		
E_P [GeV]	2.2	2.1	2.0	2.2	2.1	2.0
q^2 [GeV^2]	8.8	9.9	10.9	8.8	9.9	10.9
$f(q^2)$	1.01	1.10	1.21	0.80	0.85	0.90
Statistics	3.7	2.3	1.9	4.6	3.0	1.7
Chiral-continuum extrapolation	4.3	1.7	4.2	5.3	2.8	1.7
Light-quark mass m_{ud}	0.0	0.0	0.0	0.0	0.0	0.0
Strange-quark mass m_s	0.0	0.0	0.0	0.0	0.0	0.0
Lattice-scale uncertainty	1.2	1.2	1.2	1.5	1.5	1.5
RHQ parameter tuning	1.2	1.2	1.2	0.9	0.8	0.8
Renormalization factor	1.2	1.2	1.2	1.6	1.7	1.7
Heavy-quark discretization errors	2.5	2.5	2.5	1.8	1.8	1.8
Light-quark & gluon discretization errors	13.9	13.9	13.9	13.9	13.9	13.9
Isospin breaking	0.7	0.7	0.7	0.7	0.7	0.7
Total (%)	15.0	14.9	14.9	15.6	15.7	15.9

Table 6.14: Error budget for the $B_s \to D_s\ell\nu$ form factors at three representative q^2 values in the range of simulated lattice momenta. For convenience, we also show the corresponding Kaon and D_s meson energy, E_P. Errors are given in %. The total error is obtained by adding the individual errors in quadrature.

where $t_+ \equiv M_{B_s} + M_P$ with $P = \{K, D_s\}$ and t_0 is a free parameter which determines the range of $|z|$ in the semileptonic region. The z-variable maps the complex q^2 plane onto the unit disk $|z(q^2, t_0)| < 1$ such that $z(t_+, t_0) = -1$ and $z(\infty, t_0) = 1$ and allows for the form factors to be expressed as a convergent power series whose coefficients are constrained to be small by unitarity and heavy-quark symmetry [155–160]. This convergent power series provides a better description of semileptonic form factors compared to other functional forms [161, 162] and hence it has been adopted as the preferred method to determine CKM matrix elements by experimentalists on Babar and Belle, the Heavy Flavor Averaging Group, and the Particle Data Group [6, 163–167]. With this reasons in mind we extrapolate our lattice results to $q^2 = 0$ using the simplified series expansion [160, 168]

$$f_0(q^2) = \frac{1}{1 - q^2/M^2_{B^*_{(c)}}} \sum_{k=0}^{K} b_0^{(k)} z(q^2, t_0)^k, \tag{6.33}$$

$$f_+(q^2) = \frac{1}{1 - q^2/M^2_{B^*_{(c)}}} \sum_{k=0}^{K-1} b_+^{(k)} \left[z(q^2, t_0)^k - (-1)^{k-K} \frac{k}{K} z(q^2, t_0)^K \right]. \tag{6.34}$$

where $M^*_B(0^+) = 5.63(4)$ GeV [150], $M^*_B(1^-) = 5.3252(4)$ GeV [151] and $M^*_{B_c} = 6.330(9)$ GeV [152]. Equation (6.34) has one degree of freedom less that (6.33) because the derivative of the form factor f_+ at $q^2 = t_+(z = -1)$ must satisfy

$$\left[\frac{df_+}{dz} \right] \Bigg|_{z=-1} = 0 \tag{6.35}$$

so that the asymptotic behavior $\mathrm{Im}\, f_+(q^2) \sim (q^2 - t_+)^{3/2}$ near the $B\pi$ production threshold is preserved [160] and no analogous constraint exists for (6.33). We choose $t_0 = (M_{B_s} + M_P)(\sqrt{M_{B_s}} - \sqrt{M_P})$ where $P = \{K, D_s\}$, so that the full kinematic range is centered around the origin $z = 0$ and the magnitude of $|z|$ is minimized so that there is rapid convergence of the expansion minimizing the errors which arise due to the truncation of the z-expansion. We also implement the unitarity constraint of the coefficients b_i following [160]

$$\sum_{j,k=0}^{K} B_{jk}(t_0) b_i^{(j)}(t_0) b_i^{(k)}(t_0) \lesssim 1\,, \tag{6.36}$$

$$B_{jk}(t_0) = \sum_{n=0}^{\infty} \eta_n(t_0)\eta_{n+|j-k|}(t_0), \tag{6.37}$$

where

$$b_K = -\frac{(-1)^K}{K} \sum_{k=0}^{K-1} (-1)^k k b_k \tag{6.38}$$

and η_i are the Taylor coefficients in the expansion of

$$\Psi(z) = \frac{M^2_{B^*_{(c)}}}{4(t_+ - t_0)} \phi_i(q^2(z), t_0) \frac{(1-z)^2(1-z_*)^2}{(1-zz_*)^2}, \qquad z_* = z(M^2_{B_s}, t_0), \tag{6.39}$$

around $z = 0$. In equation (6.39) we use the outer functions [159, 160, 169]

$$\begin{aligned}
\phi_i^{B_s\to K}(q^2, t_0) = &\sqrt{\frac{3}{2K\chi_{(J^P)}}}(\sqrt{t_+ - q^2} + \sqrt{t_+ - t_0}) \\
&\times \frac{(t_+ - q^2)^{(a+1)/4}}{(t_+ - t_0)^{1/4}} (\sqrt{t_+ - q^2} + \sqrt{t_+})^{-(b+3)} \\
&\times (\sqrt{t_+ - q^2} + \sqrt{t_+ - (M_{B_s} - M_P)})^{(a/2)} \qquad (6.40)\\
\phi_+^{B_s\to D_s} = &\, 1.1213(1+z)^2(1-z)^{1/2}[(1+r)(1-z) + 2\sqrt{r}(1+z)]^{-5} \qquad (6.41)\\
\phi_0^{B_s\to D_s} = &\, 0.5299(1+z)^2(1-z)^{3/2}[(1+r)(1-z) + 2\sqrt{r}(1+z)]^{-4} \qquad (6.42)
\end{aligned}$$

where for $B_s \to K$ we have [159, 160] f_+: $(K = 48\pi, \chi_{0^+} = 5.03 \times 10^{-4}, a = 3, b = 2)$ and for f_0: $(K = 16\pi/(t_+(M_{B_s} - M_P)), \chi_{1^-} = 1.46 \times 10^{-2}, a = 1, b = 1)$, and $r = M_{B_s}/M_{D_s}$ in equations (6.41) and (6.42). The values of B_{jk} for the $B_s \to K\ell\nu$ and $B_s \to D_s\ell\nu$ form factors are given in Table 6.15.

6.3.9 Extrapolation of lattice form factors to $q^2 = 0$

We present the results of the fits to our synthetic data points for the $B_s \to K\ell\nu$ and $B_s \to D_s\ell\nu$ form factors in Appendix B —c.f. Tables B.9 and B.10 —. These tables are divided into four sections:

Table 6.15: Matrix elements $B_{jk}(t_0)$ that enter the unitarity bound (6.36). The remaining coefficients can be obtained from the relations $B_{j(j+k)} = B_{0k}$ and the symmetry property $B_{jk} = B_{kj}$.

	B_{00}	B_{01}	B_{02}	B_{03}	B_{04}	B_{05}
$f_+^{B_s\to K}$	0.0115	0.0004	-0.0076	-0.0007	0.0018	0.0004
$f_0^{B_s\to K}$	0.0926	0.0137	-0.0484	-0.0174	-0.0003	0.0024
$f_+^{B_s\to D_s}$	9.66×10^{-5}	-1.82×10^{-5}	-5.95×10^{-5}	2.50×10^{-5}	8.75×10^{-6}	-5.65×10^{-6}
$f_0^{B_s\to D_s}$	3.29×10^{-4}	-1.08×10^{-4}	-1.78×10^{-4}	1.48×10^{-4}	-5.87×10^{-6}	-3.24×10^{-5}

- The top two panels show the results of separate fits of f_0 and f_+ without any constraints on the coefficients of the z-expansion.

- In the third panel we use the equality [170]

$$f_0(q^2) = \frac{M_{B_s}^2 - q^2}{M_{B_s}^2} f_+(q^2) \tag{6.43}$$

  which holds at large recoil to impose the kinematic constraint $f_+(0) = f_0(0)$.

- In the fourth panel we present the results of fits obtained by applying both the kinematic constraint and the constraint on the sum of the coefficients of the vector form factor [171]

$$\sum_{k=0}^{N} \left(b_+^{(k)}\right)^2 \sim \left(\frac{\Lambda}{m_b}\right)^3. \tag{6.44}$$

  through Bayesian priors. Taking $\Lambda = 1000(500)$ MeV we obtain for the central value of the prior $\bar{B} = 0.01$ and Gaussian width $\sigma_B = 0.03$. We implement the Bayesian fit by minimizing the augmented $\chi^2_{\rm aug}$ [172]

$$\chi^2_{\rm aug} = \chi^2 + \frac{(\bar{B} - \sum B_{jk} b_j b_k)^2}{\sigma_B^2} \tag{6.45}$$

6.3.10 Conclusion

In Appendix B — c.f Tables B.9 and B.10 — we see that the results obtained using the kinematic constraint $f_+(0) = f_0(0)$ on its own and those obtained by also including the heavy quark constraint (6.44) are in agreement. The normalization coefficients $b^{(0)}$, slopes $b^{(1)}/b^{(0)}$ and curvatures $b^{(2)}/b^{(0)}$ are well determined by the lattice data, with central values that are stable within errors for the good quality fits —i.e. p values larger than 10% for $B_s \to K$ (constrained fits), and for all fits with $K \geq 2$ for $B_s \to D_s$ (unconstrained fits) which satisfy the unitarity constraint (6.36)—. Given that we performed correlated fits for the $B_s \to K$ form factors we may use the χ^2/dof and p-values to guide us on our choice of preferred fit for this decay. We therefore choose the kinematic and heavy quark constrained fit with truncations $K = 2/3$ for the z expansion

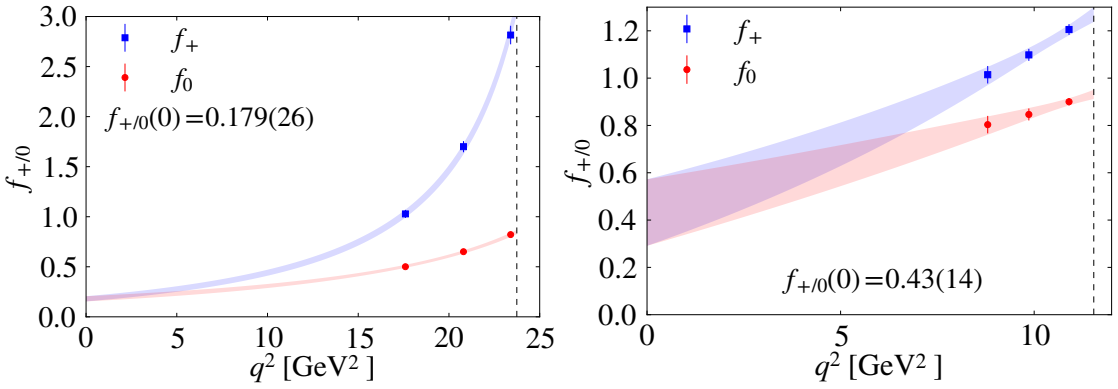

Figure 6.13: Preferred $K = 3$ fit of the $B_s \to K\ell\nu$ (left) and $B_s \to D_s\ell\nu$ (right) lattice form factors to the z-expansion (6.33)—(6.34) including the kinematic and heavy-quark constraints versus q^2. The solid curves with error bands show the fit results for $f_+(q^2)$ and $f_0(q^2)$. The vertical dashed line on the right-hand side of each plot shows $q^2 = (M_{B_s} - M_P)^2$ where $P = \{M_K, M_{D_s}\}$.

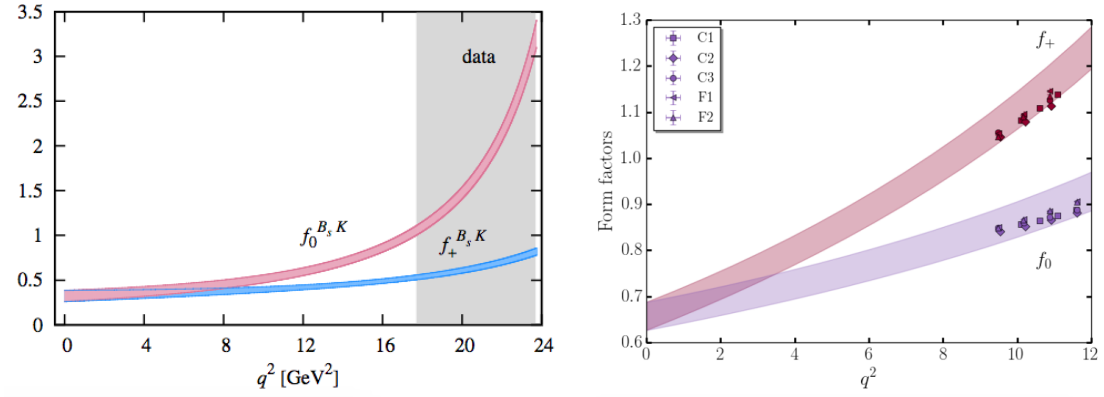

Figure 6.14: Chiral and continuum extrapolated form factors, $f_0(q^2)$ and $f_+(q^2)$ as a function of the momentum transfer. Left $B_s \to K\ell\nu$ taken from [8], right $B_s \to D_s\ell\nu$ taken from [9].

of the form factors f_+/f_0 of the $B_s \to K$ decay as our preferred fit. For uncorrelated fits the χ^2/dof and p-values are not objective measures of the quality of the fit, as such we make our choice of preferred fit for the form factors f_0 and f_+ of $B_s \to D_s$ decays by studying the effect that the number of term in the z expansion has on the error of the slopes $b^{(1)}/b^{(0)}$ and curvatures $b^{(2)}/b^{(0)}$. We therefore choose the kinematic and heavy quark constrained fit with truncations $K = 3$ for the z expansion of both form factors f_+/f_0 of the $B_s \to D_s$ decay as our preferred fit. The results obtained for our preferred fit are shown in Figure 6.13. In the q^2 region where our simulation took place —i.e. $15 < q^2 \leq q^2_{\text{max}_{B_s \to K\ell\nu}}$ and $8 < q^2 \leq q^2_{\text{max}_{B_s \to D_s\ell\nu}}$— our fit results for the form factors f_0 and f_+ are within statistical errors to the fits obtained by HPQCD —c.f Figure 6.14—. Extrapolating our results to $q^2 = 0$ we obtain the values $f_{0/+}^{B_s \to K}(0) = 0.179(26)$ and $f_{0/+}^{B_s \to D_s}(0) = 0.43(14)$. These results are in tension with those reported by HPQCD using non relativistic lattice QCD (NRQCD) [8, 9] and those obtained using Light Cone Sum Rules (LCSR) [173, 174] — c.f Table 6.16—. Our results for the form factors for

Form factor	HPQCD [8, 9]	LCSR [173, 174]	RBC/UKQCD [135]	Our result
$f_+^{B_s\to K}(0) = f_0^{B_s\to K}(0)$	0.323(63)	$0.30^{+0.04}_{-0.03}$	0.153(33)	0.179(26)
$f_+^{B_s\to D_s}(0) = f_0^{B_s\to D_s}(0)$	0.656(31)	$0.86^{+0.17}_{-0.13}$		0.43(14)

Table 6.16: Values for $B_s \to K\ell\nu$, $B_s \to D_s\ell\nu$ form factors in the physical limit at $q^2 = 0$.

the $B_s \to K\ell\nu$ decay are within statistical errors with those obtained in our previous work [135].

6.4 Rare B decays: $b \to s\ell^+\ell^-$

In this section we present our results of $B_s \to \phi\ell^+\ell^-$ form factors.

6.4.1 Operator renormalization and improvement

The perturbative coefficient ρ (4.26), and the flavour-conserving renormalization factors Z^{ll} (4.28) and Z^{bb} (4.27) are given in tables 6.4. We improve the heavy-strange vector and axial vector currents through $\mathcal{O}(\alpha_s a)$ and present the necessary matching coefficients in table 6.5. Temporal and spatial $\mathcal{O}(a)$ vector and axial-vector current operators are obtained using equations 6.5 and (6.6), where we replace V_μ^i (4.31)—(4.34) by A_μ^i (4.35)—(4.38) for axial vectors. For the tensor current we do not have one-loop results for the perturbative coefficient ρ nor for the $\mathcal{O}(a)$ improvement coefficients, as such we set the residual matching factors and $\mathcal{O}(a)$ coefficients to their mean field improved tree-level values [175],

$$T_{\mu\nu} = \sqrt{Z^{bb}Z^{ll}}\left[\bar{s}\sigma_{\mu\nu}b + ad_1\sum_{j=1}^{3}\bar{s}\sigma_{\mu\nu}\gamma_j\overrightarrow{\nabla}_j b\right] \tag{6.46}$$

where at tree-level $d_1 = 0.07293$ on the $a^{-1} = 1.785$ GeV ensemble and $d_1 = 0.069948$ on the $a^{-1} = 2.384$ GeV ensemble.

6.4.2 The form factors $f_{A_{12}}$ and $f_{T_{23}}$

In section 4.2 we have seen that to extract the form factor f_{A_2} from equation (4.18) it is necessary to use as an input parameter the form factor f_{A_1}. Similarly, the extraction of the form factor f_{T_3} from equation (4.24) requires the use of the form factor f_{T_2}. This means that although possible, the extraction of the form factors f_{A_2} and f_{T_3} is a two step process which results in a signal of lower quality than the one obtained for all other form factors. As a consequence we choose to extract the form factors $f_{A_{12}}$ and $f_{T_{23}}$ [16]

$$f_{A_{12}}(q^2) = \frac{\sqrt{q^2}|\vec{k}|}{8M_{B_s}E_\phi k_m}\epsilon^*_{0,\mu}R^{m\gamma^\mu\gamma^5}_{B_s\to\phi} \tag{6.47}$$

$$= \frac{(M_{B_s}+M_\phi)^2(M_{B_s}^2 - M_\phi^2 - q^2)f_{A_1}(q^2) - \lambda f_{A_2}}{16M_{B_s}M_\phi^2(M_{B_s}+M_\phi)}, \tag{6.48}$$

$$f_{T_{23}}(q^2) = i\frac{|\vec{k}|(M_{B_s}+M_\phi)}{4E_\phi k_m\sqrt{q^2}M_{B_s}}\epsilon^*_{0,\mu}q_\nu R^{m\sigma^{\mu\nu}\gamma^5}_{B_s\to\phi} \tag{6.49}$$

$$= \frac{M_{B_s}+M_\phi}{8M_{B_s}M_\phi^2}\left[(M_{B_s}^2 + 3M_\phi^2 - q^2)f_{T_2}(q^2) - \frac{\lambda f_{T_3}(q^2)}{M_{B_s}^2 - M_\phi^2}\right], \tag{6.50}$$

Form factor	Δm
f_{A_0}	0
f_V, f_{T_1}	45
f_{A_1}, f_{A_12}, f_{T_2}, $f_{T_{23}}$	440

Table 6.17: Mass differences (in MeV), between the initial state B_s meson and the pertinent resonance, used in the z-expansion (6.56) of the $B_s \to \phi\ell^+\ell^-$ form factors. Taken from [16].

where

$$\epsilon^*_{0,\mu} = \frac{1}{\sqrt{q^2}} \left(|\vec{k}|, (E_\phi - M_{B_s}) \frac{\vec{k}}{|\vec{k}|} \right). \tag{6.51}$$

which together with f_{A_0} and

$$V_\pm(q^2) = \frac{1}{2} \left[\left(1 + \frac{M_\phi}{M_{B_s}} \right) f_{A_1}(q^2) \mp \frac{\sqrt{\lambda}}{M_{B_s}(M_\phi + M_{B_s})} f_V(q^2) \right] \tag{6.52}$$

$$T_\pm(q^2) = \frac{1}{2M^2_{B_s}} \left[(M^2_{B_s} - M^2_\phi) f_{T_2}(q^2) \mp \sqrt{\lambda} f_{T_1}(q^2) \right] \tag{6.53}$$

form the helicity basis. In equations (6.52) and (6.53) $\lambda = 4M^2_{B_s}|\vec{k}|^2$.

6.4.3 The form factors f_V, f_{A_0}, f_{A_1}, $f_{A_{12}}$, f_{T_1}, f_{T_2} and $f_{T_{23}}$ at finite lattice spacing

Having extracted the effective masses and energies of the ϕ and B_s mesons in section 6.2, we perform correlated, constant in time fits to (4.11) to (4.23), (6.48) and (6.50) to extract the form factors f_V, f_{A_0}, f_{A_1}, $f_{A_{12}}$, f_{T_1}, f_{T_2} and $f_{T_{23}}$. We now present the results of such fits in figure 6.15—6.16 and Tables B.4—B.6. Within our fitting ranges contamination from excited states is not visible and we use the same fitting ranges for all momenta and ensembles at the same lattice spacing. Fitting ranges for the 32^3 ensembles are obtained by scaling our choices on 24^3 using the ratio of the lattice spacings.

6.4.4 $B_s \to \phi\ell^+\ell^-$ form factors chiral continuum extrapolation

We now proceed to obtain the form factor shape using pole dominance, our ansatz is

$$f_i(q, a) = \frac{c_0 + c_1(\Lambda_{\rm QCD} a)^2}{1 - \left(c_2 + c_3 \Lambda^2_{QCD} a^2 \right) q^2/(M_{B_s} + \Delta m)^2} \tag{6.54}$$

where $i = \{V, A_0, A_1, A_{12}, T_1, T_2, T_{12}\}$, $\Lambda_{\rm QCD} = 500$ MeV and Δm is the mass difference between the initial state and the pertinent resonance —c.f Table 6.17 —. The resulting

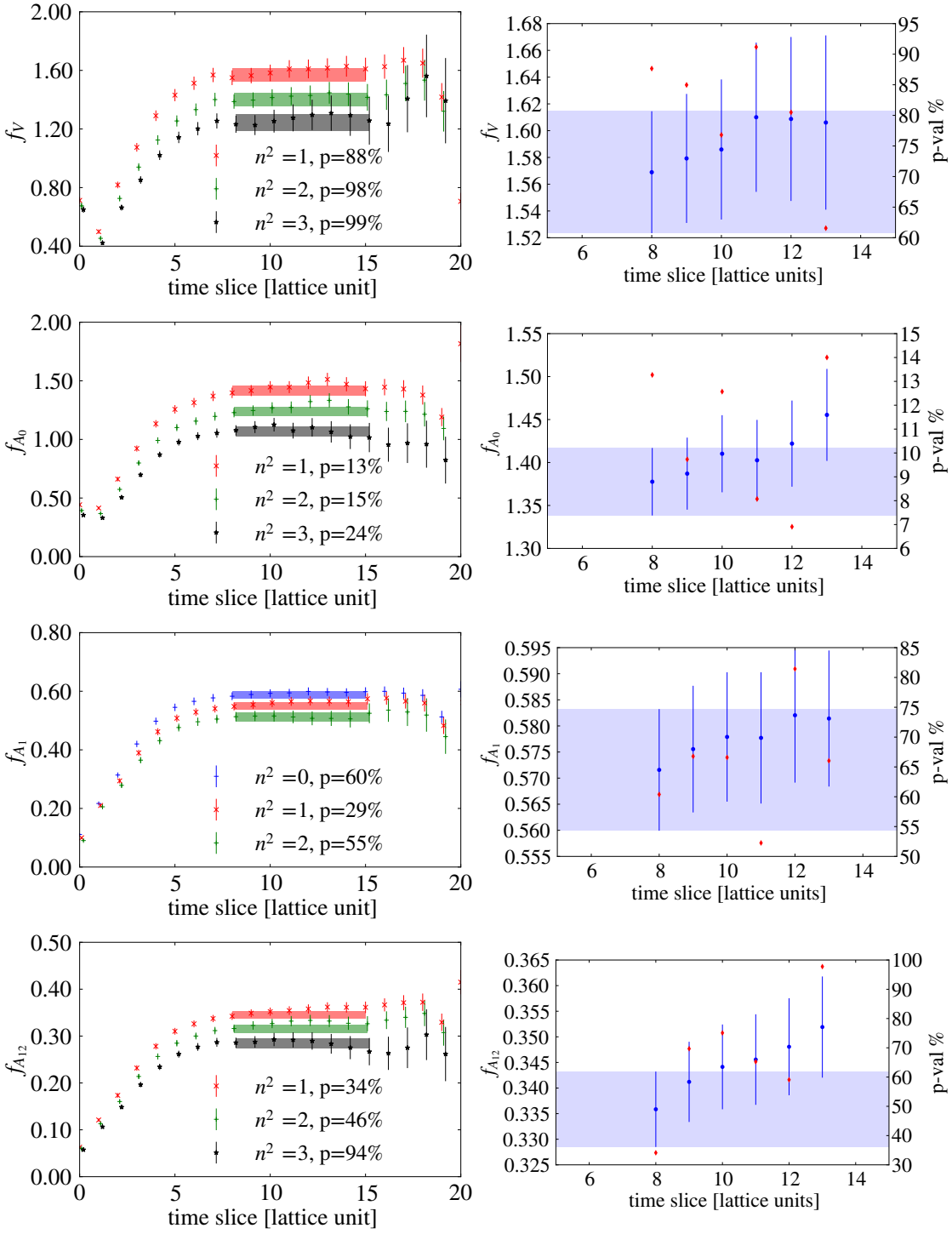

Figure 6.15: From top to bottom $B_s \to \phi\ell^+\ell^-$ form factors f_V, f_{A_0},f_{A_1}, and $f_{A_{12}}$, (left) form factors as a function of time on the $a^{-1} = 1.785(5)$ GeV ensemble with $am_l = 0.005$. (right) dependence of the form factor on the starting time slice with a fixed final time $t = 15$ at the smallest momenta $n = 0$ for f_{A_1}, $n = 1$ otherwise. The shaded band indicates the preferred fit with error, red diamonds indicate p-value.

	c_0	c_1	c_2	c_3	χ^2/dof	p
f_V	0.435(86)	0.2216(1.4465)	1.244(91)	-0.6284(1.5393)	0.64	79 %
f_{A_0}	0.428(77)	-0.4106(1.2166)	1.130(94)	0.7593(1.4779)	0.95	49 %
f_{A_1}	0.200(47)	0.96(80)	1.24(14)	-3(2)	1.07	38 %
$f_{A_{12}}$	0.127(31)	0.24278(0.50744)	1.21(17)	-1.31777(2.87626)	1.23	26 %
f_{T_1}	0.315(51)	0.0742(0.8565)	1.255(70)	-0.2740(1.1764)	0.62	81 %
f_{T_2}	0.210(48)	1.08(82)	1.16(15)	-4(2)	8.70	1 %
$f_{T_{23}}$	0.308(94)	1(1)	1.28(18)	-2.8420(3.1817)	1.03	42 %

Table 6.18: Coefficients for the continuum extrapolation of the form factors of the $B_s \to \phi\ell^+\ell^-$ decay obtained from correlated fits to (6.54).

plots are shown in Figure 6.17 and the fitting coefficients are given in Table 6.18. Variation to our fitting ansatz are explained in section 6.4.5.1 and their effect on the central value of the fit are shown in Figure 6.18

6.4.5 Systematics

A full error budget including all the sources of systematic errors for the form factors of $B_s \to \phi\ell^+\ell^-$ decays has not been finalized. We present in this section the sources of systematic errors for which a preliminary calculation has been completed.

6.4.5.1 Chiral-continuum extrapolation

The systematic uncertainty due to the chiral-continuum extrapolation of the $B_s \to \phi$ form factors is obtained by applying the following changes to the chiral-continuum fit ansatz (6.54)

1. omitting the data point at zero momentum
2. omitting the data point at the highest momentum $\vec{p} = 2\pi/L(2,0,0)$
3. including a term proportional to M_π^2 in the numerator of (6.18)

Figure 6.18 shows the relative changes of the form-factor central values under each fit variation

$$\Delta f_i = |f_i^{\text{pref.}} - f_i^{\text{alt.}}|/f_i^{\text{pref.}}\,, \tag{6.55}$$

where $i = \{V, A_0, A_1, A_{12}, T_1, T_2, T_{23}\}$. We take the largest difference between our preferred fit and any of the alternate fits as systematic uncertainty due to the chiral-continuum extrapolation.

	$f_V^{B_s\to\phi}$			$f_{A_0}^{B_s\to\phi}$		
E_P [GeV]	1.32	1.23	1.14	1.32	1.23	1.14
q^2 [GeV^2]	15.6	16.6	17.6	15.6	16.6	17.6
$f(q^2)$	1.29	1.47	1.71	1.38	1.23	1.11
Statistics	7.2	5.8	6.2	6.4	5.2	5.1
Chiral-continuum extrapolation	1.3	1.8	6.3	2.5	1.1	3.7
Renormalization factor	2.0	2.0	2.0	2.0	2.0	2.0
Total (%)	7.6	6.4	9.1	7.2	5.7	6.6

Table 6.19: Error budget for the $B_s \to \phi\ell^+\ell^-$ form factors f_V and f_{A_0} at three representative q^2 values in the range of simulated lattice momenta. For convenience, we also show the corresponding ϕ meson energy, E_P. Errors are given in %. The total error is obtained by adding the individual errors in quadrature.

	$f_{A_1}^{B_s\to\phi}$			$f_{A_{12}}^{B_s\to\phi}$		
E_P [GeV]	1.23	1.14	1.05	1.32	1.23	1.14
q^2 [GeV^2]	16.6	17.6	18.6	15.6	16.6	17.6
$f(q^2)$	0.52	0.58	0.65	0.29	0.32	0.35
Statistics	7.1	5.3	5.5	7.0	5.3	4.8
Chiral-continuum extrapolation	6.3	2.5	1.7	3.3	2.1	1.6
Renormalization factor	2.0	2.0	2.0	2.0	2.0	2.0
Total (%)	9.7	6.2	6.1	8.0	6.0	5.4

Table 6.20: Error budget for the $B_s \to \phi\ell^+\ell^-$ form factors f_{A_1} and $f_{A_{12}}$ at three representative q^2 values in the range of simulated lattice momenta. For convenience, we also show the corresponding ϕ meson energy, E_P. Errors are given in %. The total error is obtained by adding the individual errors in quadrature.

6.4.5.2 Renormalization factor

We have shown in sections 4.3 and 6.4.1 our renormalization procedure for vector and tensor currents, respectively. Following the procedure described in section 6.3.5.8 we estimate the systematic uncertainty arising from the renormalization factor of vector and axial vector currents to be $\sim 1.6\%$. The leading systematic error in the determination of the renormalization factor of tensor and pseudotensor currents is given by the use of the tree-level value $\rho_{T_{\mu\nu}} = 1$, this error has been estimated in [175] to be equal to two times the maximum value of $|\rho_{V_\mu} - 1|$ which using the values from Table 6.4 is $\sim 5\%$.

6.4.6 Error budget

We present in Tables 6.19 to 6.22 our preliminary error budget on the determination of $B_s \to \phi\ell^+\ell^-$ form factors at three representative q^2 values within the range of simulated

	$f_{T_1}^{B_s\to\phi}$			$f_{T_2}^{B_s\to\phi}$		
E_P [GeV]	1.32	1.23	1.14	1.23	1.14	1.05
q^2 [GeV^2]	15.6	16.6	17.6	16.6	17.6	18.6
$f(q^2)$	0.95	1.09	1.27	0.49	0.54	0.59
Statistics	6.4	5.2	5.2	6.9	5.4	5.4
Chiral-continuum extrapolation	2.7	0.9	9.9	6.0	4.0	10.0
Renormalization factor	5.0	5.0	5.0	5.0	5.0	5.0
Total (%)	8.6	7.3		12.2	8.4	12.4

Table 6.21: Error budget for the $B_s \to \phi\ell^+\ell^-$ form factors f_{T_1} and f_{T_2} at three representative q^2 values in the range of simulated lattice momenta. For convenience, we also show the corresponding ϕ meson energy, E_P. Errors are given in %. The total error is obtained by adding the individual errors in quadrature.

	$f_{T_{23}}^{B_s\to\phi}$		
E_P [GeV]	1.32	1.23	1.14
q^2 [GeV^2]	15.6	16.6	17.6
$f(q^2)$	0.77	0.84	0.94
Statistics	10.1	7.4	5.8
Chiral-continuum extrapolation	6.6	3.8	0.5
Renormalization factor	5.0	5.0	5.0
Total (%)	13.1	9.7	7.7

Table 6.22: Error budget for the $B_s \to \phi\ell^+\ell^-$ form factors $f_{T_{23}}$ at three representative q^2 values in the range of simulated lattice momenta. For convenience, we also show the corresponding ϕ meson energy, E_P. Errors are given in %. The total error is obtained by adding the individual errors in quadrature.

lattice momenta — c.f section 6.3.7 —. The total uncertainties range from $\sim 5\%$ to $\sim 13\%$ for all form factors.

6.4.7 Extrapolation of lattice form factors to $q^2 = 0$

We extrapolate our form factors from the rare B decay $B_s \to \phi\ell^+\ell^-$ to $q^2 = 0$ following the same procedure used for the tree level decays $B_s \to K\ell\nu$ and $B_s \to D_s\ell\nu$, that is, we remove lattice discretization effects by means of the chiral continuum extrapolation (6.54) and choose three synthetic data points in the q^2 region in which our lattice simulations where performed. We then use these synthetic data points together with their correlations to perform a z-expansion — c.f section 6.3.8 — using

$$f_i(q^2) = \frac{1}{1 - q^2/(M_{B_s} + \Delta m)^2} \sum_{k=0}^{K} b_0^{(k)} z(q^2, t_0)^k, \tag{6.56}$$

Form factor	NRQCD [16]	Our result
f_V	1.74(10)	2.20(20)
f_{A_0}	1.85(10)	1.67(12)
f_{A_1}	0.62(3)	0.67(4)
$f_{A_{12}}$	0.41(2)	0.39(4)
f_{T_1}	1.36(8)	1.63(12)
f_{T_2}	0.62(3)	0.61(3)
$f_{T_{23}}$	1.10(6)	1.02(20)

Table 6.23: Values for $B_s \to \phi\ell^+\ell^-$ form factors in the physical limit at $q^2_{\rm max}$. First numerical column results from Table XXXI of [16], second column: our results.

where $i = \{V, A_0, A_1, A_{12}, T_1, T_2, T_{12}\}$ and Δm is the mass difference between the initial state and the pertinent resonance —c.f Table 6.17 — We present the results of the fit to (6.56) of our synthetic data points for the $B_s \to \phi\ell^+\ell^-$ form factors in figure 6.19 and table B.11.

6.4.8 Conclusion

The absence of kinematic constraints on the $B_s \to \phi\ell^+\ell^-$ form factors, such as $f_i(0) = f_j(0)$ for $i \neq T_1$ and $j \neq T_2$ gives a limited choice of truncations K that can be studied. Given that we have three synthetic data points we must take $K \leq 3$ so that we have less than or equal points as fit parameters. We use as guidance our study of the z-expansion of $B_s \to K\ell\nu$ and $B_s \to D_s\ell\nu$ form factors, and the result obtained for the $B_s \to \phi\ell^+\ell^-$ form factors f_{T_1} and f_{T_2} with the kinematic constraint $f_{T_1}(0) = f_{T_2}(0)$ to choose our preferred fit. We conclude that the most sensible fit we can obtain with the available data is given by truncating the z expansion at $K = 3$. We use this truncation to extract our final result for the $B_s \to \phi\ell^+\ell^-$ form factors. Comparing our results at $q^2_{\rm max} = (M_{B_s} - M_\phi)^2$ with those obtained in lattice simulations using non relativistic QCD (NRQCD) —c.f Table 6.23— we see that within statistical errors there is agreement for all form factors except f_V and f_{T_1} which agree within $\sim 1.3\sigma$. We compare in Table 6.24 our final results with those obtained in lattice simulations that make use of NRQCD [16], we see that there is agreement within statistical errors for the form factors f_{A_1}, f_{T_1}, f_{T_2} and $f_{T_{23}}$ but there is a tension for f_V, f_{A_0} and $f_{A_{12}}$. Comparing our results with those obtained using Light Cone Sum Rules (LCSR) [17] we see agreement in all form factors except f_V.

Form factor	NRQCD [16]	LCSR [17]	Our result
f_V	0.24(7)	0.434(35)	0.97(42)
f_{A_0}	0.38(6)	0.474(37)	0.56(10)
f_{A_1}	0.29(3)	0.311(29)	0.294(84)
$f_{A_{12}}$	0.25(3)	N/A	0.154(18)
f_{T_1}	0.31(2)	0.349(33)	0.378(75)
f_{T_2}	0.31(2)	0.349(33)	0.378(75)
$f_{T_{23}}$	0.56(5)	N/A	0.45(14)

Table 6.24: Values for $B_s \to \phi\ell^+\ell^-$ form factors in the physical limit at $q^2 = 0$. First numerical column results from Table XXXI of [16], second column: results from LCSR Table VII of [17], third column: our results. N/A entries indicate that this form factors were not directly calculated, but instead the alternative form factors f_{A_2} and f_{T_3} were extracted.

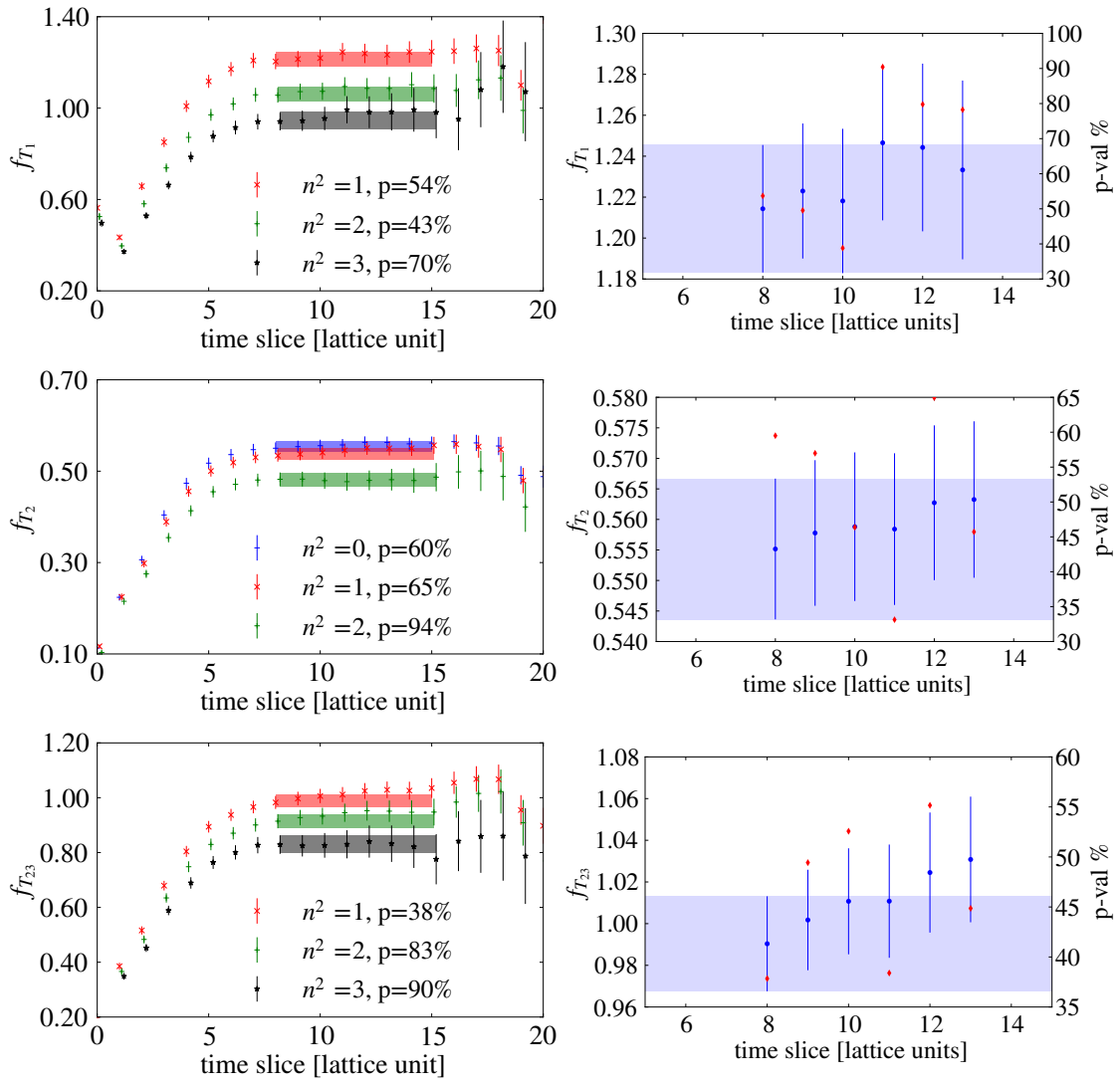

Figure 6.16: From top to bottom $B_s \to \phi\ell^+\ell^-$ form factors f_{T_1}, f_{T_2} and $f_{T_{23}}$, (left) form factors as a function of time on the $a^{-1} = 1.785(5)$ GeV ensemble with $am_l = 0.005$. (right) dependence of the form factor on the starting time slice with a fixed final time $t = 15$ at the smallest momenta $n = 0$ for f_{T_2}, $n = 1$ otherwise. The shaded band indicates the preferred fit with error, red diamonds indicate p-value.

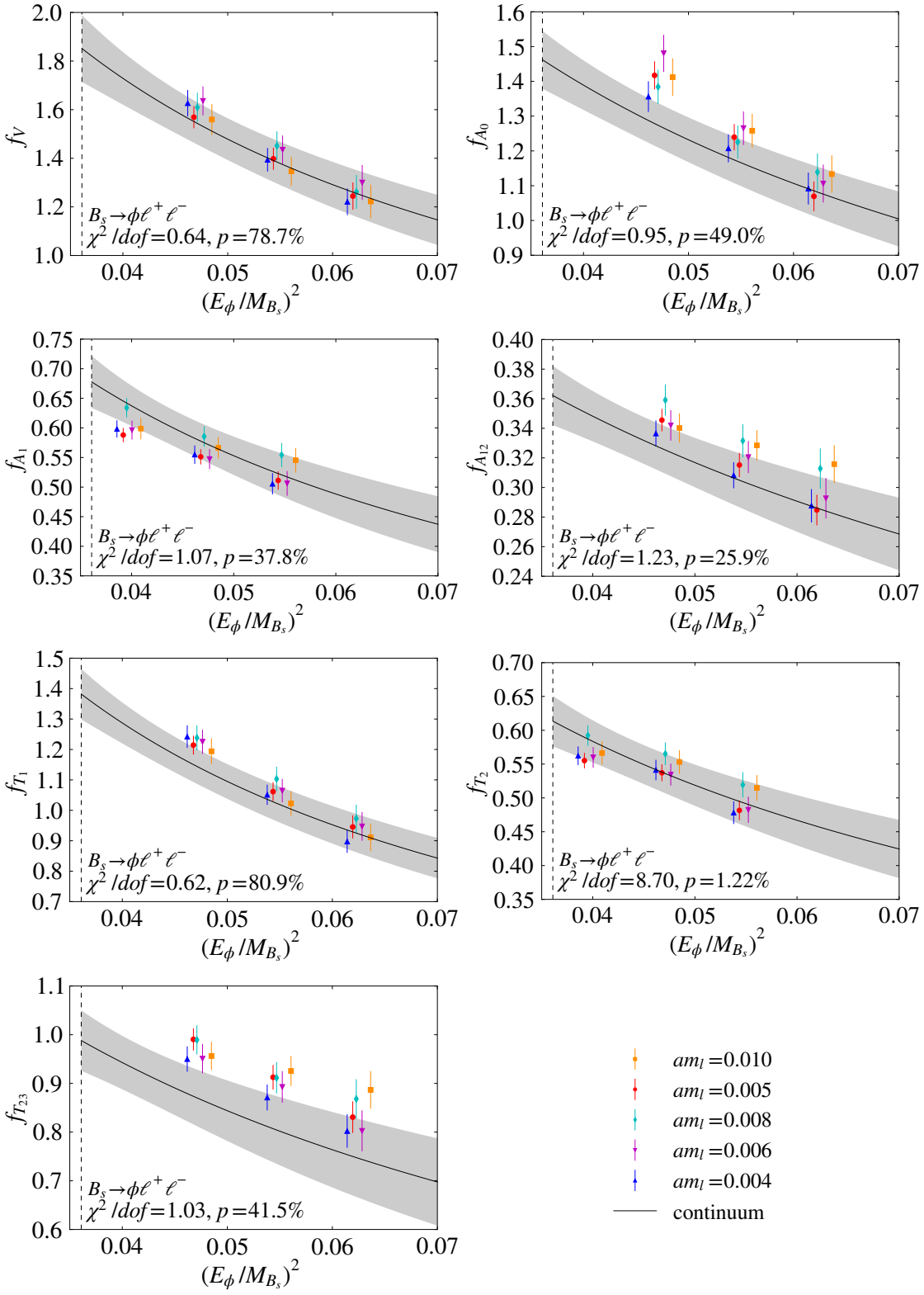

Figure 6.17: Continuum extrapolation using (6.18) for the $B_s \to \phi\ell^+\ell^-$ form factors f_V, f_{A_0},f_{A_1}, $f_{A_{12}}$, f_{T_1}, f_{T_2} and $f_{T_{23}}$. The shaded band indicates statistical errors, the vertical dashed line on the left-hand side of each plot shows the physical ϕ meson mass.

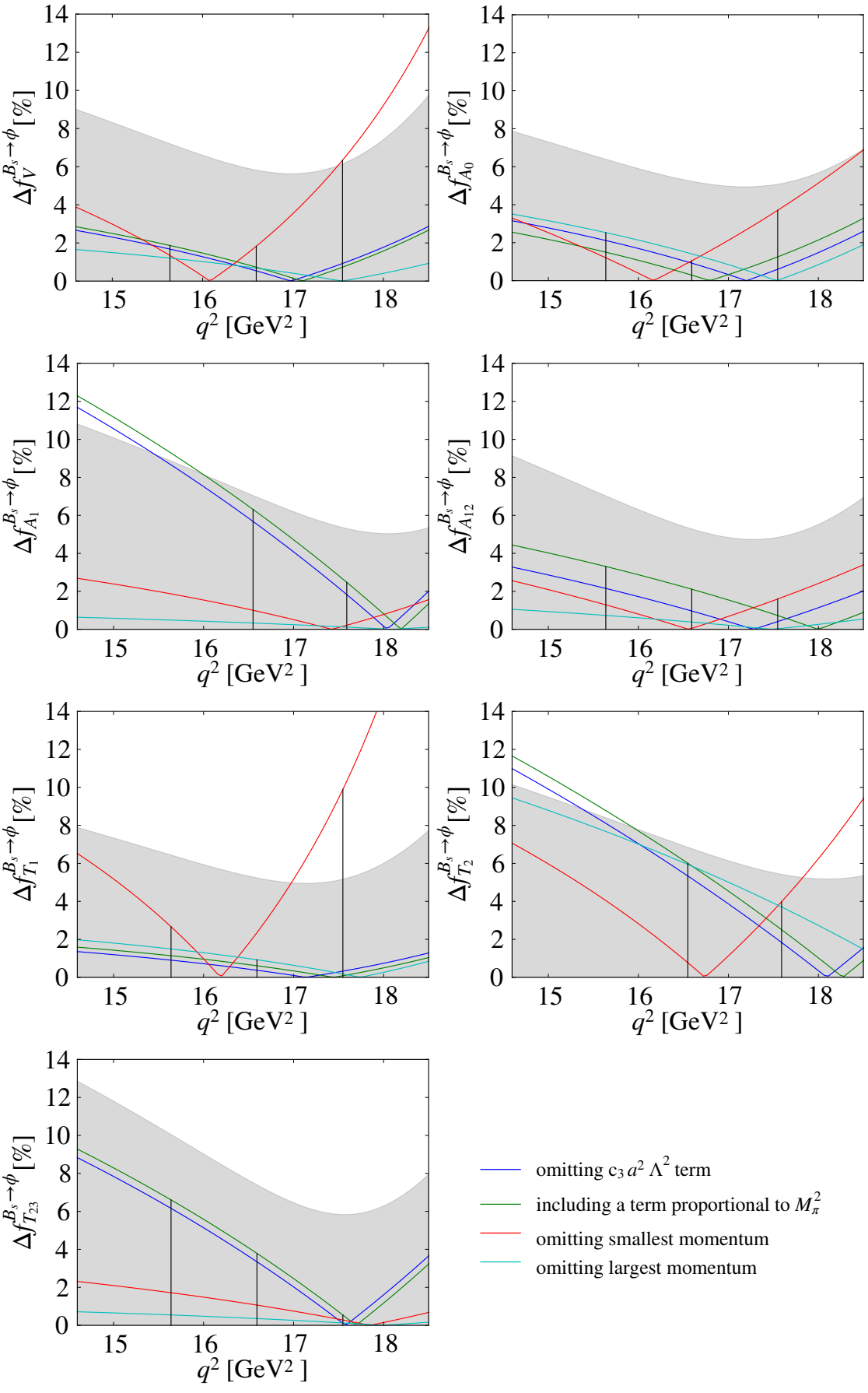

Figure 6.18: Relative change of the form-factors central value under the considered fit variations for $B_s \to \phi\ell\nu$. In each plot, the shaded band shows the statistical uncertainty of the preferred fit. The three vertical lines show the location of the synthetic data points used in the subsequent extrapolation to $q^2 = 0$.

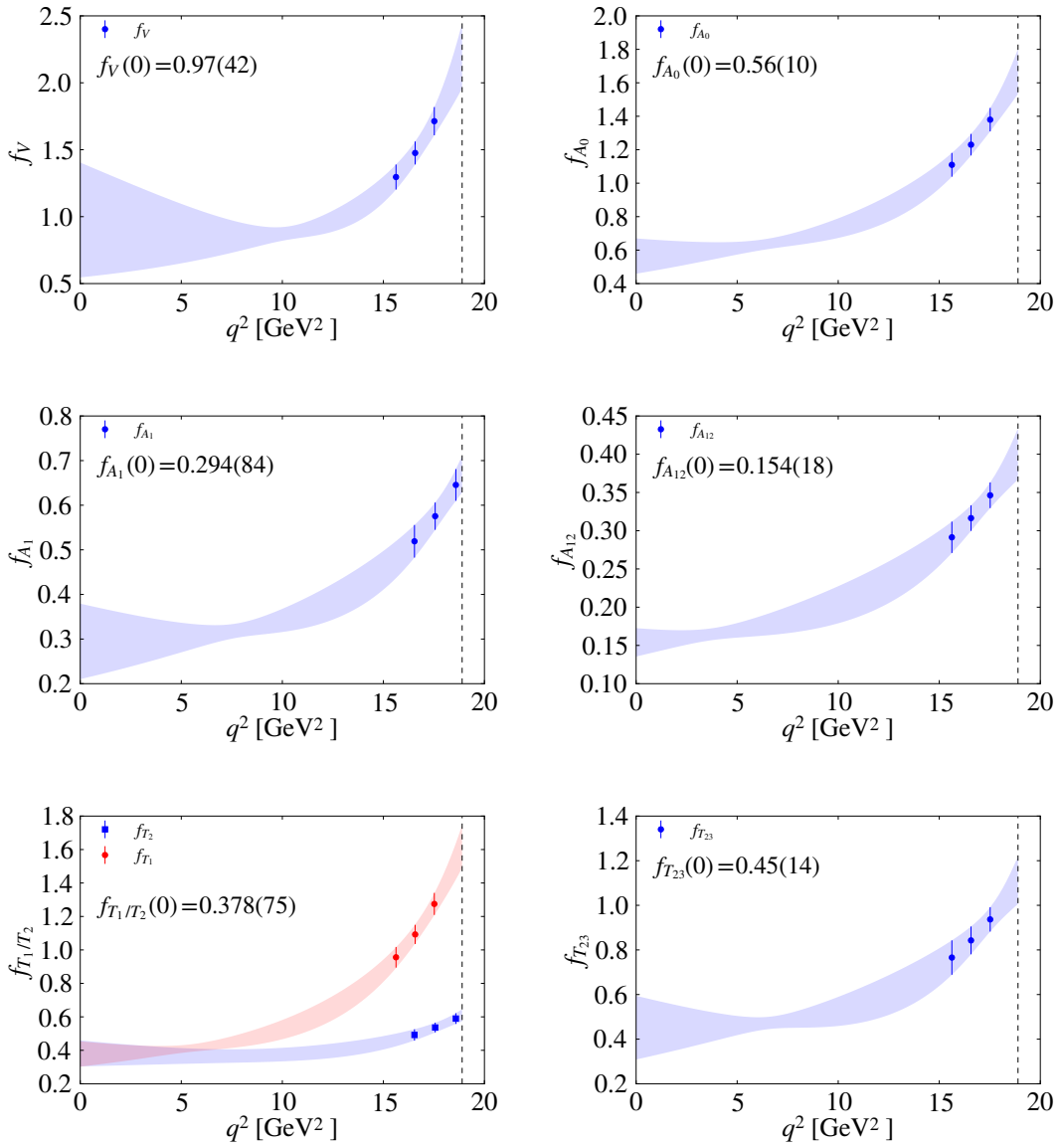

Figure 6.19: Preferred $K = 3$ fit of the $B_s \to K\ell^+\ell^-$ form factors f_V, f_{A_0},f_{A_1}, $f_{A_{12}}$, f_{T_1}, f_{T_2} and $f_{T_{23}}$ to the z-expansion (6.56). We have hard coded the kinematic constraint $f_{T_1}(0) = f_{T_2}(0)$. The solid curves with error bands show the fit results. The vertical dashed line on the right-hand side of each plot shows $q^2 = (M_{B_s} - M_\phi)^2$.

Chapter 7

Conclusions

In this work we have carried out the first calculation of $B_s \to D_s \ell\nu$ form factors using RHQ b quarks and heavy DWF c quarks. We also performed an update on the calculation of $B_s \to K\ell\nu$ form factors of reference [135] with RHQ b quarks. We independently determined the flavor conserving factor Z_V^{bb} and the perturbative coefficient ρ, which together with Z_V^{ll} are necessary for the renormalization of vector and axial vector currents. We have also calculated the one loop matching coefficients necessary to improve vector and axial vector currents to $\mathcal{O}(\alpha_s a)$.

We determined the $\mathcal{O}(a)$ improvement terms for tensor and pseudotensor currents, which together with a future determination of matching coefficients at one-loop can be used to reduce discretization errors in the heavy-strange tensor and pseudotensor currents by improving them through $\mathcal{O}(\alpha_s a)$. Working at tree-level, we performed the first calculation of $B_s \to \phi\ell^+\ell^-$ form factors with RHQ b quarks and DWF s quarks. Rare B decays are particularly challenging due to long-distance effects and the limited number of q^2 values than can be simulated.

In the region of parameter space on which our simulations were performed our fit results for the form factors f_+ and f_0 for the tree level decays $B_s \to K\ell\nu$ and $B_s \to D_s\ell\nu$ are in agreement with those obtained by the HPQCD collaboration using NRQCD [8, 9]. However, there is significant tension between our extrapolated results at $q^2 = 0$ and those obtained from LCSR [173, 174].

Our results for the rare B decay $B_s \to \phi\ell^+\ell^-$ are of particular importance as this decay, being mediated by FCNC proceeds only through box and penguin diagrams. This suppression results in a strong sensitivity to New Physics making it an ideal testing ground in the search for new particles.

Our final results for the rare B decay $B_s \to \phi\ell^+\ell^-$ form factors in the region $q^2_{\max} = (M_{B_s} - M_\phi)^2$ are mostly in agreement within statistical errors with those obtained by the Cambridge group using NRQCD [16, 176, 177], the two exceptions being the form

factors f_V and f_{T_1}. Once our results were extrapolated to $q^2 = 0$ all of our form factors except f_V were in agreement with those obtained using LCSR [17].

The calculations performed in this dissertation provide important, independent checks to existing calculations by the Cambridge group [16, 176, 177], HPQCD [9, 178], and the Fermilab/MILC [179, 180] collaborations which are all based on overlapping sets of MILC's staggered gauge field configurations, and which use NRQCD b quarks together with highly improved staggered (HISQ) and/or AsqTad light and s quarks in the valence sector.

Appendix A

Conventions

A.1 Notation

- Throughout this work in units in which $c = \hbar = 1$
- Space time coordinates:
- Minkowski metric is $g_{\mu\nu} = \text{diag}(1, -1, -1, -1)$
- Space time indices are denoted by Greek letters, latin indices indicate space components only.
- Pauli matrices:

$$\sigma_1 = \begin{bmatrix} 0 & 1 \\ 1 & 0 \end{bmatrix} \quad \sigma_2 = \begin{bmatrix} 0 & -i \\ i & 0 \end{bmatrix} \quad \sigma_3 = \begin{bmatrix} 1 & 0 \\ 0 & -1 \end{bmatrix} \tag{A.1}$$

- Gell-Mann matrices

$$\lambda_1 = \begin{bmatrix} 0 & 1 & 0 \\ 1 & 0 & 0 \\ 0 & 0 & 0 \end{bmatrix} \quad \lambda_2 = \begin{bmatrix} 0 & -i & 0 \\ i & 0 & 0 \\ 0 & 0 & 0 \end{bmatrix} \quad \lambda_3 = \begin{bmatrix} 1 & 0 & 0 \\ 0 & -1 & 0 \\ 0 & 0 & 0 \end{bmatrix} \tag{A.2}$$

$$\lambda_4 = \begin{bmatrix} 0 & 0 & 1 \\ 0 & 0 & 0 \\ 1 & 0 & 0 \end{bmatrix} \quad \lambda_5 = \begin{bmatrix} 0 & 0 & -i \\ 0 & 0 & 0 \\ i & 0 & 0 \end{bmatrix} \quad \lambda_6 = \begin{bmatrix} 0 & 0 & 0 \\ 0 & 0 & 1 \\ 0 & 1 & 0 \end{bmatrix} \tag{A.3}$$

$$\lambda_7 = \begin{bmatrix} 0 & 0 & 0 \\ 0 & 0 & -i \\ 0 & i & 0 \end{bmatrix} \quad \lambda_8 = \frac{1}{\sqrt{3}} \begin{bmatrix} 1 & 0 & 0 \\ 0 & 1 & 0 \\ 0 & 0 & -2 \end{bmatrix} \tag{A.4}$$

- Gamma matrices in Minkowski space:

$$\gamma_0 = \begin{bmatrix} \sigma_0 & 0 \\ 0 & -\sigma_0 \end{bmatrix} \quad \gamma_j = \begin{bmatrix} 0 & \sigma_j \\ -\sigma_j & 0 \end{bmatrix} \quad \gamma_5 = i\gamma_0\gamma_1\gamma_2\gamma_3 = \begin{bmatrix} 0 & \sigma_0 \\ -\sigma_0 & 0 \end{bmatrix} \tag{A.5}$$

- Gamma matrices in Euclidean space:

$$\gamma_0 = \begin{bmatrix} \sigma_0 & 0 \\ 0 & -\sigma_0 \end{bmatrix} \quad \gamma_j = \begin{bmatrix} 0 & -i\sigma_j \\ i\sigma_j & 0 \end{bmatrix} \quad \gamma_5 = i\gamma_0\gamma_1\gamma_2\gamma_3 = \begin{bmatrix} 0 & \sigma_0 \\ \sigma_0 & 0 \end{bmatrix} \tag{A.6}$$

Appendix B

Numerical results

a^{-1}[GeV]	m_l	n^2	$[t_{\min}, t_{\max}]$	$M_{B_s}^{1/2} f_\perp$	χ^2/dof	p	$[t_{\min}, t_{\max}]$	$M_{B_s}^{-1/2} f_\parallel$	χ^2/dof	p
1.785	0.005	0					[6, 10]	0.6465(73)	1.01	40 %
		1	[6, 10]	2.609(42)	2.16	7 %	[6, 10]	0.5489(75)	0.60	66 %
		2	[6, 10]	2.016(42)	2.54	4 %	[6, 10]	0.4820(99)	0.44	77 %
		3	[6, 10]	1.645(59)	1.51	19 %	[6, 10]	0.432(15)	0.54	70 %
		4	[6, 10]	1.433(83)	0.88	47 %	[6, 10]	0.420(24)	0.65	62 %
1.785	0.010	0					[6, 10]	0.6542(76)	2.44	4 %
		1	[6, 10]	2.555(38)	0.98	42 %	[6, 10]	0.5553(80)	1.06	37 %
		2	[6, 10]	1.978(41)	0.12	97 %	[6, 10]	0.497(10)	0.20	94 %
		3	[6, 10]	1.676(57)	0.38	82 %	[6, 10]	0.468(16)	0.12	97 %
		4	[6, 10]	1.502(80)	0.34	85 %	[6, 10]	0.448(22)	0.15	96 %
2.383	0.004	0					[8, 13]	0.6485(79)	0.62	73 %
		1	[8, 13]	2.582(43)	0.66	70 %	[8, 13]	0.5569(94)	0.40	90 %
		2	[8, 13]	2.046(52)	0.94	47 %	[8, 13]	0.496(13)	0.70	67 %
		3	[8, 13]	1.608(79)	1.69	10 %	[8, 13]	0.443(20)	0.99	43 %
		4	[8, 13]	1.34(14)	1.32	23 %	[8, 13]	0.394(34)	1.40	20 %
2.383	0.006	0					[8, 13]	0.6408(54)	3.57	0 %
		1	[8, 13]	2.514(32)	2.76	1 %	[8, 13]	0.5462(61)	0.91	50 %
		2	[8, 13]	2.084(39)	0.62	74 %	[8, 13]	0.4858(92)	0.56	79 %
		3	[8, 13]	1.738(56)	0.54	80 %	[8, 13]	0.439(15)	0.24	97 %
		4	[8, 13]	1.482(85)	0.69	68 %	[8, 13]	0.398(25)	0.88	52 %
2.383	0.008	0					[8, 13]	0.6537(79)	2.05	4 %
		1	[8, 13]	2.521(39)	2.34	2 %	[8, 13]	0.5666(84)	0.72	65 %
		2	[8, 13]	2.056(42)	0.49	84%	[8, 13]	0.495(11)	0.83	55 %
		3	[8, 13]	1.705(66)	1.01	42%	[8, 13]	0.453(19)	1.35	22 %
		4	[8, 13]	1.40(10)	0.26	97 %	[8, 13]	0.412(34)	1.06	38 %

Table B.1: Form factors $f_\parallel$ and $f_\perp$ on all ensembles. Results are shown for K meson momenta $\vec{p}^2 = (2\pi\vec{n}/L)^2$

m_l	m_c	n^2	$[t_{\min}, t_{\max}]$	$M_{B_s}^{1/2} f_\perp$	χ^2/dof	p	$[t_{\min}, t_{\max}]$	$M_{B_s}^{-1/2} f_\parallel$	χ^2/dof	p
0.005	0.300	0					[9, 13]	0.7637(51)	0.03	100 %
		1	[7, 13]	1.313(13)	0.74	61 %	[9, 13]	0.7380(57)	0.17	95 %
		2	[7, 13]	1.234(14)	0.73	62 %	[9, 13]	0.7144(74)	0.61	65 %
		3	[7, 13]	1.162(17)	0.95	45 %	[9, 13]	0.690(10)	1.12	34 %
		4	[7, 13]	1.111(23)	0.29	94 %	[9, 13]	0.666(14)	3.65	1 %
0.005	0.350	0					[9, 13]	0.7812(56)	0.03	100 %
		1	[7, 13]	1.239(13)	0.80	57 %	[9, 13]	0.7602(62)	0.22	92 %
		2	[7, 13]	1.175(14)	0.80	57 %	[9, 13]	0.7406(80)	0.85	49 %
		3	[7, 13]	1.115(17)	1.05	39 %	[9, 13]	0.720(11)	1.56	18 %
		4	[7, 13]	1.074(22)	0.40	88 %	[9, 13]	0.697(15)	4.40	0 %
0.005	0.400	0					[9, 13]	0.7946(61)	0.04	100 %
		1	[7, 13]	1.172(14)	0.85	53 %	[9, 13]	0.7781(69)	0.29	88 %
		2	[7, 13]	1.120(15)	0.87	51 %	[9, 13]	0.7625(88)	1.12	34 %
		3	[7, 13]	1.070(18)	1.18	31 %	[9, 13]	0.744(12)	2.07	8 %
		4	[7, 13]	1.036(22)	0.52	79 %	[9, 13]	0.723(16)	5.19	0 %
0.010	0.300	0					[9, 13]	0.7534(54)	0.36	83 %
		1	[7, 13]	1.315(13)	1.73	11 %	[9, 13]	0.7249(60)	0.34	84 %
		2	[7, 13]	1.226(15)	1.59	14 %	[9, 13]	0.7007(77)	0.34	85 %
		3	[7, 13]	1.140(18)	1.27	27 %	[9, 13]	0.680(11)	0.30	87 %
		4	[7, 13]	1.102(23)	2.35	3 %	[9, 13]	0.663(15)	0.35	84 %
0.010	0.350	0					[9, 13]	0.7692(59)	0.40	81 %
		1	[7, 13]	1.238(14)	1.85	8 %	[9, 13]	0.7451(66)	0.37	83 %
		2	[7, 13]	1.165(15)	1.66	12 %	[9, 13]	0.7250(84)	0.34	84 %
		3	[7, 13]	1.093(18)	1.50	17 %	[9, 13]	0.708(11)	0.34	85 %
		4	[7, 13]	1.068(23)	2.55	2 %	[9, 13]	0.695(16)	0.40	81 %
0.010	0.400	0					[9, 13]	0.7807(65)	0.44	78 %
		1	[7, 13]	1.169(14)	1.87	8 %	[9, 13]	0.7609(72)	0.40	80 %
		2	[7, 13]	1.108(16)	1.67	12 %	[9, 13]	0.7451(92)	0.37	83 %
		3	[7, 13]	1.046(19)	1.69	12 %	[9, 13]	0.732(12)	0.41	80 %
		4	[7, 13]	1.032(23)	2.66	1 %	[9, 13]	0.724(17)	0.49	74 %

Table B.2: Form factors $f_\parallel$ and $f_\perp$ on all ensembles with $a^{-1} = 1.785$ GeV. Results are shown for D_s meson momenta $\vec{p}^2 = (2\pi\vec{n}/L)^2$

m_l	m_c	n^2	$[t_{\min}, t_{\max}]$	$M_{B_s}^{1/2} f_\perp$	χ^2/dof	p	$[t_{\min}, t_{\max}]$	$M_{B_s}^{-1/2} f_\parallel$	χ^2/dof	p
0.004	0.280	0					[12, 17]	0.8286(69)	0.47	80 %
		1	[9, 17]	1.247(15)	1.70	9 %	[12, 17]	0.8037(78)	0.45	81 %
		2	[9, 17]	1.189(17)	1.75	8 %	[12, 17]	0.776(10)	0.41	84 %
		3	[9, 17]	1.134(20)	1.72	9 %	[12, 17]	0.747(14)	0.45	81 %
		4	[9, 17]	1.067(24)	2.21	2 %	[12, 17]	0.707(19)	0.39	86 %
0.004	0.340	0					[12, 17]	0.8515(79)	0.52	76 %
		1	[9, 17]	1.147(15)	1.86	6 %	[12, 17]	0.8310(90)	0.43	82 %
		2	[9, 17]	1.102(17)	1.98	4 %	[12, 17]	0.807(11)	0.43	83 %
		3	[9, 17]	1.059(20)	2.02	4 %	[12, 17]	0.780(15)	0.57	72 %
		4	[9, 17]	1.008(24)	2.47	1 %	[12, 17]	0.742(21)	0.47	79 %
0.006	0.280	0					[12, 17]	0.8214(56)	0.74	59 %
		1	[9, 17]	1.261(13)	1.66	10 %	[12, 17]	0.7993(64)	0.48	79 %
		2	[9, 17]	1.213(14)	2.05	4 %	[12, 17]	0.7778(83)	0.38	86 %
		3	[9, 17]	1.171(17)	2.04	4 %	[12, 17]	0.754(11)	0.32	90 %
		4	[9, 17]	1.088(21)	1.80	7 %	[12, 17]	0.742(16)	0.47	80 %
0.006	0.340	0					[12, 17]	0.8429(64)	0.83	53 %
		1	[9, 17]	1.161(13)	1.56	13 %	[12, 17]	0.8259(73)	0.47	79 %
		2	[9, 17]	1.128(15)	2.00	4 %	[12, 17]	0.8087(94)	0.33	89 %
		3	[9, 17]	1.097(17)	2.06	4 %	[12, 17]	0.788(12)	0.26	93 %
		4	[9, 17]	1.028(21)	1.91	5 %	[12, 17]	0.781(18)	0.47	80 %
0.008	0.280	0					[12, 17]	0.8301(73)	0.50	78 %
		1	[9, 17]	1.230(18)	1.45	17 %	[12, 17]	0.8099(84)	0.42	83 %
		2	[9, 17]	1.179(19)	1.40	19 %	[12, 17]	0.790(10)	0.63	67 %
		3	[9, 17]	1.127(22)	1.17	31 %	[12, 17]	0.771(15)	0.84	52 %
		4	[9, 17]	1.047(30)	1.67	10 %	[12, 17]	0.746(21)	1.53	17 %
0.008	0.340	0					[12, 17]	0.8550(84)	0.65	66 %
		1	[9, 17]	1.134(18)	1.57	13 %	[12, 17]	0.8400(96)	0.56	73 %
		2	[9, 17]	1.098(20)	1.52	14 %	[12, 17]	0.824(12)	0.83	52 %
		3	[9, 17]	1.059(22)	1.27	25 %	[12, 17]	0.808(16)	1.11	35 %
		4	[9, 17]	0.992(29)	1.68	10 %	[12, 17]	0.785(22)	1.76	12 %

Table B.3: Form factors $f_\parallel$ and $f_\perp$ on all ensembles with $a^{-1} = 2.383$ GeV. Results are shown for D_s meson momenta $\vec{p}^2 = (2\pi\vec{n}/L)^2$

a^{-1}[GeV]	m_l	n^2	$[t_{\min}, t_{\max}]$	f_V	χ^2/dof	p	$[t_{\min}, t_{\max}]$	f_{A_0}	χ^2/dof	p
1.785	0.005	0								
		1	[8, 15]	1.568(45)	0.44	88%	[8, 15]	1.417(40)	1.59	13%
		2	[8, 15]	1.397(45)	0.21	98%	[8, 15]	1.239(37)	1.53	15%
		3	[8, 15]	1.244(56)	0.18	99%	[8, 15]	1.069(42)	1.32	24%
1.785	0.010	0								%
		1	[8, 15]	1.559(63)	1.55	15%	[8, 15]	1.412(53)	0.37	92%
		2	[8, 15]	1.346(60)	2.34	2 %	[8, 15]	1.258(48)	0.50	83%
		3	[8, 15]	1.222(68)	0.59	76%	[8, 15]	1.133(53)	0.46	87%
2.383	0.004	0								
		1	[10, 20]	1.626(54)	1.49	14%	[10, 20]	1.356(44)	1.49	13%
		2	[10, 20]	1.393(48)	1.22	27%	[10, 20]	1.207(40)	1.44	15%
		3	[10, 20]	1.220(54)	0.51	88%	[10, 20]	1.091(45)	1.01	44%
2.383	0.006	0								
		1	[10, 20]	1.636(59)	0.56	85%	[10, 20]	1.480(53)	0.82	61%
		2	[10, 20]	1.435(58)	0.77	66%	[10, 20]	1.265(48)	0.93	51%
		3	[10, 20]	1.300(72)	0.76	67%	[10, 20]	1.106(54)	1.37	19%
2.383	0.008	0								
		1	[10, 20]	1.609(60)	0.62	80%	[10, 20]	1.384(49)	1.55	12%
		2	[10, 20]	1.451(59)	1.20	29%	[10, 20]	1.225(47)	0.80	63%
		3	[10, 20]	1.261(69)	0.76	67%	[10, 20]	1.139(53)	0.48	90%

Table B.4: Form factors f_V and f_{A_0} on all ensembles. Results are shown for ϕ meson momenta $\vec{p}^2 = (2\pi\vec{n}/L)^2$

a^{-1}[GeV]	m_l	n^2	$[t_{\min}, t_{\max}]$	f_V	χ^2/dof	p	$[t_{\min}, t_{\max}]$	$f_{A_{12}}$	χ^2/dof	p
1.785	0.005	0	[8, 15]	0.588(11)	0.78	60%	[8, 15]			
		1	[8, 15]	0.551(12)	1.21	29%	[8, 15]	0.3455(75)	1.13	34%
		2	[8, 15]	0.511(15)	0.85	55%	[8, 15]	0.3151(81)	0.96	46%
		3	[8, 15]				[8, 15]	0.284(10)	0.33	94%
1.785	0.010	0	[8, 15]	0.598(18)	0.81	58%	[8, 15]			
		1	[8, 15]	0.566(17)	0.92	49%	[8, 15]	0.3402(98)	0.59	77%
		2	[8, 15]	0.545(20)	1.23	28%	[8, 15]	0.328(10)	1.40	20%
		3	[8, 15]				[8, 15]	0.315(12)	2.09	4%
2.383	0.004	0	[10, 20]	0.598(14)	1.81	5%	[10, 20]			
		1	[10, 20]	0.554(15)	1.42	16%	[10, 20]	0.3364(88)	1.72	7%
		2	[10, 20]	0.505(17)	1.70	7%	[10, 20]	0.3082(88)	1.54	12%
		3	[10, 20]				[10, 20]	0.287(11)	1.19	29%
2.383	0.006	0	[10, 20]	0.596(16)	1.55	12%	[10, 20]			
		1	[10, 20]	0.547(16)	1.01	43%	[10, 20]	0.341(10)	1.52	13%
		2	[10, 20]	0.506(20)	2.04	3%	[10, 20]	0.320(10)	1.11	35%
		3	[10, 20]				[10, 20]	0.292(13)	1.19	29%
2.383	0.008	0	[10, 20]	0.634(16)	0.77	66%	[10, 20]			
		1	[10, 20]	0.585(17)	1.13	34%	[10, 20]	0.359(10)	0.41	94%
		2	[10, 20]	0.554(20)	1.81	5%	[10, 20]	0.331(11)	0.73	70%
		3	[10, 20]				[10, 20]	0.312(13)	0.45	92%

Table B.5: Form factors f_{A_1} and $f_{A_{12}}$ on all ensembles. Results are shown for ϕ meson momenta $\vec{p}^2 = (2\pi\vec{n}/L)^2$

a^{-1}[GeV]	m_l	n^2	$[t_{\min}, t_{\max}]$	f_{T_1}	χ^2/dof	p	f_{T_2}	χ^2/dof	p	$f_{T_{23}}$	χ^2/dof	p
1.785	0.005	0	[8, 15]				0.553(11)	0.86	54%			
		1	[8, 15]	1.186(30)	0.93	48%	0.533(12)	0.79	59%	0.984(22)	1.03	41%
		2	[8, 15]	1.037(30)	1.20	30%	0.477(14)	0.33	94%	0.904(25)	0.47	86%
		3	[8, 15]	0.925(37)	0.72	66%				0.822(32)	0.45	87%
1.785	0.010	0	[8, 15]				0.566(17)	0.58	77%			
		1	[8, 15]	1.194(42)	1.02	42%	0.553(17)	0.47	86%	0.956(29)	0.61	75%
		2	[8, 15]	1.022(40)	2.09	4%	0.514(19)	0.64	72%	0.925(30)	1.14	33%
		3	[8, 15]	0.911(45)	0.57	78%				0.886(38)	1.16	32%
2.383	0.004	0	[10, 20]				0.560(13)	1.55	12%			
		1	[10, 20]	1.223(36)	2.15	2%	0.537(15)	1.78	6%	0.945(25)	1.69	8%
		2	[10, 20]	1.035(32)	1.73	7%	0.475(16)	1.53	12%	0.865(26)	2.06	2%
		3	[10, 20]	0.884(36)	1.79	6%				0.794(34)	1.72	7%
2.383	0.006	0	[10, 20]				0.559(15)	1.85	5%			
		1	[10, 20]	1.225(39)	1.32	21%	0.534(16)	0.92	52%	0.950(29)	1.74	7%
		2	[10, 20]	1.064(38)	1.62	10%	0.482(19)	1.02	43%	0.892(32)	1.09	37%
		3	[10, 20]	0.947(47)	1.89	4%				0.802(42)	1.07	38%
2.383	0.008	0	[10, 20]				0.592(15)	0.28	99%			
		1	[10, 20]	1.238(40)	0.75	68%	0.565(16)	0.51	89%	0.989(30)	0.24	99%
		2	[10, 20]	1.103(40)	1.39	18%	0.519(18)	1.49	14%	0.911(32)	0.35	97%
		3	[10, 20]	0.972(45)	0.57	84%				0.868(40)	0.44	93%

Table B.6: Form factors f_{T_1} and f_{T_2} and f_{T_23} on all ensembles. Results are shown for ϕ meson momenta $\vec{p}^2 = (2\pi\vec{n}/L)^2$

(am_{sea}, fit type, form factor)	χ^2/dof	fitted value($k^2 = 1$)	c_0	c_1	c_2	c_3	c_4
m005, I,$f_\parallel$	0.313	0.7995(71)	0.508(10)	0.282(12)	-0.0203(31)		
m005, I,$f_\perp$	0.909	1.130(13)	2.015(27)	-0.755(26)	-0.0526(49)		
m005, II,$f_\parallel$	0.048	0.7978(71)	0.5624(91)	0.225(11)	-0.0648(49)	0.0471(54)	
m005, II,$f_\perp$	0.323	1.099(13)	2.348(27)	-1.106(27)	-0.199(11)	0.1550(96)	
m005, III,$f_\parallel$	0.321	0.7989(71)	0.509(10)	0.282(12)	-0.0219(27)	0.00042(0.00077)	
m005, III,$f_\perp$	0.666	1.136(13)	2.045(27)	-0.756(26)	-0.0808(82)	0.0051(15)	
m005, IV,$f_\parallel$	0.041	0.7973(71)	0.5626(91)	0.225(11)	-0.0658(56)	0.0468(51)	0.00035(0.00077)
m005, IV,$f_\perp$	0.026	1.106(13)	2.370(27)	-1.100(27)	-0.224(13)	0.1521(96)	0.0049(15)
m010, I,$f_\parallel$	0.642	0.7881(77)	0.513(11)	0.266(13)	-0.0192(33)		
m010, I,$f_\perp$	1.409	1.130(14)	2.009(29)	-0.751(27)	-0.0503(54)		
m010, II,$f_\parallel$	0.293	0.7860(77)	0.5815(99)	0.194(12)	-0.0756(53)	0.0595(59)	
m010, II,$f_\perp$	0.764	1.096(14)	2.392(31)	-1.153(30)	-0.219(12)	0.178(10)	
m010, III,$f_\parallel$	0.386	0.7853(77)	0.516(11)	0.266(13)	-0.0269(29)	0.00200(82)	
m010, III,$f_\perp$	1.053	1.138(14)	2.048(28)	-0.751(27)	-0.0873(89)	0.0067(17)	
m010, IV,$f_\parallel$	0.013	0.7833(77)	0.5833(99)	0.195(12)	-0.0814(61)	0.0578(56)	0.00193(82)
m010, IV,$f_\perp$	0.339	1.105(14)	2.423(31)	-1.146(30)	-0.252(14)	0.174(10)	0.0065(17)

Table B.7: Coefficients for different fits — c.f section 6.3.2.1 — for the renormalized and $\mathcal{O}(\alpha_s a)$ improved form factors $f_\parallel$ and $f_\perp$ of the decay $B_s \to D_s \ell\nu$

(am_{sea}, fit type, form factor)	χ^2/dof	fitted value($k^2=1$)	c_0	c_1	c_2	c_3	c_4
m004, I,$f_\parallel$	0.195	0.8091(82)	0.583(14)	0.308(20)	-0.0286(41)		
m004, I,$f_\perp$	0.319	1.178(14)	1.973(29)	-0.910(33)	-0.0435(55)		
m004, II,$f_\parallel$	0.157	0.8089(82)	0.621(11)	0.261(19)	-0.0591(61)	0.0377(79)	
m004, II,$f_\perp$	0.048	1.174(14)	2.259(31)	-1.263(37)	-0.168(12)	0.154(12)	
m004, III,$f_\parallel$	0.070	0.8113(82)	0.580(13)	0.308(20)	-0.0223(34)	-0.00164(91)	
m004, III,$f_\perp$	0.371	1.178(14)	1.974(29)	-0.910(33)	-0.0446(92)	0.00020(0.00170)	
m004, IV,$f_\parallel$	0.001	0.8111(82)	0.620(11)	0.259(19)	-0.0541(70)	0.0395(74)	-0.00167(90)
m004, IV,$f_\perp$	0.058	1.174(14)	2.259(31)	-1.263(37)	-0.168(14)	0.154(12)	0.00006(0.00170)
m006, I,$f_\parallel$	0.202	0.8199(67)	0.577(11)	0.316(16)	-0.0191(35)		
m006, I,$f_\perp$	0.470	1.208(13)	1.996(26)	-0.906(29)	-0.0387(47)		
m006, II,$f_\parallel$	0.073	0.8196(67)	0.6257(97)	0.256(15)	-0.0593(48)	0.0496(65)	
m006, II,$f_\perp$	0.179	1.205(13)	2.271(26)	-1.245(31)	-0.157(10)	0.1461(98)	
m006, III,$f_\parallel$	0.213	0.8193(67)	0.577(11)	0.316(16)	-0.0207(28)	0.00042(0.00081)	
m006, III,$f_\perp$	0.548	1.208(13)	1.996(26)	-0.906(29)	-0.0391(76)	0.00006(0.00144)	
m006, IV,$f_\parallel$	0.070	0.8191(67)	0.6260(96)	0.257(15)	-0.0604(56)	0.0492(62)	0.00038(0.00081)
m006, IV,$f_\perp$	0.215	1.205(13)	2.271(26)	-1.245(31)	-0.157(11)	0.1461(98)	-0.00004(0.00144)
m008, I,$f_\parallel$	0.079	0.8281(87)	0.558(15)	0.348(21)	-0.0183(45)		
m008, I,$f_\perp$	0.332	1.181(16)	1.924(31)	-0.849(35)	-0.0409(61)		
m008, II,$f_\parallel$	0.013	0.8279(87)	0.601(12)	0.295(19)	-0.0544(62)	0.0446(82)	
m008, II,$f_\perp$	0.118	1.178(16)	2.224(34)	-1.218(41)	-0.171(13)	0.159(12)	
m008, III,$f_\parallel$	0.086	0.8278(87)	0.558(14)	0.348(21)	-0.0193(39)	0.00026(0.00102)	
m008, III,$f_\perp$	0.361	1.183(16)	1.935(32)	-0.849(35)	-0.050(10)	0.00172(0.00191)	
m008, IV,$f_\parallel$	0.012	0.8276(87)	0.601(12)	0.295(19)	-0.0551(72)	0.0443(77)	0.00022(0.00101)
m008, IV,$f_\perp$	0.116	1.180(16)	2.231(35)	-1.215(41)	-0.178(15)	0.158(12)	0.00157(0.00192)

Table B.8: Coefficients for different fits — c.f section 6.3.2.1 — for the renormalized and $\mathcal{O}(\alpha_s a)$ improved form factors $f_\parallel$ and $f_\perp$ of the decay $B_s \to D_s \ell\nu$ (cont)

	f_+						f_0							
K	$b^{(0)}$	$b^{(1)}/b^{(0)}$	$b^{(2)}/b^{(0)}$	$b^{(3)}/b^{(0)}$	$\sum B_{mn}b_m b_n$	K	$b^{(0)}$	$b^{(1)}/b^{(0)}$	$b^{(2)}/b^{(0)}$	$b^{(3)}/b^{(0)}$	$\sum B_{mn}b_m b_n$	$f(q^2=0)$	χ^2/dof	p
1	0.450(14)				0.002							0.450(14)	75.5	0%
						1	0.2108(54)				0.004	0.2108(54)	25.9	0%
2	0.355(16)	-3.16(35)			0.022							0.179(26)	1.84	17%
						2	0.2370(67)	0.6983(67)			0.008	0.2611(92)	7.04	1%
3	0.338(20)	-5.(1)	-14(1)		0.372							-0.0297(0.1564)		
						3	0.217(10)	-1.042(10)	-8.04(72)		0.337	0.146(44)		
2	0.398(10)	-2.084(86)			0.014	2	0.2423(63)	0.738(89)			0.009	0.2684(87)	5.00	0%
3	0.372(14)	-2.32(13)	1(1)		0.024	2	0.2367(67)	0.689(93)			0.008	0.2605(92)	3.88	2%
2	0.355(16)	-3.16(35)			0.022	3	0.2218(85)	-0.51(39)	-5(1)		0.175	0.178(26)	1.01	36%
3	0.354(16)	-3.40(48)	-3(2)		0.035	3	0.217(10)	-0.93(71)	-7(3)		0.298	0.153(43)	1.48	22%
2	0.398(10)	-2.083(86)			0.014	2	0.2423(63)	0.738(89)			0.009	0.2684(87)	3.75	0%
3	0.373(13)	-2.30(12)	1.41(88)		0.022	2	0.2370(66)	0.692(92)			0.008	0.2609(91)	2.65	5%
2	0.355(16)	-3.15(34)			0.022	3	0.2220(85)	-0.50(39)	-5(1)		0.171	0.179(26)	0.73	53%
3	0.355(16)	-3.27(38)	-2(1)		0.027	3	0.2200(89)	-0.71(50)	-6(2)		0.231	0.166(31)	0.98	37%

Table B.9: Coefficients of the z-parametrization of the $B_s \to K\ell\nu$ decay form factors f_0 (6.33) and f_+ (6.34). First panel unconstrained fits, second panel fits subject to the constraint $f_+(q^2=0) = f_0(q^2=0)$, the third panel shows results for fits including the constraint of panel two plus the unitarity constraint $\sum B_{jk}b_j b_k$. Results shown are for correlated fits.

			f_+						f_0					
K	$b^{(0)}$	$b^{(1)}/b^{(0)}$	$b^{(2)}/b^{(0)}$	$b^{(3)}/b^{(0)}$	$\sum B_{mn}b_m b_n$	K	$b^{(0)}$	$b^{(1)}/b^{(0)}$	$b^{(2)}/b^{(0)}$	$b^{(3)}/b^{(0)}$	$\sum B_{mn}b_m b_n$	$f(q^2=0)$	χ^2/dof	p
1	0.846(15)				6.915							0.846(15)	4.03	2%
						1	0.644(12)				0.000	0.644(12)	0.57	56%
2	0.677(67)	-11(5)			0.006							0.44(15)	0.07	79%
						2	0.586(61)	-4.130(61)			0.002	0.51(12)	0.01	90%
3	0.759(37)	0.753(0.868)	25(1)		4.320							0.957(61)		
						3	0.623(39)	1.899(39)	135.(82)		2.315	0.735(36)		
2	0.694(61)	-9(4)			0.005	2	0.573(64)	-5(4)			0.003	0.48(13)	0.07	97%
3	0.688(63)	-9(4)	35.262(38.918)		0.096	2	0.587(61)	-4.068(4.280)			0.002	0.51(12)	0.03	97%
2	0.678(67)	-11(5)			0.006	3	0.575(63)	-6(5)	-43.154(46.208)		0.193	0.44(15)	0.04	95%
3	0.740(40)	-1.76(16)	20(9)		2.579	3	0.640(37)	4.47(58)	19(1)		4.945	0.839(26)	0.00	93%
2	0.693(60)	-9(4)			0.005	2	0.573(63)	-5(4)			0.003	0.48(13)	0.06	99%
3	0.693(60)	-9(4)	5(3)		0.012	2	0.577(64)	-4(4)			0.003	0.49(13)	0.05	98%
2	0.677(66)	-11(5)			0.006	3	0.574(63)	-6(5)	-44.748(45.465)		0.208	0.44(14)	0.03	99%
3	0.676(65)	-11(4)	-14(2)		0.009	3	0.572(62)	-6.(4)	-53(4)		0.295	0.43(14)	0.05	95%

Table B.10: Coefficients of the z-parametrization of the $B_s \to D_s \ell\nu$ decay form factors f_0 (6.33) and f_+ (6.34). First panel unconstrained fits, second panel fits subject to the constraint $f_+(q^2=0) = f_0(q^2=0)$, the third panel shows results for fits including the constraint of panel two plus the unitarity contrain $\sum B_{jk} b_j, b_k$. Results shown are for uncorrelated fits.

Form factor	$b^{(0)}$	$b^{(1)}/b^{(0)}$	$b^{(2)}/b^{(0)}$	$f(q^2=0)$
f_V	0.561(33)	2.227(4.064)	93(7)	0.97(42)
f_{A_0}	0.476(41)	-0.124(0.872)	31.999(38.286)	0.56(10)
f_{A_1}	0.239(21)	0.00978(1.95269)	37.829(47.563)	0.294(84)
$f_{A_{12}}$	0.143(17)	-0.98(12)	24.477(38.282)	0.154(18)
f_{T_1}	0.257(28)	2(1)	43(3)	0.378(75)
f_{T_2}	0.353(40)	-3.56(55)	57(4)	0.378(75)
$f_{T_{23}}$	0.369(51)	-0.655(1.7112)	45.148(66.511)	0.45(14)

Table B.11: Coefficients of the z-parametrization (6.56) truncated at $K = 3$ for the $B_s \to \phi\ell\nu$ decay form factors. Results shown are for uncorrelated fits.

	q^2	$f_+^{B_s\to K}$			$f_0^{B_s\to K}$		
	[GeV^2]	1.07	0.77	0.53	1.07	0.77	0.53
f_+	1.07	1.6139e-03	2.0018e-03	2.9658e-03	5.2035e-04	5.1376e-04	6.0122e-04
	0.77	2.0018e-03	3.0997e-03	3.9310e-03	6.2021e-04	7.4453e-04	8.9291e-04
	0.53	2.9658e-03	3.9310e-03	8.5804e-03	9.0353e-04	1.0595e-03	1.3423e-03
f_0	1.07	5.2035e-04	6.2021e-04	9.0353e-04	2.5828e-04	2.2629e-04	2.6213e-04
	0.77	5.1376e-04	7.4453e-04	1.0595e-03	2.2629e-04	2.8290e-04	3.4583e-04
	0.53	6.0122e-04	8.9291e-04	1.3423e-03	2.6213e-04	3.4583e-04	4.4509e-04

Table B.12: Variance-covariance matrix for the $B_s \to K\ell\nu$ form factors at three representative q^2 values

	q^2	$f_+^{B_s\to D_s}$			$f_0^{B_s\to D_s}$		
	[GeV^2]	2.2	2.1	2.0	2.2	2.1	2.0
f_+	2.2	1.3687e-03	8.7742e-04	1.2447e-04	1.2463e-03	8.4080e-04	2.6153e-04
	2.1	8.7742e-04	6.4369e-04	2.8231e-04	7.6535e-04	5.6025e-04	2.6533e-04
	2.0	1.2447e-04	2.8231e-04	5.1792e-04	4.6244e-05	1.3981e-04	2.6689e-04
f_0	2.2	1.2463e-03	7.6535e-04	4.6244e-05	1.3654e-03	9.0960e-04	2.3755e-04
	2.1	8.4080e-04	5.6025e-04	1.3981e-04	9.0960e-04	6.3880e-04	2.3756e-04
	2.0	2.6153e-04	2.6533e-04	2.6689e-04	2.3751e-04	2.3756e-04	2.3487e-04

Table B.13: Variance-covariance matrix for the $B_s \to D_s\ell\nu$ form factors at three representative q^2 values

	q^2	$f_V^{B_s\to\phi}$			$f_{A_0}^{B_s\to\phi}$		
	[GeV^2]	15.6	16.6	17.6	15.6	16.6	17.6
f_V	15.6	1.7062e-06	1.4360e-06	8.9286e-07			
	16.6	1.4360e-06	1.4436e-06	1.3833e-06			
	17.6	8.9286e-07	1.3833e-06	2.1661e-06			
f_{A_0}	15.6				9.8533e-07	8.3852e-07	5.8806e-07
	16.6				8.3852e-07	8.0977e-07	7.4194e-07
	17.6				5.8806e-07	7.4194e-07	9.5731e-07

Table B.14: Variance-covariance matrix for the $B_s \to \phi\ell^+\ell^-$ form factors f_V and f_{A_0} at three representative q^2 values. We present the block diagonal covariance matrix for the form factors f_V and f_{A_0} as the correlation between these two form factors does not enter in our fits.

	q^2	$f_{A_1}^{B_s\to\phi}$			$f_{A_{12}}^{B_s\to\phi}$		
	[GeV^2]	16.6	17.6	18.6	15.6	16.6	17.6
f_{A_1}	16.6	2.6149e-07	1.9648e-07	9.4682e-08			
	17.6	1.9648e-07	1.8275e-07	1.5719e-07			
	18.6	9.4682e-08	1.5719e-07	2.4511e-07			
$f_{A_{12}}$	15.6				8.2016e-08	6.2420e-08	3.3725e-08
	16.6				6.2420e-08	5.4681e-08	4.2821e-08
	17.6				3.3725e-08	4.2821e-08	5.4881e-08

Table B.15: Variance-covariance matrix for the $B_s \to \phi\ell\ell$ form factors f_{A_1} and $f_{A_{12}}$ at three representative q^2 values. We present the block diagonal covariance matrix for the form factors f_{A_1} and $f_{A_{12}}$ as the correlation between these two form factors does not enter in our fits.

	q^2	$f_{T_1}^{B_s\to\phi}$			$f_{T_2}^{B_s\to\phi}$		
	[GeV^2]	15.6	16.6	17.6	16.6	17.6	18.6
f_{T_1}	15.6	7.4206e-07	6.4486e-07	4.3749e-07	2.3406e-07	2.0420e-07	1.5920e-07
	16.6	6.4486e-07	6.4011e-07	5.9672e-07	2.3959e-07	2.2090e-07	1.9094e-07
	17.6	4.3749e-07	5.9672e-07	8.4603e-07	2.3627e-07	2.3838e-07	2.3669e-07
f_{T_2}	16.6	2.3406e-07	2.3959e-07	2.3627e-07	2.2153e-07	1.7567e-07	1.0922e-07
	17.6	2.0420e-07	2.2090e-07	2.3838e-07	1.7567e-07	1.6576e-07	1.4893e-07
	18.6	1.5920e-07	1.9094e-07	2.3669e-07	1.0922e-07	1.4893e-07	2.0069e-07

Table B.16: Variance-covariance matrix for the $B_s \to \phi\ell\ell$ form factors f_{T_1} and f_{T_2} at three representative q^2 values. We present the full covariance matrix as we made use of it for the extrapolation of the form factors to $q^2 = 0$ with the contraint $f_{T_1}(0) = f_{T_2}(0)$.

	q^2	$f_{T_{23}}^{B_s\to\phi}$		
	[GeV^2]	15.6	16.6	17.6
$f_{T_{23}}$	15.6	1.1589e-06	8.9954e-07	4.9062e-07
	16.6	8.9954e-07	7.5988e-07	5.3286e-07
	17.6	4.9062e-07	5.3286e-07	5.8275e-07

Table B.17: Variance-covariance matrix for the $B_s \to \phi\ell^+\ell^-$ form factor $f_{T_{23}}$ at three representative q^2 values.

References

[1] W. Altmannshofer and D. M. Straub, "New physics in $b \to s$ transitions after LHC run 1," *Eur. Phys. J.*, vol. C75, no. 8, p. 382, 2015.

[2] A. Bharucha, D. M. Straub, and R. Zwicky, "$B \to V\ell^+\ell^-$ in the Standard Model from light-cone sum rules," *JHEP*, vol. 08, p. 098, 2016.

[3] R. Aaij *et al.*, "Angular analysis and differential branching fraction of the decay $B_s^0 \to \phi\mu^+\mu^-$," *JHEP*, vol. 09, p. 179, 2015.

[4] S. Descotes-Genon, T. Hurth, J. Matias, and J. Virto, "Optimizing the basis of $B \to K^*ll$ observables in the full kinematic range," *JHEP*, vol. 05, p. 137, 2013.

[5] R. Aaij *et al.*, "Measurement of Form-Factor-Independent Observables in the Decay $B^0 \to K^{*0}\mu^+\mu^-$," *Phys. Rev. Lett.*, vol. 111, p. 191801, 2013.

[6] C. Patrignani *et al.*, "Review of Particle Physics," *Chin. Phys.*, vol. C40, no. 10, p. 100001, 2016.

[7] Y. Aoki *et al.*, "Continuum Limit Physics from 2+1 Flavor Domain Wall QCD," *Phys.Rev.*, vol. D83, p. 074508, 2011.

[8] C. Bouchard, G. P. Lepage, C. Monahan, H. Na, and J. Shigemitsu, "$B_s \to K\ell\nu$ form factors from lattice QCD," *Phys.Rev.*, vol. D90, no. 5, p. 054506, 2014.

[9] C. J. Monahan, H. Na, C. M. Bouchard, G. P. Lepage, and J. Shigemitsu, "$B_s \to D_s\ell\nu$ Form Factors and the Fragmentation Fraction Ratio f_s/f_d," *Phys. Rev.*, vol. D95, no. 11, p. 114506, 2017.

[10] C. Allton *et al.*, "Physical Results from 2+1 Flavor Domain Wall QCD and SU(2) Chiral Perturbation Theory," *Phys. Rev.*, vol. D78, p. 114509, 2008.

[11] T. Blum *et al.*, "Domain wall QCD with physical quark masses," *Phys. Rev.*, vol. D93, no. 7, p. 074505, 2016.

[12] P. A. Boyle *et al.*, "in preparation," 2016.

[13] Y. Shamir, "Chiral fermions from lattice boundaries," *Nucl. Phys.*, vol. B406, pp. 90–106, 1993.

[14] V. Furman and Y. Shamir, "Axial symmetries in lattice QCD with Kaplan fermions," *Nucl. Phys.*, vol. B439, pp. 54–78, 1995.

[15] C. Lehner, 2014. in preparation.

[16] R. R. Horgan, Z. Liu, S. Meinel, and M. Wingate, "Lattice QCD calculation of form factors describing the rare decays $B \to K^* \ell^+ \ell^-$ and $B_s \to \phi \ell^+ \ell^-$," *Phys. Rev.*, vol. D89, no. 9, p. 094501, 2014.

[17] P. Ball and R. Zwicky, "$B_{d,s} \to \rho, \omega, K^*, \phi$ decay form-factors from light-cone sum rules revisited," *Phys. Rev.*, vol. D71, p. 014029, 2005.

[18] J. Flynn, A. J uttner, T. Kawanai, E. Lizarazo, and O. Witzel, "Hadronic form factors for rare semileptonic B decays," *PoS*, vol. LATTICE2015, p. 345, 2016.

[19] E. Lizarazo and O. Witzel, "Non-perturbative determinations of B-meson decay constants and semi-leptonic form factors," *PoS*, vol. ICHEP2016, p. 558, 2016.

[20] J. Flynn, T. Izubuchi, A. Juttner, T. Kawanai, C. Lehner, E. Lizarazo, A. Soni, J. T. Tsang, and O. Witzel, "Form factors for semi-leptonic B decays," 2016.

[21] S. L. Glashow, J. Iliopoulos, and L. Maiani, "Weak Interactions with Lepton-Hadron Symmetry," *Phys. Rev.*, vol. D2, pp. 1285–1292, 1970.

[22] M. Kobayashi and T. Maskawa, "CP Violation in the Renormalizable Theory of Weak Interaction," *Prog. Theor. Phys.*, vol. 49, pp. 652–657, 1973.

[23] N. Cabibbo, "Unitary symmetry and leptonic decays," *Phys. Rev. Lett.*, vol. 10, pp. 531–532, 1963.

[24] G. Aad *et al.*, "Observation of a new particle in the search for the Standard Model Higgs boson with the ATLAS detector at the LHC," *Phys. Lett.*, vol. B716, pp. 1–29, 2012.

[25] S. Chatrchyan *et al.*, "Observation of a new boson at a mass of 125 GeV with the CMS experiment at the LHC," *Phys. Lett.*, vol. B716, pp. 30–61, 2012.

[26] A. D. Sakharov, "Violation of CP Invariance, c Asymmetry, and Baryon Asymmetry of the Universe," *Pisma Zh. Eksp. Teor. Fiz.*, vol. 5, pp. 32–35, 1967. [Usp. Fiz. Nauk161,61(1991)].

[27] A. G. Cohen, D. B. Kaplan, and A. E. Nelson, "Progress in electroweak baryogenesis," *Ann. Rev. Nucl. Part. Sci.*, vol. 43, pp. 27–70, 1993.

[28] A. Riotto and M. Trodden, "Recent progress in baryogenesis," *Ann. Rev. Nucl. Part. Sci.*, vol. 49, pp. 35–75, 1999.

[29] W.-S. Hou, "Source of CP Violation for the Baryon Asymmetry of the Universe," *Chin. J. Phys.*, vol. 47, p. 134, 2009.

[30] K. G. Wilson, "CONFINEMENT OF QUARKS," *Phys. Rev.*, vol. D10, pp. 2445–2459, 1974.

[31] E. Eichten, "Heavy Quarks on the Lattice," *Nucl. Phys. Proc. Suppl.*, vol. 4, p. 170, 1988.

[32] N. Isgur and M. B. Wise, "WEAK TRANSITION FORM-FACTORS BETWEEN HEAVY MESONS," *Phys. Lett.*, vol. B237, pp. 527–530, 1990.

[33] N. Isgur and M. B. Wise, "Weak Decays of Heavy Mesons in the Static Quark Approximation," *Phys. Lett.*, vol. B232, pp. 113–117, 1989.

[34] E. Eichten and B. R. Hill, "An Effective Field Theory for the Calculation of Matrix Elements Involving Heavy Quarks," *Phys. Lett.*, vol. B234, pp. 511–516, 1990.

[35] H. Georgi, "An effective field theory for heavy quarks at low- energies," *Phys. Lett.*, vol. B240, pp. 447–450, 1990.

[36] E. Eichten and B. R. Hill, "STATIC EFFECTIVE FIELD THEORY: 1/m CORRECTIONS," *Phys. Lett.*, vol. B243, pp. 427–431, 1990.

[37] W. E. Caswell and G. P. Lepage, "Effective Lagrangians for Bound State Problems in QED, QCD, and Other Field Theories," *Phys. Lett.*, vol. 167B, pp. 437–442, 1986.

[38] B. Thacker and G. Lepage, "Heavy quark bound states in lattice QCD," *Phys.Rev.*, vol. D43, pp. 196–208, 1991.

[39] G. P. Lepage, L. Magnea, C. Nakhleh, U. Magnea, and K. Hornbostel, "Improved nonrelativistic QCD for heavy quark physics," *Phys. Rev.*, vol. D46, pp. 4052–4067, 1992.

[40] A. X. El-Khadra, A. S. Kronfeld, and P. B. Mackenzie, "Massive Fermions in Lattice Gauge Theory," *Phys. Rev.*, vol. D55, pp. 3933–3957, 1997.

[41] S. Aoki, Y. Kuramashi, and S. Tominaga, "Relativistic heavy quarks on the lattice," *Prog.Theor.Phys.*, vol. 109, pp. 383–413, 2003.

[42] N. H. Christ, M. Li, and H.-W. Lin, "Relativistic Heavy Quark Effective Action," *Phys.Rev.*, vol. D76, p. 074505, 2007.

[43] Y. Iwasaki, "Renormalization group analysis of lattice theories and improved lattice action. 2. four-dimensional nonabelian su(n) gauge model," *UTHEP-118*, 1983.

[44] R. C. Brower, H. Neff, and K. Orginos, "The Móbius Domain Wall Fermion Algorithm," 2012.

[45] F. Abe *et al.*, "Observation of top quark production in $\bar{p}p$ collisions," *Phys. Rev. Lett.*, vol. 74, pp. 2626–2631, 1995.

[46] K. Kodama *et al.*, "Observation of tau neutrino interactions," *Phys. Lett.*, vol. B504, pp. 218–224, 2001.

[47] P. Fayet, "Supersymmetric theories of particles and interactions," *Physica Scripta*, vol. 1987, no. T15, p. 46, 1987.

[48] L. Susskind, "Dual symmetric theory of hadrons. 1.," *Nuovo Cim.*, vol. A69, pp. 457–496, 1970.

[49] Y. Nambu, "Quasiparticles and Gauge Invariance in the Theory of Superconductivity," *Phys. Rev.*, vol. 117, pp. 648–663, 1960.

[50] J. Goldstone, "Field Theories with Superconductor Solutions," *Nuovo Cim.*, vol. 19, pp. 154–164, 1961.

[51] J. Goldstone, A. Salam, and S. Weinberg, "Broken Symmetries," *Phys. Rev.*, vol. 127, pp. 965–970, 1962.

[52] A. V. Manohar and M. B. Wise, "Heavy quark physics," *Camb. Monogr. Part. Phys. Nucl. Phys. Cosmol.*, vol. 10, pp. 1–191, 2000.

[53] K. Fujikawa, "Path Integral Measure for Gauge Invariant Fermion Theories," *Phys. Rev. Lett.*, vol. 42, pp. 1195–1198, 1979.

[54] K. G. Wilson, "Non-lagrangian models of current algebra," *Phys. Rev.*, vol. 179, pp. 1499–1512, Mar 1969.

[55] K. G. Wilson and W. Zimmermann, "Operator product expansions and composite field operators in the general framework of quantum field theory," *Communications in Mathematical Physics*, vol. 24, no. 2, pp. 87–106, 1972.

[56] A. J. Buras, A. Czarnecki, M. Misiak, and J. Urban, "Completing the NLO QCD calculation of anti-B $\to$ X(s gamma)," *Nucl. Phys.*, vol. B631, pp. 219–238, 2002.

[57] P. Gambino, M. Gorbahn, and U. Haisch, "Anomalous dimension matrix for radiative and rare semileptonic B decays up to three loops," *Nucl. Phys.*, vol. B673, pp. 238–262, 2003.

[58] W. Altmannshofer, P. Ball, A. Bharucha, A. J. Buras, D. M. Straub, and M. Wick, "Symmetries and Asymmetries of $B \to K^* \mu^+ \mu^-$ Decays in the Standard Model and Beyond," *JHEP*, vol. 01, p. 019, 2009.

[59] R. Aaij *et al.*, "Angular analysis of the $B^0 \to K^{*0} \mu^+ \mu^-$ decay using 3 fb^{-1} of integrated luminosity," *JHEP*, vol. 02, p. 104, 2016.

[60] S. Wehle *et al.*, "Lepton-Flavor-Dependent Angular Analysis of $B \to K^* \ell^+ \ell^-$," *Phys. Rev. Lett.*, vol. 118, no. 11, p. 111801, 2017.

[61] R. Aaij *et al.*, "Differential branching fractions and isospin asymmetries of $B \to K^{(*)}\mu^+\mu^-$ decays," *JHEP*, vol. 06, p. 133, 2014.

[62] R. Aaij *et al.*, "Measurements of the S-wave fraction in $B^0 \to K^+\pi^-\mu^+\mu^-$ decays and the $B^0 \to K^*(892)^0\mu^+\mu^-$ differential branching fraction," *JHEP*, vol. 11, p. 047, 2016.

[63] R. Aaij *et al.*, "Test of lepton universality using $B^+ \to K^+\ell^+\ell^-$ decays," *Phys. Rev. Lett.*, vol. 113, p. 151601, 2014.

[64] S. Fajfer, J. F. Kamenik, and I. Nisandzic, "On the $B \to D^*\tau\bar{\nu}_\tau$ Sensitivity to New Physics," *Phys. Rev.*, vol. D85, p. 094025, 2012.

[65] J. A. Bailey *et al.*, "Refining new-physics searches in $B \to D\tau\nu$ decay with lattice QCD," *Phys. Rev. Lett.*, vol. 109, p. 071802, 2012.

[66] J. Lees *et al.*, "Evidence for an excess of $\bar{B} \to D^{(*)}\tau^-\bar{\nu}_\tau$ decays," *Phys.Rev.Lett.*, vol. 109, p. 101802, 2012.

[67] S. Nandi, S. K. Patra, and A. Soni, "Correlating new physics signals in $B \to D^{(*)}\tau\nu_\tau$ with $B \to \tau\nu_\tau$," 2016.

[68] S. Descotes-Genon, L. Hofer, J. Matias, and J. Virto, "On the impact of power corrections in the prediction of $B \to K^*\mu^+\mu^-$ observables," *JHEP*, vol. 12, p. 125, 2014.

[69] S. J ager and J. Martin Camalich, "Reassessing the discovery potential of the $B \to K^*\ell^+\ell^-$ decays in the large-recoil region: SM challenges and BSM opportunities," *Phys. Rev.*, vol. D93, no. 1, p. 014028, 2016.

[70] J. Lyon and R. Zwicky, "Resonances gone topsy turvy - the charm of QCD or new physics in $b \to s\ell^+\ell^-$?," 2014.

[71] M. Ciuchini, M. Fedele, E. Franco, S. Mishima, A. Paul, L. Silvestrini, and M. Valli, "$B \to K^*\ell^+\ell^-$ decays at large recoil in the Standard Model: a theoretical reappraisal," *JHEP*, vol. 06, p. 116, 2016.

[72] B. Capdevila, S. Descotes-Genon, L. Hofer, and J. Matias, "Hadronic uncertainties in $B \to K^*\mu^+\mu^-$: a state-of-the-art analysis," *JHEP*, vol. 04, p. 016, 2017.

[73] V. G. Chobanova, T. Hurth, F. Mahmoudi, D. Martinez Santos, and S. Neshatpour, "Large hadronic power corrections or new physics in the rare decay B $\to$ K* μ^+ μ^-," *JHEP*, vol. 07, p. 025, 2017.

[74] U.-G. Meißner and W. Wang, "$\mathbf{B_s} \to \mathbf{K}^{(*)}\ell\bar{\nu}$, Angular Analysis, S-wave Contributions and $|\mathbf{V_{ub}}|$," *JHEP*, vol. 1401, p. 107, 2014.

[75] Q.-S. Yan, C.-S. Huang, W. Liao, and S.-H. Zhu, "Exclusive semileptonic rare decays $B \to K, K^* \ell^+ \ell^-$ in supersymmetric theories," *Phys. Rev.*, vol. D62, p. 094023, 2000.

[76] S. R. Choudhury, A. S. Cornell, N. Gaur, and G. C. Joshi, "Supersymmetric effects on forward backward asymmetries of $B \to K \ell^+ \ell^-$," *Phys. Rev.*, vol. D69, p. 054018, 2004.

[77] Y. Sakaki and H. Tanaka, "Constraints on the charged scalar effects using the forward-backward asymmetry on $B^- \to D(^*)\tau\nu$," *Phys. Rev.*, vol. D87, no. 5, p. 054002, 2013.

[78] G. Burdman, "Short distance coefficients and the vanishing of the lepton asymmetry in $B \to$ V ℓ^+ lepton-," *Phys. Rev.*, vol. D57, pp. 4254–4257, 1998.

[79] S. Fukae, C. S. Kim, and T. Yoshikawa, "A Systematic analysis of the lepton polarization asymmetries in the rare B decay, $B \to X(s)\tau^+\tau^-$," *Phys. Rev.*, vol. D61, p. 074015, 2000.

[80] T. M. Aliev, D. A. Demir, and M. Savci, "Probing the sources of CP violation via $B \to K^* \ell^+ \ell^-$ decay," *Phys. Rev.*, vol. D62, p. 074016, 2000.

[81] A. Ali, E. Lunghi, C. Greub, and G. Hiller, "Improved model independent analysis of semileptonic and radiative rare B decays," *Phys. Rev.*, vol. D66, p. 034002, 2002.

[82] G. Hiller and F. Kruger, "More model-independent analysis of $b \to s$ processes," *Phys. Rev.*, vol. D69, p. 074020, 2004.

[83] C. Bobeth, G. Hiller, and G. Piranishvili, "Angular distributions of $\bar{B} \to \bar{K} \ell^+ \ell^-$ decays," *JHEP*, vol. 12, p. 040, 2007.

[84] G. Hiller and M. Schmaltz, "Diagnosing lepton-nonuniversality in $b \to s\ell\ell$," *JHEP*, vol. 02, p. 055, 2015.

[85] M. Tanaka, "Charged Higgs effects on exclusive semitauonic B decays," *Z. Phys.*, vol. C67, pp. 321–326, 1995.

[86] M. Tanaka and R. Watanabe, "Tau longitudinal polarization in $B \to D\tau\nu$ and its role in the search for charged Higgs boson," *Phys. Rev.*, vol. D82, p. 034027, 2010.

[87] M. Huschle *et al.*, "Measurement of the branching ratio of $\bar{B} \to D^{(*)}\tau^-\bar{\nu}_\tau$ relative to $\bar{B} \to D^{(*)}\ell^-\bar{\nu}_\ell$ decays with hadronic tagging at Belle," *Phys. Rev.*, vol. D92, no. 7, p. 072014, 2015.

[88] S. Bifani, "Search for new physics with $b \to s\ell^+\ell^-$." LHC seminar, 2017.

[89] S. Descotes-Genon, J. Matias, and J. Virto, "Understanding the $B \to K^* \mu^+ \mu^-$ Anomaly," *Phys. Rev.*, vol. D88, p. 074002, 2013.

[90] W. Altmannshofer and D. M. Straub, "New Physics in $B \to K^* \mu\mu$?," *Eur. Phys. J.*, vol. C73, p. 2646, 2013.

[91] R. Gauld, F. Goertz, and U. Haisch, "On minimal Z' explanations of the $B \to K^* \mu^+ \mu^-$ anomaly," *Phys. Rev.*, vol. D89, p. 015005, 2014.

[92] B. Stech, "Weak two-body decays of heavy mesons," in *Flavor mixing and CP violation. proceedings, 5th Moriond workshop, la plagne, france, january 13-19, 1985*, pp. 151–162, 1985.

[93] M. Wirbel, B. Stech, and M. Bauer, "Exclusive Semileptonic Decays of Heavy Mesons," *Z. Phys.*, vol. C29, p. 637, 1985.

[94] M. Creutz, *Quarks, gluons and lattices*. Cambridge Monographs on Mathematical Physics, Cambridge, UK: Cambridge Univ. Press, 1985.

[95] T. DeGrand and C. E. Detar, *Lattice methods for quantum chromodynamics*. 2006.

[96] C. Gattringer and C. B. Lang, "Quantum chromodynamics on the lattice," *Lect. Notes Phys.*, vol. 788, pp. 1–343, 2010.

[97] J. Smit, "Introduction to quantum fields on a lattice: A robust mate," *Cambridge Lect. Notes Phys.*, vol. 15, pp. 1–271, 2002.

[98] D. J. Gross and F. Wilczek, "Ultraviolet Behavior of Nonabelian Gauge Theories," *Phys. Rev. Lett.*, vol. 30, pp. 1343–1346, 1973.

[99] H. D. Politzer, "Reliable Perturbative Results for Strong Interactions?," *Phys. Rev. Lett.*, vol. 30, pp. 1346–1349, 1973.

[100] M. Creutz, L. Jacobs, and C. Rebbi, "Monte Carlo Study of Abelian Lattice Gauge Theories," *Phys. Rev.*, vol. D20, p. 1915, 1979. [,182(1979)].

[101] P. T. Matthews and A. Salam, "The green's functions of quantised fields," *Il Nuovo Cimento (1943-1954)*, vol. 12, pp. 563–565, Oct 1954.

[102] P. T. Matthews and A. Salam, "Propagators of quantized field," *Il Nuovo Cimento (1955-1965)*, vol. 2, pp. 120–134, Jul 1955.

[103] T. Takaishi, "Heavy quark potential and effective actions on blocked configurations," *Phys. Rev.*, vol. D54, pp. 1050–1053, 1996.

[104] P. de Forcrand *et al.*, "Renormalization group flow of su(3) lattice gauge theory: Numerical studies in a two coupling space," *Nucl. Phys.*, vol. B577, pp. 263–278, 2000.

[105] M. Luscher and P. Weisz, "On-shell improved lattice gauge theories," *Commun. Math. Phys.*, vol. 97, p. 59, 1985.

[106] B. Sheikholeslami and R. Wohlert, "Improved Continuum Limit Lattice Action for QCD with Wilson Fermions," *Nucl.Phys.*, vol. B259, p. 572, 1985.

[107] H. B. Nielsen and M. Ninomiya, "No Go Theorem for Regularizing Chiral Fermions," *Phys. Lett.*, vol. 105B, pp. 219–223, 1981.

[108] P. H. Ginsparg and K. G. Wilson, "A Remnant of Chiral Symmetry on the Lattice," *Phys. Rev.*, vol. D25, p. 2649, 1982.

[109] D. B. Kaplan, "A Method for simulating chiral fermions on the lattice," *Phys. Lett.*, vol. B288, pp. 342–347, 1992.

[110] H. Neuberger, "Exactly massless quarks on the lattice," *Phys. Lett.*, vol. B417, pp. 141–144, 1998.

[111] H. Neuberger, "More about exactly massless quarks on the lattice," *Phys. Lett.*, vol. B427, pp. 353–355, 1998.

[112] A. Borici, "Truncated overlap fermions: The Link between overlap and domain wall fermions," in *Lattice fermions and structure of the vacuum. Proceedings, NATO Advanced Research Workshop, Dubna, Russia, October 5-9, 1999*, pp. 41–52, 1999.

[113] K. Symanzik, "Continuum Limit and Improved Action in Lattice Theories. 1. Principles and ϕ^4 Theory," *Nucl. Phys.*, vol. B226, pp. 187–204, 1983.

[114] K. Symanzik, "Continuum Limit and Improved Action in Lattice Theories. 2. O(N) Nonlinear Sigma Model in Perturbation Theory," *Nucl. Phys.*, vol. B226, pp. 205–227, 1983.

[115] G. C. Wick, "The Evaluation of the Collision Matrix," *Phys. Rev.*, vol. 80, pp. 268–272, 1950. [,592(1950)].

[116] S. Gusken, K. Schilling, R. Sommer, K. H. Mutter, and A. Patel, "Mass Splittings in the Baryon Octet and the Nucleon σ Term in Lattice QCD," *Phys. Lett.*, vol. B212, pp. 216–220, 1988.

[117] C. R. Allton *et al.*, "Gauge invariant smearing and matrix correlators using Wilson fermions at Beta = 6.2," *Phys. Rev.*, vol. D47, pp. 5128–5137, 1993.

[118] C. Best, M. Gockeler, R. Horsley, E.-M. Ilgenfritz, H. Perlt, P. E. L. Rakow, A. Schafer, G. Schierholz, A. Schiller, and S. Schramm, "Pion and rho structure functions from lattice QCD," *Phys. Rev.*, vol. D56, pp. 2743–2754, 1997.

[119] M. G. Alford, T. Klassen, and P. Lepage, "The D234 action for light quarks," *Nucl.Phys.Proc.Suppl.*, vol. 47, pp. 370–373, 1996.

[120] J. A. Bailey, C. Bernard, C. DeTar, M. Di Pierro, A. X. El-Khadra, R. T. Evans, E. D. Freeland, E. Gamiz, S. Gottlieb, U. M. Heller, J. E. Hetrick, A. S. Kronfeld, J. Laiho, L. Levkova, P. B. Mackenzie, M. Okamoto, J. N. Simone, R. Sugar, D. Toussaint, and R. S. Van de Water, "$b \to \pi\ell\nu$," *Phys. Rev. D*, vol. 79, p. 054507, Mar 2009.

[121] G. Burdman, Z. Ligeti, M. Neubert, and Y. Nir, "The Decay B $\to$ pi lepton neutrino in heavy quark effective theory," *Phys. Rev.*, vol. D49, pp. 2331–2345, 1994.

[122] D. Bećirević, S. Prelovsek, and J. Zupan, "$B \to \pi$ and $B \to K$ transitions in standard and quenched chiral perturbation theory," *Phys.Rev.*, vol. D67, p. 054010, 2003.

[123] A. X. El-Khadra *et al.*, "Semileptonic decays $b \to \pi\ell\nu$ and $D \to \pi\ell\nu$ from lattice qcd," *Phys.Rev.*, vol. D64, p. 014502, 2001.

[124] A. S. Kronfeld, "Perturbative and nonperturbative corrections to B $\to$ D(*) lepton neutrino*," *Nucl. Phys. Proc. Suppl.*, vol. 83, pp. 307–309, 2000.

[125] J. N. Simone, S. Hashimoto, A. X. El-Khadra, A. S. Kronfeld, P. B. Mackenzie, and S. M. Ryan, "The $B \to D^*\ell\nu$ form factor at zero recoil," *Nucl. Phys. Proc. Suppl.*, vol. 83, pp. 334–336, 2000.

[126] J. Harada *et al.*, "Application of heavy quark effective theory to lattice QCD. 2. Radiative corrections to heavy light currents," *Phys.Rev.*, vol. D65, p. 094513, 2002.

[127] N. Yamada, S. Aoki, and Y. Kuramashi, "Perturbative determination of mass dependent renormalization and improvement coefficients for the heavy-light vector and axial-vector currents with relativistic heavy and domain-wall light quarks," *Nucl. Phys.*, vol. B713, pp. 407–437, 2005.

[128] C. Lehner and S. Meinel, "Private communication."

[129] M. Luscher, "Volume Dependence of the Energy Spectrum in Massive Quantum Field Theories. 1. Stable Particle States," *Commun. Math. Phys.*, vol. 104, p. 177, 1986.

[130] P. Boyle, L. Del Debbio, A. Khamseh, A. Jüttner, F. Sanfilippo, and J. T. Tsang, "Domain Wall Charm Physics with Physical Pion Masses: Decay Constants, Bag and ξ Parameters," *PoS*, vol. LATTICE2015, p. 336, 2016.

[131] P. Boyle, A. Jüttner, M. K. Marinkovic, F. Sanfilippo, M. Spraggs, and J. T. Tsang, "An exploratory study of heavy domain wall fermions on the lattice," *JHEP*, vol. 04, p. 037, 2016.

[132] P. Boyle, L. Del Debbio, A. Jüttner, A. Khamseh, F. Sanfilippo, J. T. Tsang, and O. Witzel, "Charm Physics with Domain Wall Fermions and Physical Pion Masses," 2016.

[133] H.-W. Lin and N. Christ, "Non-perturbatively Determined Relativistic Heavy Quark Action," *Phys.Rev.*, vol. D76, p. 074506, 2007.

[134] Y. Aoki, N. H. Christ, J. M. Flynn, T. Izubuchi, C. Lehner, M. Li, H. Peng, A. Soni, R. S. Van de Water, and O. Witzel, "Nonperturbative tuning of an improved relativistic heavy-quark action with application to bottom spectroscopy," *Phys. Rev.*, vol. D86, p. 116003, 2012.

[135] J. M. Flynn, T. Izubuchi, T. Kawanai, C. Lehner, A. Soni, R. S. Van de Water, and O. Witzel, "$B \to \pi \ell \nu$ and $B_s \to K \ell \nu$ form factors and $|V_{ub}|$ from 2+1-flavor lattice QCD with domain-wall light quarks and relativistic heavy quarks," *Phys. Rev.*, vol. D91, no. 7, p. 074510, 2015.

[136] A. Ali Khan, S. Aoki, G. Boyd, R. Burkhalter, S. Ejiri, M. Fukugita, S. Hashimoto, N. Ishizuka, Y. Iwasaki, K. Kanaya, T. Kaneko, Y. Kuramashi, T. Manke, K. Nagai, M. Okawa, H. P. Shanahan, A. Ukawa, and T. Yoshié, "Light hadron spectroscopy with two flavors of dynamical quarks on the lattice," *Phys. Rev. D*, vol. 65, p. 054505, Feb 2002.

[137] J. D. Bratt, R. G. Edwards, M. Engelhardt, P. Hägler, H. W. Lin, M. F. Lin, H. B. Meyer, B. Musch, J. W. Negele, K. Orginos, A. V. Pochinsky, M. Procura, D. G. Richards, W. Schroers, and S. N. Syritsyn, "Nucleon structure from mixed action calculations using $2 + 1$ flavors of asqtad sea and domain wall valence fermions," *Phys. Rev. D*, vol. 82, p. 094502, Nov 2010.

[138] B. Efron, *The Jackknife, the Bootstrap, and Other Resampling Plans.* CBMS-NSF Regional Conference Series in Applied Mathematics, Society for Industrial and Applied Mathematics, 1982.

[139] J. Shao and D. Tu, *The jackknife and bootstrap.* Berlin; New York: Springer-Verlag Inc, 1995.

[140] M. Quenouille, "Approximation tests of correlation in time series," *J. R. Statist. Soc.*, vol. B11, pp. 68–84, 1949.

[141] J. Tukey, "Bias and confidence in not quite large samples," *Ann. Math. Statist.*, vol. 29, p. 614, 1958.

[142] A. Ali Khan *et al.*, "Light hadron spectroscopy with two flavors of dynamical quarks on the lattice," *Phys. Rev.*, vol. D65, p. 054505, 2002. [Erratum: Phys. Rev.D67,059901(2003)].

[143] N. H. Christ *et al.*, "B-meson decay constants from 2+1-flavor lattice QCD with domain-wall light quarks and relativistic heavy quarks," *Phys.Rev.*, vol. D91, p. 054502, 2015.

[144] M. B. Wise, "Chiral perturbation theory for hadrons containing a heavy quark," *Phys. Rev.*, vol. D45, no. 7, p. R2188, 1992.

[145] G. Burdman and J. F. Donoghue, "Union of chiral and heavy quark symmetries," *Phys. Lett.*, vol. B280, pp. 287–291, 1992.

[146] T.-M. Yan, H.-Y. Cheng, C.-Y. Cheung, G.-L. Lin, Y. C. Lin, and H.-L. Yu, "Heavy quark symmetry and chiral dynamics," *Phys. Rev.*, vol. D46, pp. 1148–1164, 1992. [Erratum: Phys. Rev.D55,5851(1997)].

[147] A. F. Falk and B. Grinstein, "Anti-B $\to$ Anti-K e^+e^- in Chiral Perturbation Theory," *Nucl. Phys.*, vol. B416, pp. 771–785, 1994.

[148] J. Flynn and C. Sachrajda, "SU(2) chiral perturbation theory for K(l3) decay amplitudes," *Nucl.Phys.*, vol. B812, pp. 64–80, 2009.

[149] J. Bijnens and I. Jemos, "Hard Pion Chiral Perturbation Theory for $B \to \pi$ and $D \to \pi$ Formfactors," *Nucl.Phys.*, vol. B840, pp. 54–66, 2010.

[150] W. A. Bardeen, E. J. Eichten, and C. T. Hill, "Chiral multiplets of heavy - light mesons," *Phys.Rev.*, vol. D68, p. 054024, 2003.

[151] J. Beringer *et al.*, "Review of Particle Physics (RPP)," *Phys.Rev.*, vol. D86, p. 010001, 2012.

[152] E. B. Gregory, C. T. H. Davies, E. Follana, E. Gamiz, I. D. Kendall, G. P. Lepage, H. Na, J. Shigemitsu, and K. Y. Wong, "Prediction of the B_c^* mass in full lattice qcd," *Phys. Rev. Lett.*, vol. 104, p. 022001, Jan 2010.

[153] M. B. Oktay and A. S. Kronfeld, "New lattice action for heavy quarks," *Phys.Rev.*, vol. D78, p. 014504, 2008.

[154] S. Aoki *et al.*, "Review of lattice results concerning low-energy particle physics," *Eur. Phys. J.*, vol. C77, no. 2, p. 112, 2017.

[155] C. G. Boyd, B. Grinstein, and R. F. Lebed, "Constraints on form-factors for exclusive semileptonic heavy to light meson decays," *Phys.Rev.Lett.*, vol. 74, pp. 4603–4606, 1995.

[156] L. Lellouch, "Lattice constrained unitarity bounds for anti-B0 $\to \pi^+\ell^+\nu^-$ decays," *Nucl.Phys.*, vol. B479, pp. 353–391, 1996.

[157] C. G. Boyd and M. J. Savage, "Analyticity, shapes of semileptonic form-factors, and anti-B $\to$; pi lepton anti-neutrino," *Phys.Rev.*, vol. D56, pp. 303–311, 1997.

[158] C. Bourrely, B. Machet, and E. de Rafael, "Semileptonic Decays of Pseudoscalar Particles ($M \to M' \ell \nu_\ell$) and Short Distance Behavior of Quantum Chromodynamics," *Nucl.Phys.*, vol. B189, p. 157, 1981.

[159] M. C. Arnesen, B. Grinstein, I. Z. Rothstein, and I. W. Stewart, "A precision model independent determination of —V(ub)— from B $\to \pi \ell \nu$," *Phys. Rev. Lett.*, vol. 95, p. 071802, 2005.

[160] C. Bourrely, I. Caprini, and L. Lellouch, "Model-independent description of B →; pi l nu decays and a determination of —V(ub)—," *Phys.Rev.*, vol. D79, p. 013008, 2009.

[161] D. Becirevic and A. B. Kaidalov, "Comment on the heavy to light form-factors," *Phys.Lett.*, vol. B478, pp. 417–423, 2000.

[162] P. Ball and R. Zwicky, "New results on B →; pi, K, eta decay formfactors from light-cone sum rules," *Phys.Rev.*, vol. D71, p. 014015, 2005.

[163] P. del Amo Sanchez *et al.*, "Study of $B \to \pi \ell \nu$ and $B \to \rho \ell \nu$ Decays and Determination of $|V_{ub}|$," *Phys.Rev.*, vol. D83, p. 032007, 2011.

[164] H. Ha *et al.*, "Measurement of the decay $B^0 \to \pi^- \ell^+ \nu$ and determination of $|V_{ub}|$," *Phys.Rev.*, vol. D83, p. 071101, 2011.

[165] J. Lees *et al.*, "Branching fraction and form-factor shape measurements of exclusive charmless semileptonic B decays, and determination of $|V_{ub}|$," *Phys.Rev.*, vol. D86, p. 092004, 2012.

[166] A. Sibidanov *et al.*, "Study of Exclusive $B \to X_u \ell \nu$ Decays and Extraction of $\|V_{ub}\|$ using Full Reconstruction Tagging at the Belle Experiment," *Phys.Rev.*, vol. D88, no. 3, p. 032005, 2013.

[167] Y. Amhis *et al.*, "Averages of b-hadron, c-hadron, and τ-lepton properties as of summer 2016," 2016.

[168] A. Bharucha, T. Feldmann, and M. Wick, "Theoretical and Phenomenological Constraints on Form Factors for Radiative and Semi-Leptonic B-Meson Decays," *JHEP*, vol. 1009, p. 090, 2010.

[169] J. A. Bailey *et al.*, "$B \to D \ell \nu$ form factors at nonzero recoil and $|V_{cb}|$ from 2+1-flavor lattice QCD," *Phys. Rev.*, vol. D92, no. 3, p. 034506, 2015.

[170] M. Beneke and T. Feldmann, "Symmetry breaking corrections to heavy to light B meson form-factors at large recoil," *Nucl.Phys.*, vol. B592, pp. 3–34, 2001.

[171] T. Becher and R. J. Hill, "Comment on form-factor shape and extraction of —V(ub)— from $B \to \pi \ell \nu$," *Phys.Lett.*, vol. B633, pp. 61–69, 2006.

[172] G. Lepage *et al.*, "Constrained curve fitting," *Nucl.Phys.Proc.Suppl.*, vol. 106, pp. 12–20, 2002.

[173] R.-H. Li, C.-D. Lu, and Y.-M. Wang, "Exclusive B(s) decays to the charmed mesons $D(s)^+(1968, 2317)$ in the standard model," *Phys. Rev.*, vol. D80, p. 014005, 2009.

[174] G. Duplancic and B. Melic, "B, B(s) $\to$ K form factors: An Update of light-cone sum rule results," *Phys. Rev.*, vol. D78, p. 054015, 2008.

[175] W. Detmold and S. Meinel, "$\Lambda_b \to \Lambda \ell^+ \ell^-$ form factors, differential branching fraction, and angular observables from lattice QCD with relativistic b quarks," *Phys. Rev.*, vol. D93, no. 7, p. 074501, 2016.

[176] R. R. Horgan, Z. Liu, S. Meinel, and M. Wingate, "Calculation of $B^0 \to K^{*0} \mu^+ \mu^-$ and $B_s^0 \to \phi \mu^+ \mu^-$ observables using form factors from lattice QCD," *Phys. Rev. Lett.*, vol. 112, p. 212003, 2014.

[177] R. R. Horgan, Z. Liu, S. Meinel, and M. Wingate, "Rare B decays using lattice QCD form factors," *PoS*, vol. LATTICE2014, p. 372, 2015.

[178] C. Bouchard, G. P. Lepage, C. Monahan, H. Na, and J. Shigemitsu, "Standard Model Predictions for $B \to K \ell^+ \ell^-$ with Form Factors from Lattice QCD," *Phys. Rev. Lett.*, vol. 111, no. 16, p. 162002, 2013. [Erratum: Phys. Rev. Lett.112,no.14,149902(2014)].

[179] J. A. Bailey *et al.*, "$B \to K l^+ l^-$ decay form factors from three-flavor lattice QCD," *Phys. Rev.*, vol. D93, no. 2, p. 025026, 2016.

[180] D. Du, A. X. El-Khadra, S. Gottlieb, A. S. Kronfeld, J. Laiho, E. Lunghi, R. S. Van de Water, and R. Zhou, "Phenomenology of semileptonic B-meson decays with form factors from lattice QCD," *Phys. Rev.*, vol. D93, no. 3, p. 034005, 2016.